A Study of the Static to Kinetic Friction Transition of Polymers

by

Edward Chungjen Lee

Thesis submitted to the Faculty of the

Virginia Polytechnic Institute and State University

in partial fulfillment of the requirements for the degree of

MASTER OF SCIENCE

in

Mechanical Engineering

APPROVED:

Dr. Norman S. Eiss, Chairman

Dr. Reginald G. Mitchiner

Dr. Michael J. Furey

May 1995
Blacksburg, Virginia

C.2

A Study of the Static to Kinetic Friction Transition of Polymers

by

Edward C. Lee

Norman S. Eiss, Jr., Chairman

Mechanical Engineering

(ABSTRACT)

This study investigates the transition from static to kinetic friction for structural polymers and continues previous research conducted by Dr. N. S. Eiss, B. McCann, and R. Molique. A new test apparatus which simultaneously measures friction, normal load, and relative velocity was developed to study this transition. The polymers used in this study were nylon, ABS, polycarbonate, and fiberglass filled and unfilled polypropylene. Creep effects of polymers on the static coefficient and thus the drop in friction was investigated. Friction tests were conducted to determine the effect of normal load, surface roughness, and material composition on the transition from static to kinetic friction. A double value friction-velocity relationship was found whenever a drop in friction occurred. The material composition seems have a larger effect on friction induced vibrations than surface roughness. A few conclusions about why certain static to kinetic transitions occur are made.

Acknowledgments

The completion of this study would not be possible without the assistance of many people not mentioned in the acknowledgments. I would like to thank Dr. Norman S. Eiss for his patience, guidance, and support over the past two years on this project. Working with Dr. Eiss on this study has been an excellent learning experience with many challenges and responsibilities. I would also like to thank the members of my committee, Dr. Reginald G. Mitchiner and Dr. Michael J. Furey, for sharing their time and knowledge with me.

I am thankful to the Mechanical Engineering Department and the Ford Motor Company for sponsoring and providing the necessary resources to complete the project. I would also like to thank the following people who were extremely helpful in completing this project:

- The Mechanical Engineering machine shop and electrical shop personnel, especially Jerry Lucas, Ben Poe, and Billy Sheppard for their assistance and guidance on the construction of the new test apparatus.
- Rob Molique and Alan Arkus for all their help in developing the new test apparatus
- Dr. Larry D. Mitchell, Dr. Bhawani Tripathy, and Jorge Hanchi for all their assistance and insight in helping to complete this project.
- Dr. Paulo D' Souza and Mike McLeod whom assisted me on the injection molding and stress strain testing of my test samples.
- Ben Tritt, Chris Smith, Matt Schroeder, Mark Freeman, and Doug Patterson for making my time spent in the lab more enjoyable.

Finally I would like to thank my family whose support, love, and understanding has helped me get here today.

Table of Contents

List of Figures

List of Tables

1.0 Introduction

One of the most beneficial applications of plastics today is found in automotive interiors. Material development for plastics has produced suitable resins for this application because the size and complexity of the modern dashboard demands good resin flow properties coupled with stiffness, good impact resistance, color fastness and resistance to heat distortion[1]. Injection molded thermoplastic resins are typically incorporated and include Acrylonitrile-Butadiene-Styrene (ABS), and polypropylene. Unfortunately noise in the form of squeak or squeal emanates from the instrument panel and interior trim components when subjected to vibrations caused by the engine or the road. This noise is generated when relative motion between two parts exist and energy is released during every slip. This slip excites the instrument panel and transforms some energy into noise. Various techniques to prevent noise such as lubrication, separation, or bonding of these components are not possible or are expensive. It is believed that squeak and squeal noises can be reduced by selecting materials which do not exhibit stick slip frictional behavior.

Previous researchers on this project who worked with Dr. N. S. Eiss were B. P. McCann and R. S. Molique. McCann concluded that unstable frictional behavior is more likely to occur for smooth surfaces and/or higher loads. Molique's research generally agreed with McCann's but also concluded that static and kinetic friction are controlled by the same friction mechanisms. McCann and Molique conducted tests on the same pin-on-disk machine which was originally designed to measure wear and steady state friction values. In this study, a new test apparatus was developed to study the transition from static-to-kinetic friction.

The objectives of this project were:

1. To design, construct, and develop a new test apparatus to measure friction, normal load, and velocity simultaneously. This apparatus served two purposes: to study the friction-velocity relationship and to investigate the transition from static-to-kinetic friction.
2. To study the relationship between creep, material composition, normal load, and surface roughness to the transition from static-to-kinetic friction and how these variables affect friction induced oscillations.
3. To support or dispute conclusions on the friction-velocity relationship and transitional friction behavior of McCann, Molique, and other researchers by measuring friction and velocity during the slip phase of stick-slip cycles.
4. To identify material properties and/or system parameters which predict frictional oscillations.

2.0 Literature Review

2.1 Mechanisms of Polymer Friction

Friction is the resistive force which prevents one body from sliding over another. Two mechanisms contribute to resist motion between two contacting bodies: adhesion and plowing. When two surfaces are loaded in contact the asperities deform to support the load. Surfaces in contact will always have asperities that are elasticity or plastically deformed. The combined area of the contacting area is termed the real area of contact and is smaller than the apparent area of contact. The total interaction between contacting asperities contribute to friction and the deforming of the surface by the mechanisms of plowing or breaking of the adhesive bonds. These mechanism dissipate energy supplied by the work done by the applied force.

When two surfaces are loaded together, the contacting asperities deform to support the load. At any load, the tips of the asperities are under high pressure and deform plastically. This plastic flow increases the real area of contact by growth of the original asperity contacts and deformation of new asperity contacts. The real area of contact increases during this time until the asperities can elastically support the load. Strong adhesive bonds between the contacting asperities are formed within the real area of

contact. The tangential force to overcome adhesion is equal to the real area of contact, A, times the shear strength on the interface, s:

$$F_{adhesion} = A*s.$$

Thus, the contribution of the adhesion component to friction is the force required to break the interfacial adhesive bonds formed between contacting asperities.

The plowing component of friction is the force required to plow the asperities by plastic deformation. The asperities deform each other and cause some vertical motion to occur. The magnitude of the contribution of plowing to friction depends on surface roughness and the relative hardness of the two materials.

For polymers, the real area of contact is dependent on many factors including contact pressure, temperature, and sliding velocity. For polymers, frictional losses occur in two regions of deformation; the interfacial zone, where adhesion and plowing occur and the deformation zone, where visco-elastic deformation below the surface causes hysteresis losses[2].

Deformation losses for polymers during sliding are more dependent on temperature and strain rate than metals. Significant heating occurs because polymers tend have a low thermal conductivity. Because of low melting temperatures the heating leads to softening of the surface layer. For polymers, viscous losses in the surface layers is the main contributor to friction. At low sliding speeds, where frictional heating is deemed negligible, polymer friction depends on the roughness[2].

2.1.1 Creep Behavior

The static coefficient of friction for some polymers has been shown to increase with stick time, a relationship which has been attributed to creep[3]. Creep is defined as the dimensional change of a thermoplastic part subjected to long term constant load, such as the necking of the cross-section of the material which occurs under tensile loads. For compressive loads the cross-section area of the material would increase. This dimensional change depends upon factors such as the amount of applied load, temperature, duration of load, and the amount and the direction of orientation in the part. For a visco-elastic material, deformation due to creep will recover somewhat after the load is removed. The percent recovery depends on the elapsed time since load removal and on the duration and magnitude of the applied load[4].

2.1.2 Static and Kinetic Friction

Two explanations are offered for the static friction being higher than kinetic. The first one is based on creep which causes the real area of contact to increase during long periods of loading. During sliding there is less time for creep which causes the real area to be less than that prior to sliding. The adhesion model of friction predicts that the static friction would be higher because of the larger area of contact. The second explanation is based on microslips. Microslips occur when contacting asperities deform plastically as the tangential load is increased. When a new asperity is encountered the microslip is stopped. This process continues until gross sliding occurs. The value of the friction force when sliding commences is the maximum resistance of the asperity contacts. The kinetic value

is lower because it is the time average of the resistance of the contacting asperities which form the contact[5,6].

2.2 Friction Induced Oscillations

Friction induced oscillations are in the form of stick slip or harmonic oscillations which occur during sliding. During static loading, the tangential force will store elastic energy in the deformable components of the system. The resistive force at the interface remains equal and opposite to the tangential applied force. Both increase at the same rate in order to keep the system in static equilibrium and thus, remain stationary. Once the tangential force exceeds the frictional resistance the system starts to slide. If kinetic friction is less than the static friction, the potential energy stored in the system components transforms into kinetic energy as the system increases in velocity. If a cyclic exchange of potential and kinetic energy occurs, vibrations result. These vibrations can be in the form of single stick slip, multiple stick slip, or harmonic oscillations[5,7].

2.2.1 Harmonic Oscillations and Stick Slip

Harmonic oscillations are characterized by their sinusoidal content. The system usually oscillates at one of the damped natural frequencies of the system[8,9]. Stick-slip has a saw tooth waveform where the friction force gradually increases during stick and rapidly drops during slip. The frequency of stick-slip is determined by the difference between static and kinetic friction, the natural frequency of the sliding system, and the

average sliding velocity. The stick-slip frequency is generally lower than the system natural frequency. An example of stick-slip is shown in figure 2.1.

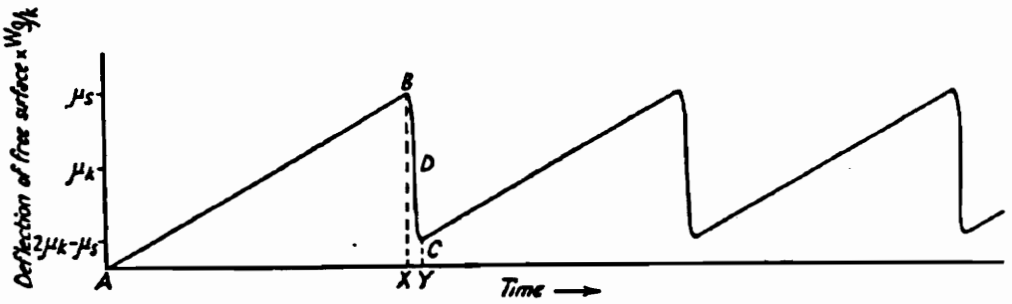

Figure 2.1 Illustration of stick-slip, taken from [28].

Two conditions tend to encourage stick slip: 1) When potential energy is stored in the system. This is true for any friction measuring apparatus which deflects to measure friction force, 2) When the friction-velocity curve has a negative slope which signifies friction decreases with increasing velocity. This occurs when a drop in friction results in a kinetic friction lower than static friction. It is also well known that experimental conditions affect the transition from static to kinetic friction. Stick-slip amplitude has been known to increase with increasing relative humidity and contact spot size[10].

The widely accepted causes for stick slip is that the static friction force exceeds the kinetic friction force or that the friction coefficient drops rapidly at small speeds[11, 12, 13, 14, 15, 16]. The static coefficient is higher than the kinetic coefficient of friction due to molecular adhesion between the surfaces and time dependent effects, such as creep[11,

17]. The time dependence of the static friction coefficient has been studied by many researchers This relationship indicates as stick times shorten then there is less time for static friction to increase[11]. Thus, the static and kinetic friction mechanisms are the same if no time is allowed during the stick phase[18].

During long contact times the real area of contact increases requiring a larger tangential shearing force. Once the shear strength of the junctions is reached, failure occurs which decreases the contact area. A force imbalance between the applied force and friction occurs. The sliding surfaces must then accelerate to the new equilibrium force, the kinetic friction, which opposes motion of the surfaces until the relative velocity returns to zero.

2.2.2 Friction Induced Noise

The relationship between self-excited frictional vibrations and noise emission has been studied by numerous researchers. Symmons and McNulty have found that metal on metal interfaces exhibit vibrations similar to harmonic oscillation while metal-plastic systems showed stick-slip behavior. The harmonic oscillations produced no noise emissions while the-stick slip oscillation produce significant noise emissions[19]. Thus, acoustical emissions are caused by the immediate drop in friction force during the initial slip. This imparts an impulse force to the system which excites the system into vibrations and acoustical output.

Friction noises are caused by a complex set of mechanisms such as adhesion and fusion, in addition to velocity characteristics of the friction force. Frictional noises are

also affected by surface roughness, contact area, load, damping characteristic of the material, temperature, and humidity[20, 21, 22].

2.2.3 Controlling Stick Slip

The chance of stick slip occurring can be reduced by increasing the sliding velocity, stiffening the elastic members, or increasing the damping of the elastic member. Self excited vibrations cannot be eliminated by increasing the velocity. Increasing the sliding velocity reduces contact time between asperities so that the asperities do not have adequate time to respond to the application of the normal stress[23]. Stiffening the elastic members reduces the amount of stored potential energy and damping dissipates the energy during slip.

Polymer additives and fillers do affect friction characteristics and the friction-velocity relationship is useful in determining when stick slip is likely to occur. For instance, McCann found that the addition of silicone oil to polymers reduced the overall friction force because the adhesive force at the interface was reduced[24]. But the silicone oil did not eliminate stick slip because there was a negative friction-velocity relationship.

Surface roughness also affects frictional behavior of both metals and polymers. In the classic metal-on-metal friction, an increase in the surface roughness generally increases the coefficient of friction[25]. But this is not the case for polymer-on-polymer or metal-on-polymer friction. McCann has shown that for polymers the coefficient of friction decreases for increasing surface roughness. This is due to decrease in contact area over which adhesive forces can act. The force of adhesion is reduced at the interface without

the corresponding increase in friction due to deformation. McCann's research has shown that smooth-on-smooth contact for polymers tends to promote stick slip behavior[24].

2.2.4 The Friction-Velocity Relationship

The change in velocity with friction force can be plotted to obtain a curve. Many researchers agree that a negative slope to the friction-velocity curve causes negative damping to the system resulting in self excited vibrations. Harmonic oscillation occurs if the slope of the negative friction-velocity relationship is small[20]. The exact friction-velocity relationship is dependent on the frictional behavior of the polymer.

There is considerable disagreement regarding the experimental determination of the friction-velocity relationship by averaging the kinetic friction and velocity during stick slip. Ko and Brockley have compared a friction-velocity curve obtained by averaging kinetic friction and one obtained by their acceleration-velocity-displacement(AVD) method[30]. The AVD method determines the friction-velocity relationship by measuring acceleration, velocity, and displacement and substituting this data into linear ordinary differential equations of motion. At low velocities the first method showed a decrease in friction while their method showed an increase in friction.

Antoniou, Cameron, and Gentle also question the averaging of kinetic friction[31]. But they also criticize the AVD method because error due to "parasitic interference(e.g. triggering oscillation interference) and calibration and hysteresis errors(each transducer has its own response which does not coincide absolutely with the responses of the other two transducers)" will distort the friction-velocity relationship. Incidentally, these authors

used a pin-on-disk apparatus and also mathematically manipulated the test data to find the relationship[31].

Many researchers have found the friction-velocity relationship to be doubled valued. Some have considered the bifurcation to be due to hysteresis in the relationship between acceleration and deceleration of the velocity during slip[32].

2.3 Mechanical Properties of Polymers

Crystallization controls to a large degree the physical and mechanical properties of a polymer[4, 33, 34]. Polypropylene and Nylon 66 are semi-crystalline polymers which tend to have molecules arranged in an ordered structure. Polycarbonate and ABS are amorphous solid polymers which are considered to be a random tangle of molecules. The molecules of an amorphous polymers when stretched may be aligned along the stretch direction, and would be considered an oriented amorphous polymer but not a crystalline polymer.

Fillers such as fiberglass increase the tensile strength, modulus, and reduce mold shrinkage at an expense to elongation. The fiberglass fillers also have high aspect ratios which tend to align themselves in the direction of the filling flow lines in the molded part. Glass fillers are generally isotropic which means stresses around these particles are evenly distributed. Load on the plastic composite is transferred from the continuous phase(resin) to the discontinuous phase(filler) through the effect of shear at the resin-fiber interface. Thus, the ultimate properties of the composite are dependent on the extent of bonding

between the two phases, the surface area of the filler, and the extent of the packing of the filler particles[4].

Yield behavior of polymers is temperature and strain rate dependent and appears as necking or brittle fracture[34]. For strain softening materials, the force required to deform the material after yield is less than that required to yield the material. For strain hardening materials such as ABS and polycarbonate, the actual load or nominal stress on the specimen decreases during necking, but the true stress may increase due to the reduction in cross-sectional area. Necking occurs when the directional properties of the molecular orientation are changed in the direction to the draw. The stiffness of the necked material along the direction of the draw is increased. Initially nominal stress decreases as the molecular orientation begins to reorganize. The free volume in the molecular structure is being filled as the molecular orientation begins to align in the direction of the draw.

2.4 Friction Measuring Equipment

Numerous configurations are used to measure frictional behavior. The sliding block, inclined plane, and deflection of an elastic beam configurations were summarized by Dorinson and Ludema[35]. In the slider block method, sliding motion is initiated by an actuator and the friction and displacement is measured by a force transducer and linear variable displacement transformer (LVDT), respectively. The inclined plane method has a motor which tilts the plane until slips occurs. A switch is activated at this time to stop the motor and the angle of tilt is measured. This test can measure only the static friction. A

third device measures friction by deflection of an elastic beam and is commonly used on pin-on-disk test machines.

Several devices were designed specifically to measure the transition from static to kinetic friction. Oscillating devices were used to indirectly measure frictional oscillations by measuring the angular displacement and angular velocity of a ring-like body. The output was obtained by mathematically manipulating the experimental data[32]. Ko and Brockley obtained friction-velocity curves by simultaneously measuring force, velocity, and acceleration on a test apparatus whose measurements are based on deflecting an elastic member[30]. Output was obtained by substituting the data into linear differential equations of motion, and then plotting the friction-velocity curve. Eguchi and Yamamoto used a sliding mechanism which measured friction by strain gages and acceleration by an accelerometer to study stick-slip oscillations[3]. In most cases the friction-velocity relationship was obtained indirectly.

2.5 Effect of Inertial Vibrations on Measurements

Vibrations of the measuring equipment has been known to effect the accuracy of friction measurements[30, 36]. Inertial effects of the friction tester may actually cause the transition from static to kinetic to occur at lower static coefficient values and suppress stick slip[36]. The inertial effects occur when a vibratory component is added to the constant load acting on a friction sliding part. To prevent inertial effects on friction measurements the measuring system must be dampened and stiffened[37].

Friction measurement inconsistencies were found to be associated with surface roughness effects, lubrication, and environmental factors, forced vibration of the apparatus, and self-induced frictional oscillations. These inconsistencies can be controlled by better surface preparation, control of lubrication conditions and chemistry of the surfaces, and using inert or vacuum environments[30].

Previous friction studies by McCann and Molique were conducted on a pin-on-disk machine which measured friction by the deflection of a elastic member. The elastic member of this machine is represented by the cantilever beam illustrated in figure 2.2. The problem with the pin-on-disk machine was that the beam usually vibrated once slip occurred due to the drop in friction force. This vibration occurs because of the cyclic interchange of potential energy stored in the beam during deflection by the friction force and the kinetic energy of the moving beam. The vibrations prevent accurate measurements of the friction force. In addition the beam vibrations cause the pin to move and the relative velocity is no longer equal to the disk velocity. Another source of vibration may be due to "running in" of the pin and the disk. The shearing and/or breaking of the asperities on either pin or disk surface may cause small deflections in the beam.

A test apparatus was developed for this study to overcome the limitations of the previous machines and is described in section 3.1. As mentioned before, many researchers believe that kinetic friction forces measured by displacement methods do not always give an accurate representation of the friction values especially during stick slip. The new test apparatus simultaneously and directly measures friction, velocity, and normal load. The

friction-velocity relationship can be directly plotted without averaging the kinetic friction or mathematical manipulation.

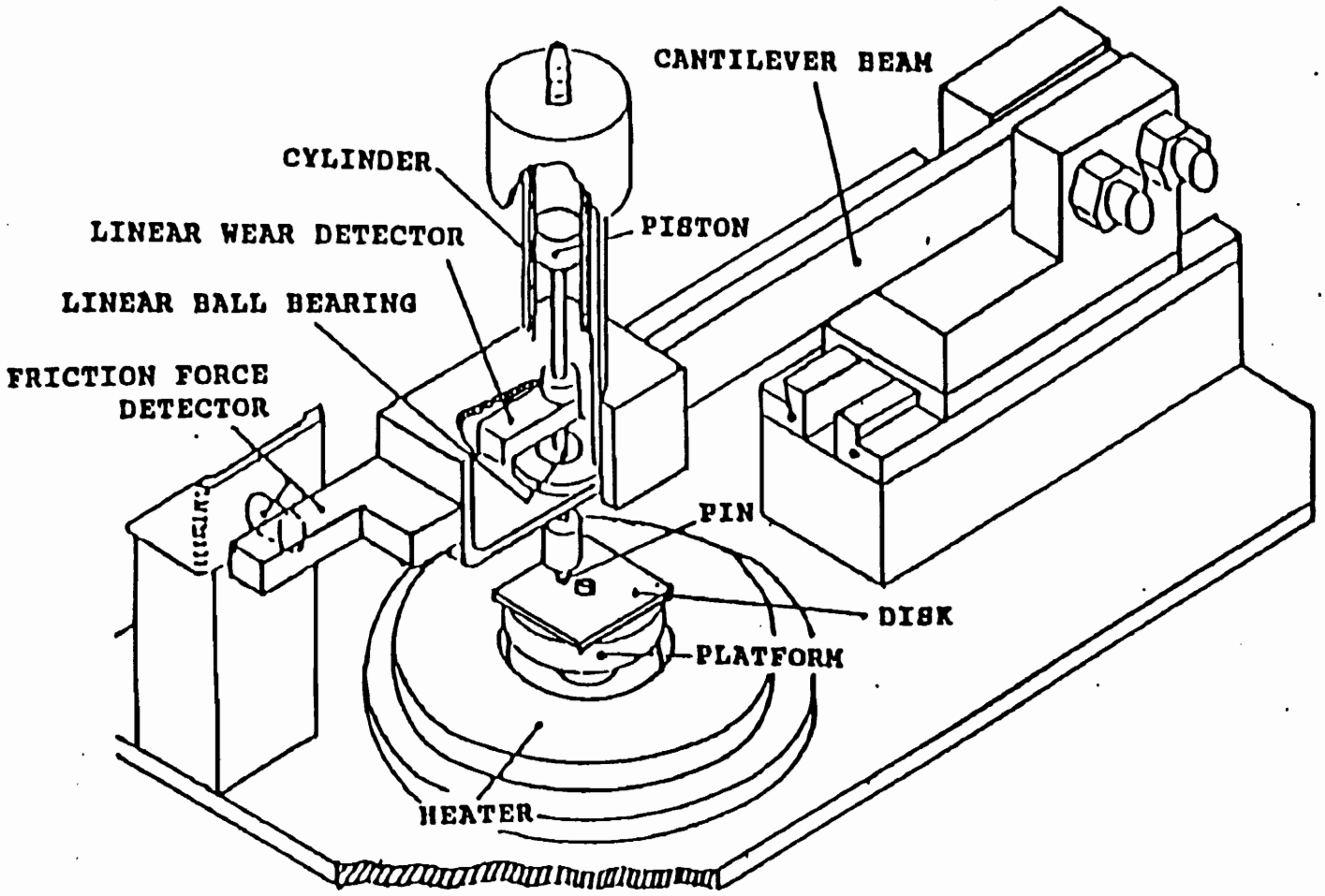

Figure 2.2 Illustration of pin-on-disk machine used by McCann and Molique.

3.0 Experimental Setup and Procedures

This chapter discusses the new test apparatus and procedures used in this study. The first section describes the new test apparatus used to collect friction data. Further details about the transducers and components utilized by the new test apparatus are included in the appendix. Section 3.2 describes the materials tested. Material preparation and surface analysis techniques are reported in section 3.3. The test conditions and procedures for this study are outlined in section 3.4. Measurement of creep and friction are discussed in section 3.5. Stress strain measurements are explained in section 3.5. Finally, section 3.7 outlines the tests to determine the effect of system stiffness on experimental results.

3.1 The Linear Friction Tester

The new test apparatus has been designed to reduce the vibration problems associated with the original pin-on-disk machine. Figure 3.1 illustrates the new test apparatus. The basic philosophy was to design a machine to accurately measure static to kinetic friction transitions by stiffening the force measuring element so that its inertial forces are small compared to the friction and its motion was small compared to the relative displacements between the contacting elements. The advantage of the new machine is that accurate and instantaneous friction and velocity data can be simultaneously obtained and plotted.

The simplest means of creating an accurately measurable relative velocity between two surfaces is to keep one surface stationary and measure the absolute velocity of the other. The friction is measured by a transducer attached to the stationary sample.

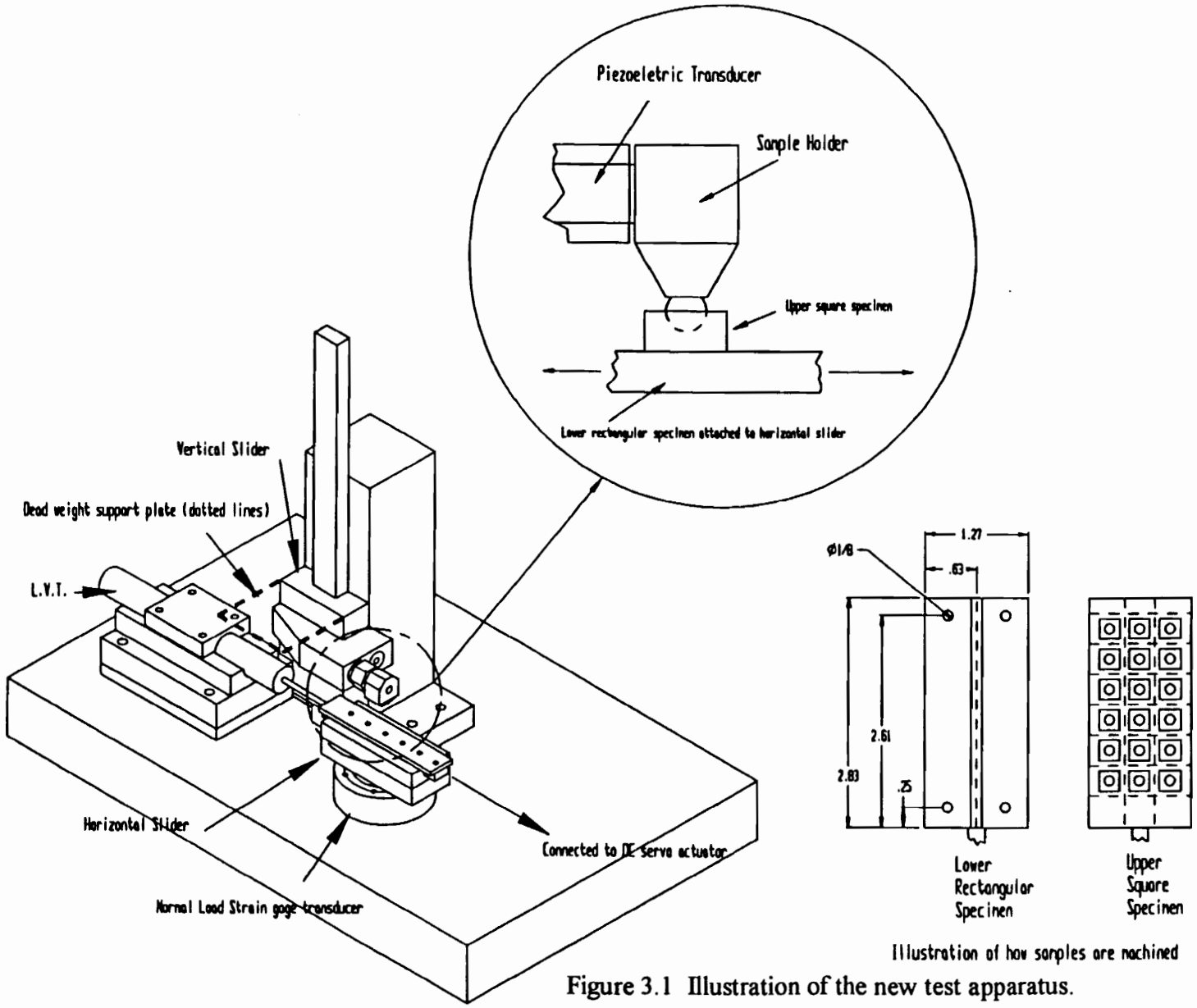

Figure 3.1 Illustration of the new test apparatus.

Attaching the force transducer to the moving sample would lessen the accuracy of its measurement due to the dynamic effects discussed in section 2.5. This attachment to the stationary member simplifies the transducer mounting and prevents disconnecting and reconnecting the transducer when specimens are changed.

The friction transducer is attached to a vertical linear slider with recirculating bearings which also supports the dead weights to keep them in alignment with the sample contact area. The dead weights provided the normal load. This slider can be lifted approximately 8 inches above the contact position to change samples. The lateral stiffness of the vertical slider is twice that of the friction transducer bracket. This is important because the sample attached to the force transducer must be held stationary when subjected to changing friction. A stiff mounting for the stationary sample reduces motion between the stationary sample and the moving sample during step changes in friction (which occur for some materials during the transition from static to kinetic friction.) This increases the accuracy of velocity measurements because the actual relative velocity (V_{moving}-$V_{stationary}$) is close to the measured absolute velocity of the moving sample.

The friction is measured by a PCB Piezotronics, 208AO2 series piezoelectric force transducer. This force transducer produces a proportional output within a load range of 0 to 100 pounds. When the transducer is DC coupled its time constant is greater than 1000 seconds. This was experimentally confirmed when a step force was applied to the transducer resulting in a 1% drop in the signal during a time span of 10 seconds.

Changes in normal load at the interface are measured by a Sensotec Model 41 strain gauge transducer. This is a full bridge strain gage load cell which measures loads up to 10 pounds. In this study the samples were subjected to loads for 5 minutes to reduce the effect of creep on friction measurements. Since the output of a strain gage type

transducer is constant for a constant applied load it is ideally suited for measuring changes in loads after a long static contact period.

Relative velocity is measured by a Lucas Schaevitz VT-Z Series linear velocity transducer. It produces a DC voltage output directly proportional to changes in velocity. This transducer is connected directly to the horizontal slider.

Sliding motion is provided by in-line direct current (DC) servo linear actuator. Velocity variations are minimized by the actuator's direct drive flexible coupling, acme screw drive, and feedback controller.

The actuator is connected to the machine through a series of elastomeric members which serve three purposes:

1. To store potential energy which allows stick slip behavior to occur.
2. To allow minor off-axis alignment between the actuator and friction tester.
3. To dampen vibrations from the actuator.

The stiffness of the sliding system is determined by the combination of these elastomeric members which connect the actuator to the slider.

Data is collected by the Global Lab data acquisition software and a personal computer based analog to digital A/D board. A sampling rate of 6000 Hz was used to ensure an acceptable number of points to capture the transition from static to kinetic friction. The choice of sampling rate was based on the computer simulation of the test apparatus presented in section 5.2.

3.2 Materials

The materials used in this project came from various vendors who supply resins to the Ford Motor Company. Appendix I contains a complete listing of different polymers available for future testing. In this study, four major classes of polymers were tested for

general relationships between creep effects, surface roughness, normal load, material composition and the transition from static and kinetic friction. These materials include: acrylonitrile-butadiene styrene (ABS), polypropylene(PP), polycarbonate(PC), and nylon. Five polymers were selected based on the least amount of additives, fillers, and/or reinforcements in their composition. Glass filled polypropylene and unfilled polypropylene were chosen to compare the effects of reinforcements and fillers on frictional properties. Table 3.1 lists the manufacturer, composition, and additives of each polymer.

Table 3.1 List of Materials and Composition

#	Manufacturer	Polymer	Composition	%
1	Allied Signal	CAPRON 8233GH3	Nylon 6/6 Glass fiber Reinforcement	 33
2	DOW Chemicals	Pulse 930 ABS Engr Resin FP770031*	ABS resin and bisphenol A/phosgen resin terminated with p-tertiary butyl phenol	100
3	Miles	APEC HT DP9-9351 1510 Black*	Modified Polycarbonate Bisphenol A Polycarbonate Methylene Chloride	min 70 max 30 <3 ppm
4	Ferro	Polypropylene NPP00GW01BK*	Unfilled	n/a
5	Ferro	Polypropylene HPP30GR05BK*	Fiberglass/mineral Filled	n/a

3.3 Sample Preparation

The polymers were injection molded in the Polymer Processing Lab at Virginia Tech with molds purchase with funds from the Ford Motor Company. All materials were vacuum dried for 3 - 6 hours prior to injection molding. The molds consisted of 2.83 by 1.26 inch plaques with six available surface roughnesses: Montana BG, Stipple #1, Naples FY, SPI-SPE #1, SPI-SPE #3, and SPI-SPE #5. Molding conditions for these particular

materials are described in appendix G. Surface profiles of the samples were taken with a Tencor Alpha-Step 500 surface profilometer. The ten point heights of the surfaces are shown in table 3.2 for comparison of the surface roughnesses. The ten point height is determined by the formula:

$$\text{Ten point Height} = \frac{\Sigma(\text{5 highest peaks}) - \Sigma(\text{5 Lowest Valleys})}{5}$$

All measurements were made parallel to mold flow direction except those marked with * which were measured perpendicular to the mold flow direction. Only one measurement was made for each surface roughness. Surface measurements for the nylon surface could not be obtained.

Table 3.2 Surface Roughnesses of ABS, Filled and unfilled PP, and PC

	10 Point Height, μm			
	ABS	**PC**	**Filled PP**	**Unfilled PP**
Montana BG	53.6	18.7	71.5 70.4*	78.6 63.7*
Naples FY	36.4	53.5	77.3 81.0*	80.8 93.4*
SPI-SPE #1	1.2	0.98	11.5 10.9*	2.318 N/A
Stipple #1	37.3	25.9	44 45.6*	39.2 43.4*

The test apparatus requires two different sized polymer samples to test the polymer-on-polymer surface interaction(see figure 3.1). These samples were milled from the molded plaques. The lower sample is a 2.83 by 0.63 inch rectangle with holes on each

end where screws secure the specimen to the horizontal slider. The upper 1/4 inch square sample has a 1/32 inch deep hemispherical cavity on top to provide for the self-alignment of the flat-on-flat contact. The former is the moving sample and the latter is the stationary sample. Prior to testing all samples were deburred, washed in mild detergent to remove surface debris, and allowed to air dry.

3.4 Test Conditions and Procedures

The following test conditions were observed unless stated otherwise. All friction data in this study were obtained with the same surface roughness and material rubbing against each other. All tests were conducted by pushing the sample in the direction away from the actuator. The leading edge of the upper square sample was kept perpendicular to the direction of sliding to maintain consistency between tests. Surface velocity of the moving sample was 0.0005 meters per second. For most conditions, four replicate tests were conducted.

3.5 Measurement of Creep and Friction

The first series of experiments involved tests to measure how creep during time of loading affects static and kinetic friction. These static contact time tests were conducted with fiberglass reinforced nylon. The second series of tests were conducted to determine how material composition, normal load, and surface roughness affect the static coefficient of friction and the transition from static to kinetic friction. Also investigated were how these parameters affect stable or unstable friction conditions in terms of steady sliding, stick slip, or single stick behavior, and the friction-velocity relationship. The materials used in the second set of tests were polycarbonate, glass filled and unfilled polypropylene, and ABS.

3.5.1 Static Contact Time Tests

Static contact time tests were conducted with fiberglass filled nylon because it had been previously injection molded and machined while the other samples were still being injection molded. The filled nylon samples were tested in timed intervals of 0.5, 1, 2, 3, and 5 minutes under two loads, 10.7 and 20.7 Newtons, and the four surface roughnesses. Each condition was replicated four times with virgin surfaces used in each replicated.

Another round of tests covered the contact time from 0 to 0.5 minutes reusing the specimens from the first test which appeared to be undamaged. These tests involved one replicate for each tests of the 30, 15, 10, and 0 second duration under the two loads for the Montana surface.

3.5.2 Friction Tests

The second session of tests involved the four remaining materials, four surface roughnesses, a high load of 20.7 Newtons, and a low load of 10.7 Newtons. Four replicate tests were conducted for each condition to obtain statistically significant data. A flow chart of the test program is shown below in figure 3.2.

Tests were run at 70-78°F room temperature and 20 - 40% relative humidity. The samples were also statically loaded for 5 minutes before starting the actuator to reduce the effect of creep on friction measurements.

3.6 Stress Strain Tests

Stress strain testing was the only technique performed to characterize the material to explain possible relationships between mechanical and frictional behavior. The four materials denoted with an asterisk in table 3.1 were tested on a Instron stress strain apparatus to measure mechanical behavior. SPI-SPE #1 was the surface roughness of the

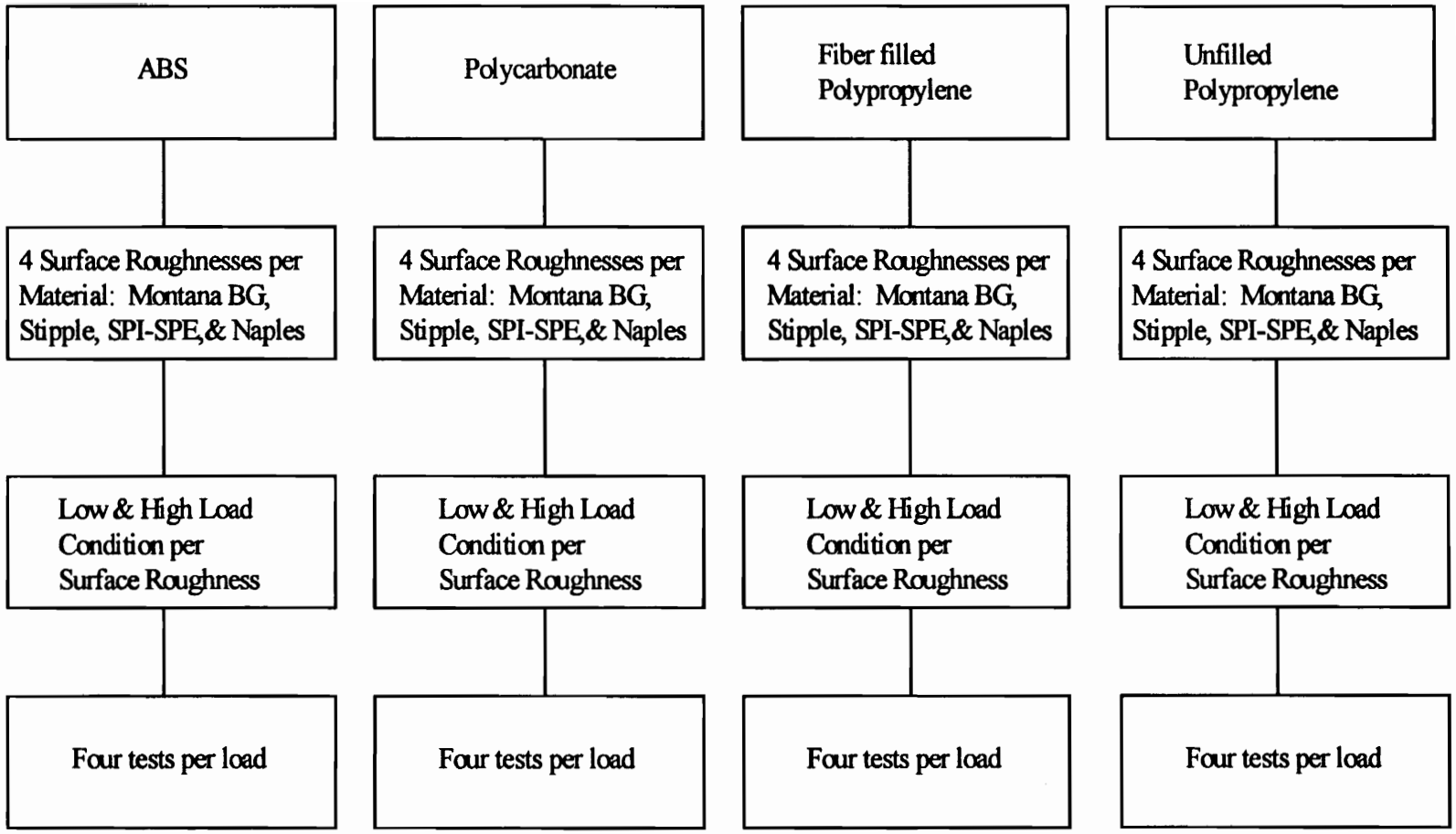

Total number of tests per polymer: 32

Total number of tests: 128

Figure 3.2 Flow Chart of Test Program

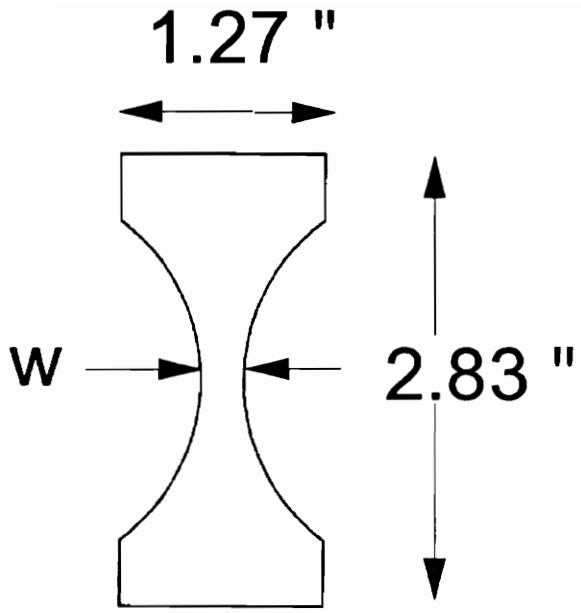

Figure 3.3 Illustration of "dog bone" shape used in stress strain testing.

samples tested. The plaques were machined to a "dog bone" shape and loaded in tension until failure occurred(see figure 3.3).

3.7 Tests to Determine Effect of Elastomeric Combinations on Friction Measurements

Different combinations of elastomeric members were tested to determine their effect on friction measurements. Pulse 930 ABS samples and four different stiffness combinations were utilized in these tests. The natural frequencies of the lower slider and elastic members was measured with the upper square specimen removed. The natural frequencies of the four combinations of elastomeric members tested were: 100, 67, 58, 54 Hz.

Table 3.3 List of different Elastomeric Combinations

Elastomeric Combination	Natural Frequency, Hz
4 VBM 1028 in series	58
3 VBM 1020 in series	54
1 VBM 1028	100
1 VBM 1020 and 1 VBM 1028 in series	67

VBM 1020 and VBM 1028 are the manufacturers designation for the elastomeric members. The VBM 1020 elastic member has a #4-40 threads and the VBM 1028 elastic member has #6-32 threads.

Chapter 4 Results

4.1 Time Dependent Static Contact Tests

Figures 4.1 to 4.8 show the static and kinetic coefficients of friction of filled nylon for each surface roughness, at different time intervals under the two loads tested. The confidence limits indicate that surface roughness and normal load have no significant effect on creep. However, the magnitude of the static friction coefficient is strongly correlated with static contact time. This shows evidence of creep behavior. These tests also show that the static coefficient of friction stabilizes after a static contact time of 5 minutes. Consequently, all friction tests were preceded by a 5 minute static loading time to minimize creep effects on the static friction value.

In the second round of tests as the contact time approaches zero, the static and kinetic coefficient of friction are statistically similar (see figure 4.9-4.10). The statistically similar values of static and kinetic coefficients of friction for the same contact time with different surfaces and loads show that surface roughness and normal load have a minimal affect on the static and kinetic friction as a function of contact times.

Figure 4.11-4.12 show the results of static contact time tests of 2 and 5 minutes conducted for polycarbonate and unfilled polypropylene. Figure 4.11 shows the magnitude of the static and kinetic coefficient of friction to be independent of static contact time for the Montana surface for unfilled polypropylene. In figure 4.12 the SPI-SPE #1 surface for polycarbonate reveals a kinetic friction greater in magnitude than the static friction. Molique reported several cases of this phenomenon in his thesis.[28] Also note that the static coefficient of friction for polycarbonate is increasing with time of contact.

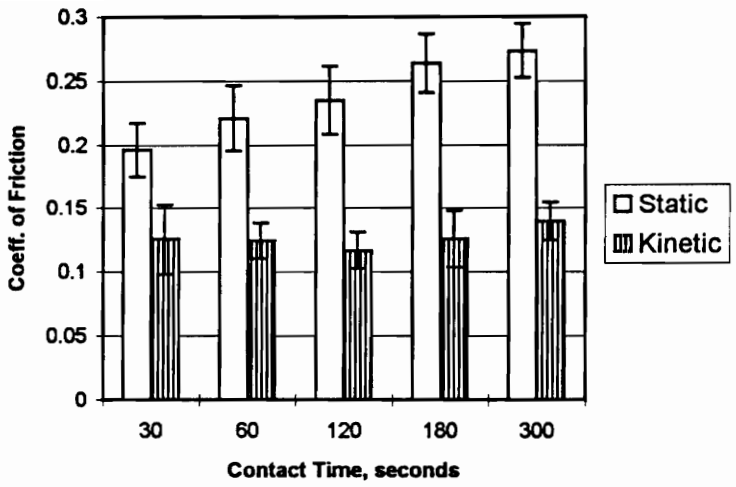

Figure 4.1 Static and kinetic coefficient of friction vs. contact time for filled nylon, Montana surface, under a 10.7 Newton load. I equals 95% confidence limits.

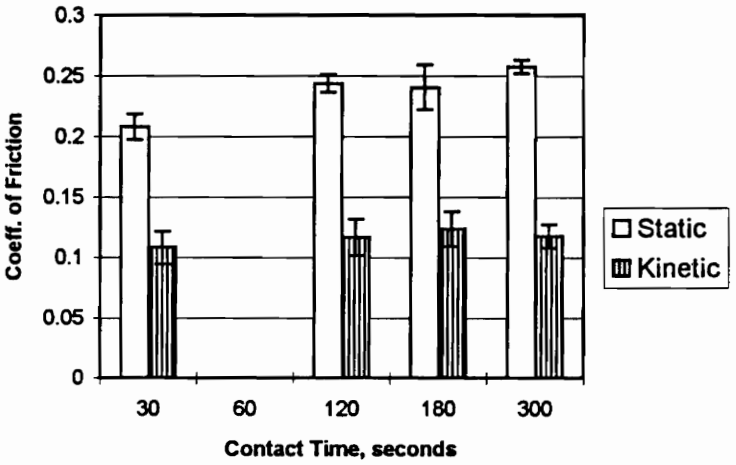

Figure 4.2 Static and kinetic coefficient of friction vs. contact time for filled nylon, Montana surface, under a 20.7 Newton load. I equals 95% confidence limits.

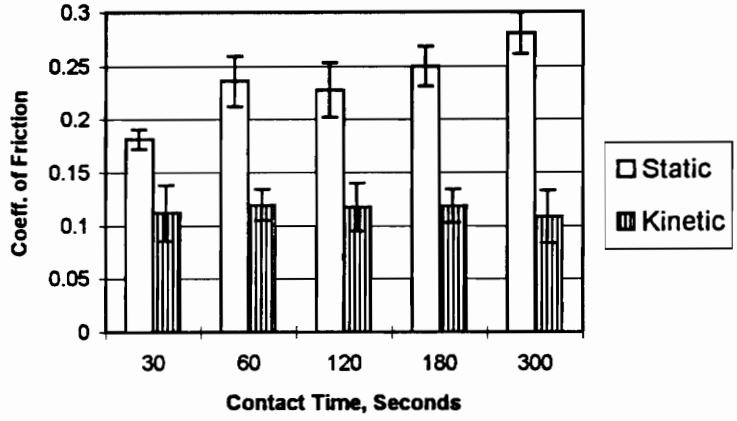

Figure 4.3 Static and kinetic coefficient of friction vs. contact time for filled nylon, Naples surface, under a 10.7 Newton load. I equals 95% confidence limits.

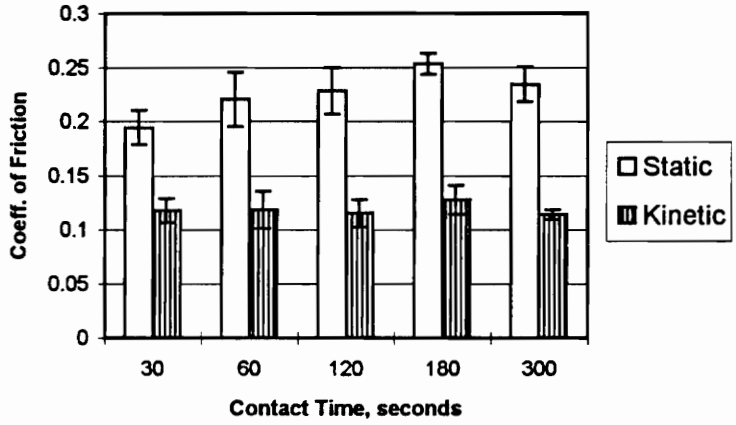

Figure 4.4 Static and kinetic coefficient of friction vs. contact time for filled nylon, Naples surface, under a 20.7 Newton load. I equals 95% confidence limits.

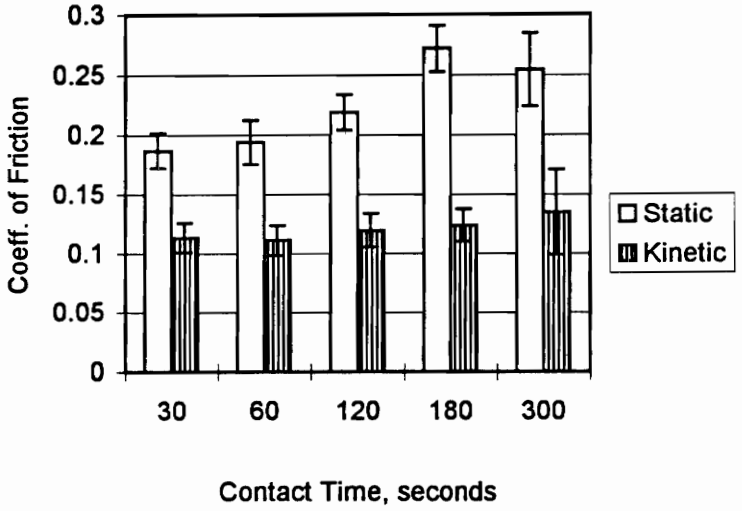

Figure 4.5 Static and kinetic coefficient of friction vs. contact time for filled nylon, SPI-SPE #1 surface, under a 10.7 Newton load. I equals 95% confidence limits.

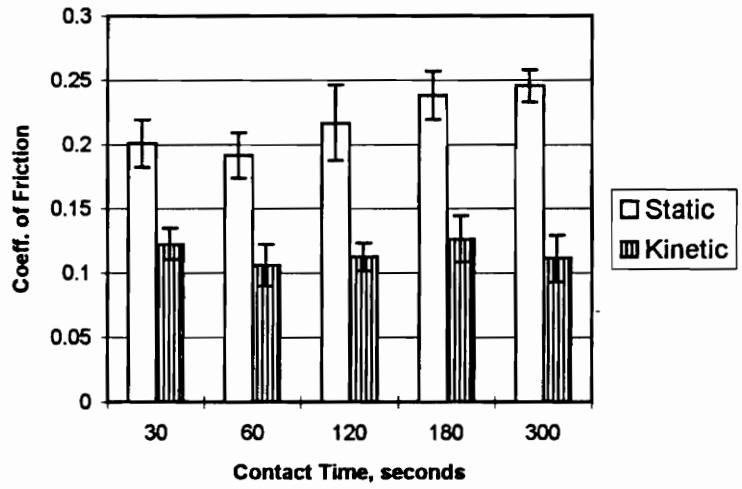

Figure 4.6 Static and kinetic coefficient of friction vs. contact time for filled nylon, SPI-SPE #1 surface, under a 20.7 Newton load. I equals 95% confidence limits.

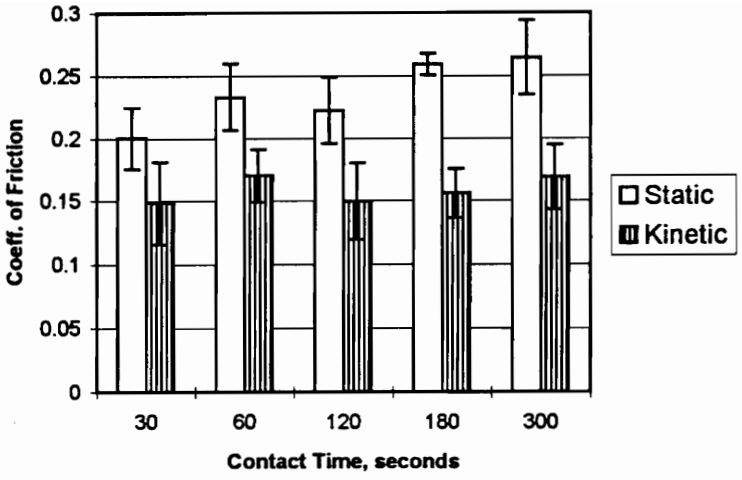

Figure 4.7 Static and kinetic coefficient of friction vs. contact time for filled nylon, Stipple surface, under a 10.7 Newton load. I equals 95% confidence limits.

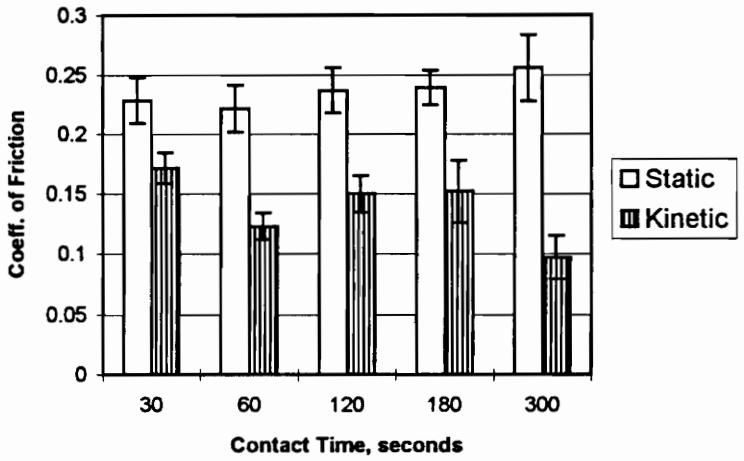

Figure 4.8 Static and kinetic coefficient of friction vs. contact time for filled nylon, Stipple surface, under a 20.7 Newton load. I equals 95% confidence limits.

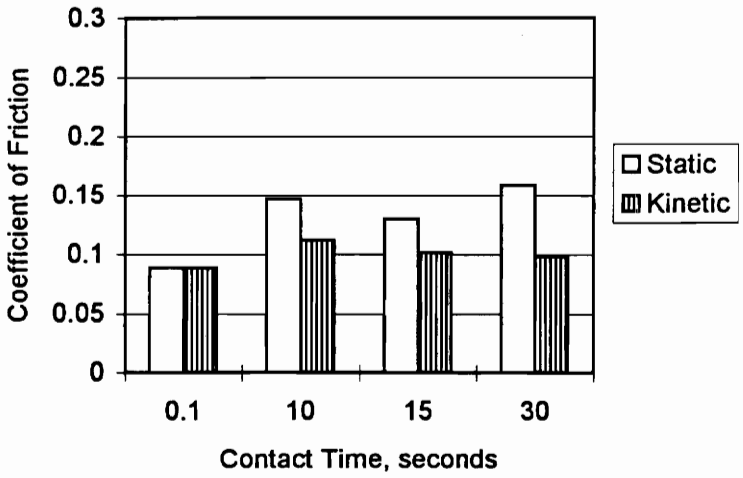

Figure 4.9 Static and kinetic coefficient of friction vs. contact time for filled nylon, Montana surface, under a 10.7 Newton load.

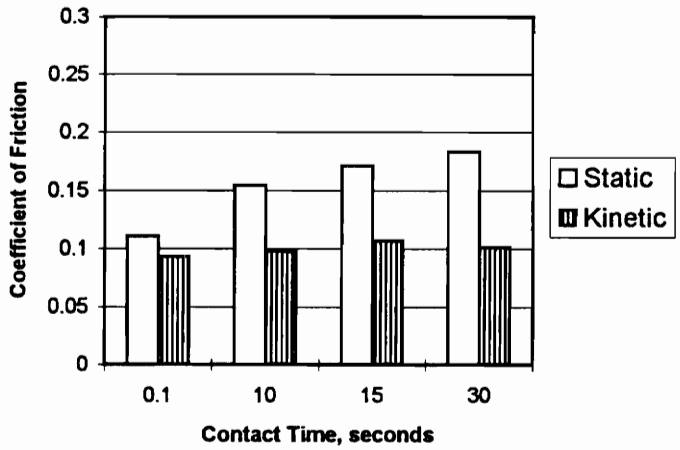

Figure 4.10 Static and kinetic coefficient of friction vs. contact time for filled nylon, Montana surface, under a 20.7 Newton load.

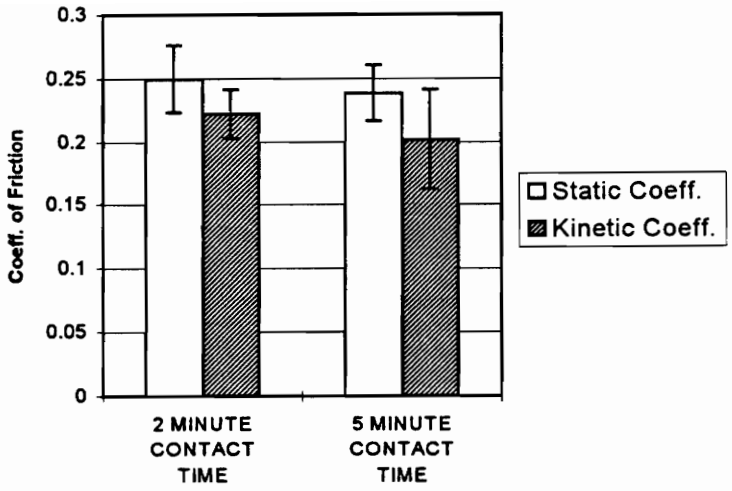

Figure 4.11 Static and kinetic coefficient of friction vs. contact time for unfilled polypropylene, Montana surface, under a 20.7 Newton load. I equals 95% confidence limits.

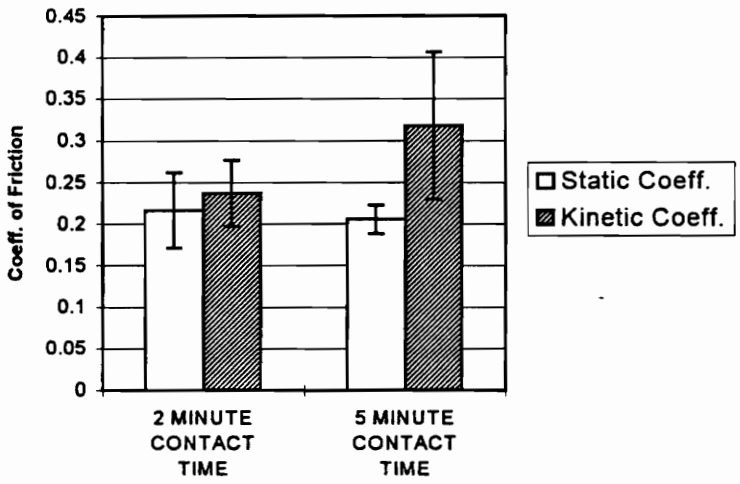

Figure 4.12 Static and kinetic coefficient of friction vs. contact time for polycarbonate, SPI-SPE #1 surface, under a 20.7 Newton load. I equals 95% confidence limits.

4.2 A Catalogue of Friction Transition Tests

A category of frictional behaviors has been tabulated in table 4.1 for friction measurements with a static contact time of 5 minutes. The materials listed include ABS, fiberglass filled and unfilled polypropylene, and polycarbonate. All four surfaces and both loading conditions are included.

Each column in the table classifies kinetic friction into multiple stick-slip, single stick-slip, steady sliding, and single stick. Multiple stick-slip has a saw tooth form after the first slip, single stick-slip has one stick cycle after the initial slip, steady sliding occurs when the static and kinetic coefficients are equal, and single stick occurs in cases where sliding occurs after the initial drop in static friction(see figure 4.13-4.16).

Each row separates kinetic friction into: increasing, constant, and fluctuating kinetic friction. The increasing kinetic friction category simply means the friction time trace curves show that the kinetic friction increased to a mean value over a period of time after the initial slip. Constant kinetic friction means that the kinetic friction varied less than 10 percent from the mean. Lastly, fluctuating kinetic friction means that variations were greater than 10 percent and appear to be harmonic oscillations.

Four distinct static-to-kinetic friction transitions have also been observed and tabulated in table 4.2:

1. A gradual drop in friction where energy is gradually released into the system. See figure 4.16.
2. A sudden step like drop in friction which quickly releases energy into the system, in which cases stick-slip only occur. See figure 4.13-4.14.
3. A smooth transition where the static and kinetic friction coefficients are the same. See figure 4.15.
4. A kinetic friction greater than the static friction. See figure 4.17.

Table 4.1 A Catalogue of Frictional Behaviors

	Multiple Stick-slip	Single Stick-slip	Single Stick	Steady Sliding
μ_k Increases $\mu_k < \mu_s$	ABLS-1 ABHS-1 PCHN-4 ABLS-C,D ABHS-C,D	ABHS-3	FPLS-1 PCHN-1,2,3 ABLS-A,B ABHS-A,B PCLM-A,B,C,D	
$\mu_k > \mu_s$			PCLS-1,2,3,4 PCHS-1,2,3,4,5,6 UPLS-1,2,4,3 UPHS-1,2,3,4	
μ_k is Constant $\mu_k < \mu_s$	ABLS-2 ABHS-2	ABLS-3,4 ABHS-4 FPHS-1,2,3	FPLS-2,3,4 FPHS-4 UPLM-1,2,3,4	UPLI-1,2,3,4 UPHI-1,2,3,4 UPLN-1,2,3,4 UPHN-1,2,3,4
μ_k Fluctuates	ABLM-1,3 ABHM-1,3,4 ABLN-1,2,3 ABHN-1 PCLM-1,4 PCHM-1 ABHM-C ABLN-A ABHN-B PCHM-A,C,D ABHM-X	ABLM-2,4 ABHM-2 ABLN-4 ABHN-2,3,4 FPLM-1,2,3,4 FPHM-1,2,3,4 FPLN-1,2,4,3 FPHN-1,2,3,4 PCHI-1,2,3,4 PCLM-2,.3 PCLN-1,2,3,4 ABHM-A,B ABLN-B,C,D ABHN-A,C,D ABLM-A,B,C,D PCHM-B	ABLI-1,2,3,4 ABHI-1,2,3,4 FPLI-1,2,3,4 FPHI-1,2,3,4 PCHM-2,3,4 PCLI-1,2,3*,4 UPHM-3,4 ABLI-A,B,C,D ABHI-A,B,C,D ABHS-W,V,Y,X, Z ABHM-U, Y	UPHM-1,2

Denotation:

The first two letters denote material composition	The third letter denotes normal load	The fourth letter denotes surface roughness
AB-ABS	L- Low load, 10.7 Newtons	I-Stipple #1
PC-polycarbonate	H-High Load, 20.7 Newtons	M-Montana BG
FP-Fiberglass filled polypropylene		N-Naples FY
UP-Unfilled Polypropylene		S-SPI-SPE #1

The numbers or letters following the dash indicate the replicate number and experimental setup

1,2,3,4	4 VBM1028s in series	X,Y,W,Z	1 VBM1028
A,B,C,D -	3 VBM 1020s in series	U,V	1 VBM1020 & 1 VBM1028 in series

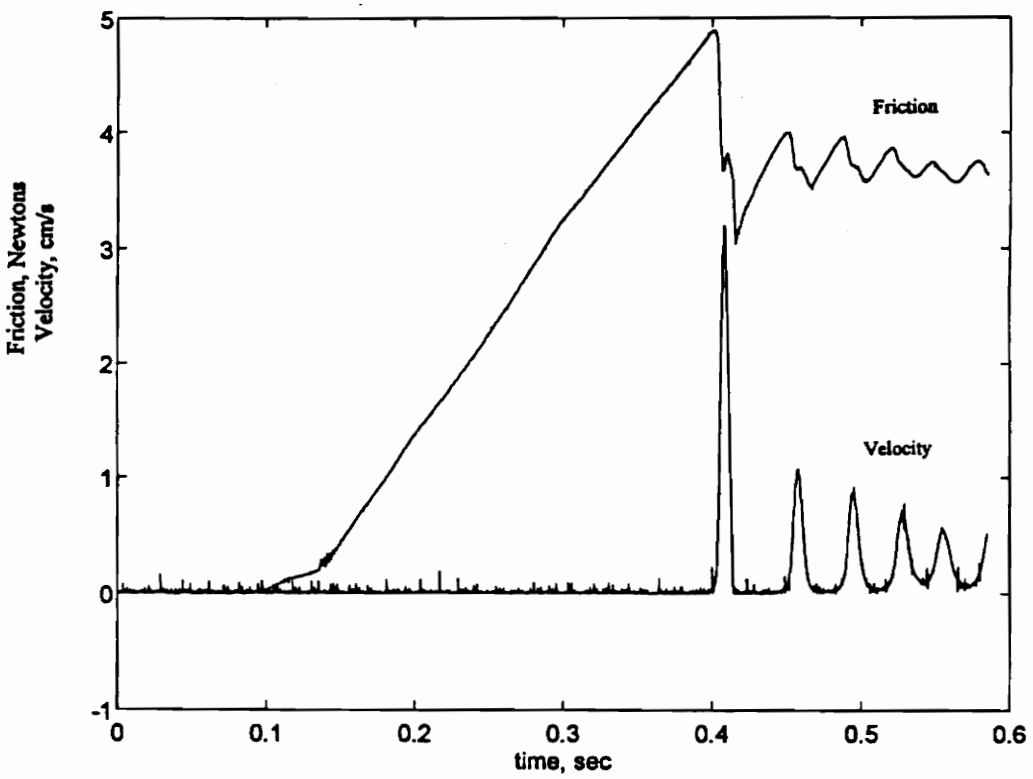

Figure 4.13 Friction-time plot of multiple stick slip for ABS SPI-SPE #1 surface under a 20.7 Newton load.

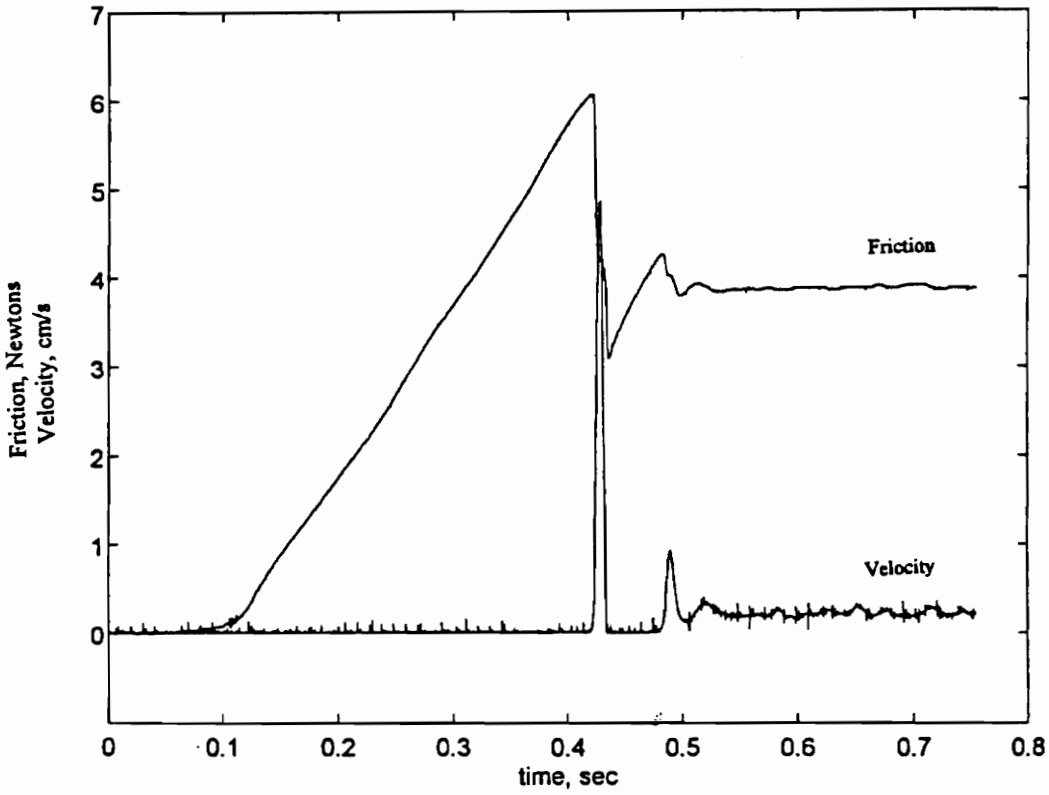

Figure 4.14 Friction-time plot of single stick slip for ABS SPI-SPE #1 surface under a 20.7 Newton load.

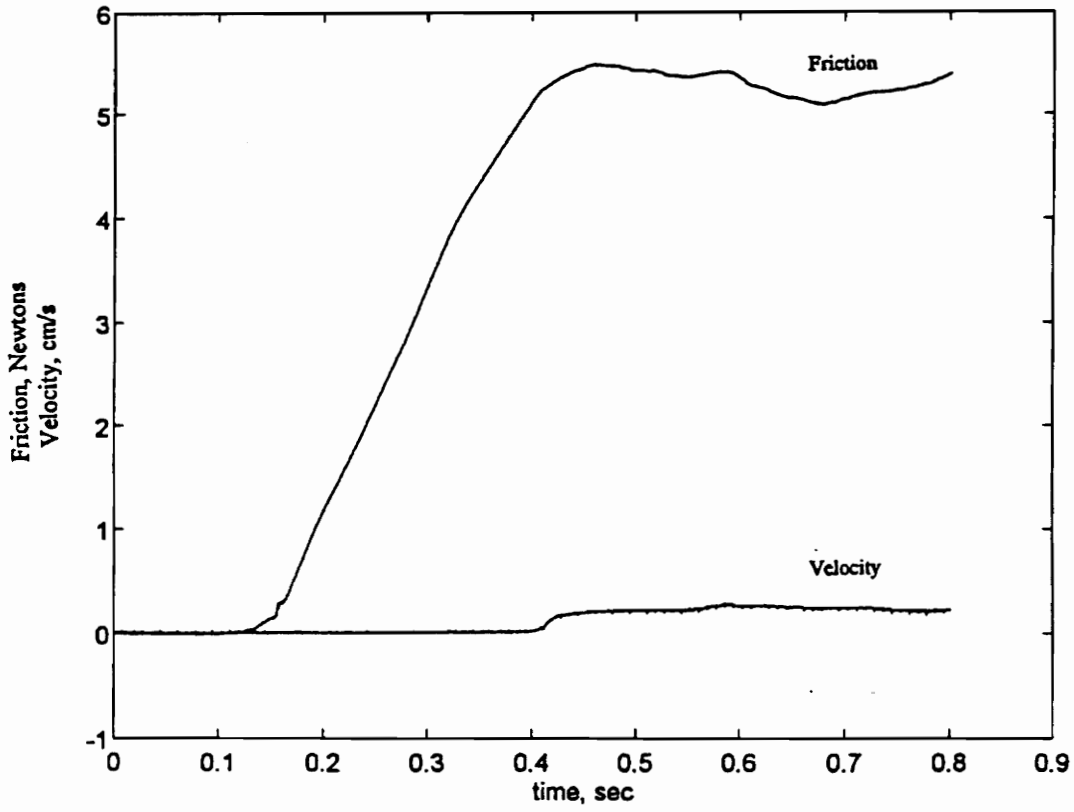

Figure 4.15 Friction-time plot of smooth transition from static to kinetic friction for unfilled polypropylene Naples surface under a 20.7 Newton load.

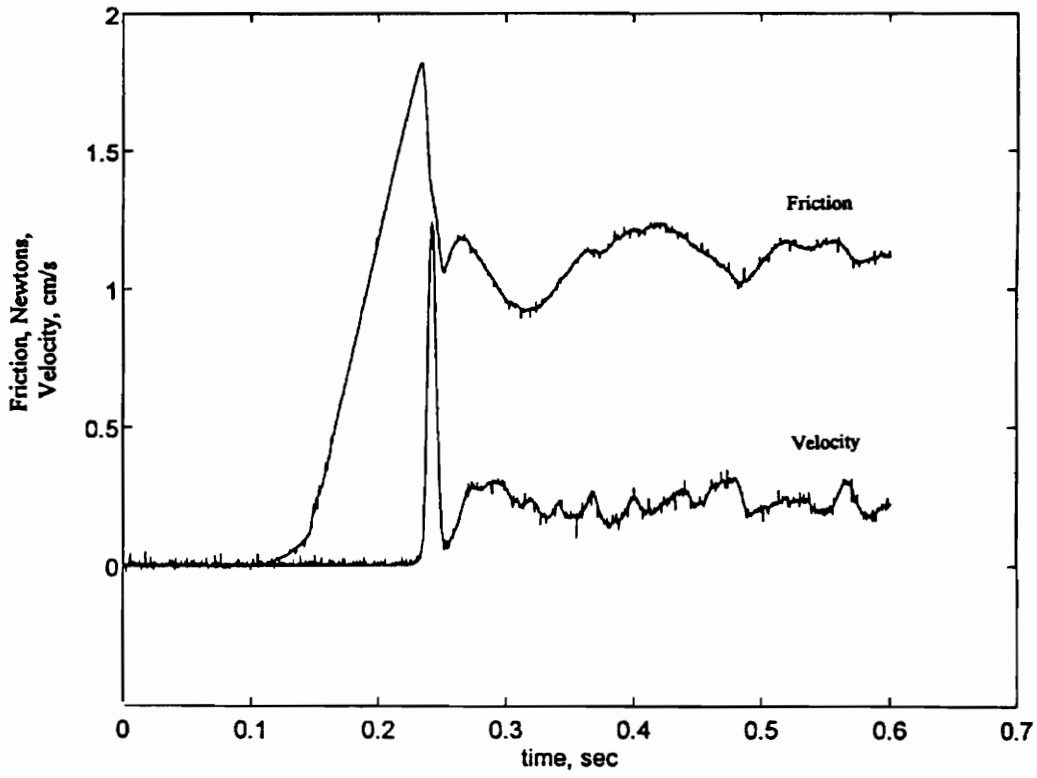

Figure 4.16 Friction-time plot of single stick for ABS Stipple surface under a 10.7 Newton load.

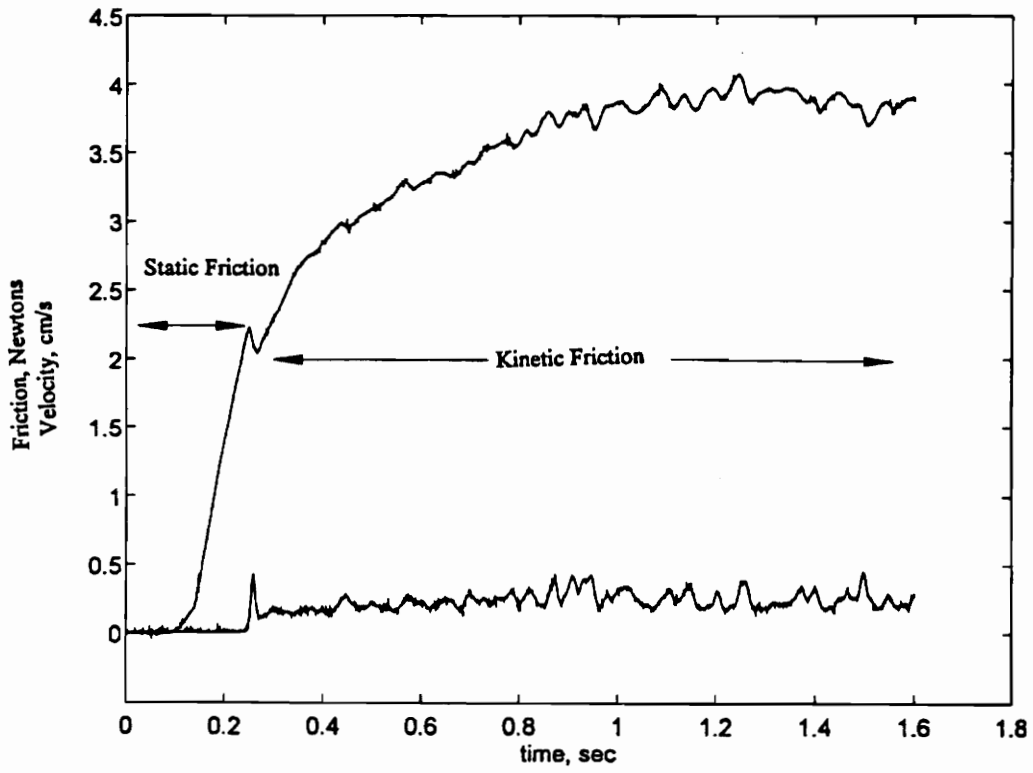

Figure 4.17 Friction-time plot of polycarbonate SPI-SPE #1 surface under a 20.7 Newton load showing kinetic friction higher than static friction..

Table 4.2 A Catalogue of Friction Transitions

CASE 1 Gradual drop from static-to-kinetic	CASE 2 Sharp drop from static-to-kinetic		CASE 3 Smooth transition from static-to-kinetic	CASE 4 Kinetic friction is greater than static friction
ABLI-2,3,4 ABHI-1,2,3 FPLI-1,2,3,4 FPHI-1,2,3,4 FPLN-1,2,3,4 PCLI-1,2,3,4 PCLN-4 PCHN-1 UPLM-1,2,3,4 UPHM-3,4	ABLI-1 ABHI-4 ABLM1,2,3,4 ABHM-12,3,4 ABLN-1,2,3,4 ABHN-1,2,3,4 ABLS-1,2,3,4, ABHS-1,2,3,4 FPLM-1,2,3,4 FPHM-1,2,3,4 FPHN-1,2,3,4 FPLS-1,2,3,4 FPHS-1,2,3,4	PCHI-1,2,3,4 PCLM1,2,3,4 PCHM-1,2,3,4 PCHM-1,2,3,4 PCLN-1,2,3 PCHN-2,3,4	UPLI-1,2,3,4 UPHI-1,2,3,4 UPHM-1,2 UPLN-1,2,3,4 UPHN-1,2,3,4	PCLS-1,2,3,4,5,6 PCHS-1,2,3,4 UPLS-1,2,3,4 UPHS-12,3,4

Figure 4.18-4.21 show the average static and kinetic friction coefficients of four replicate tests as a function of surface roughness and normal load. These plots are useful in determining how the coefficients of friction are affected by different surface roughnesses. Note that the static and kinetic friction coefficients for unfilled PP are much higher than the other materials for surfaces, especially for the SPI-SPE surface. The smooth SPI-SPE surface for PC, unfilled PP, and ABS show higher friction coefficients when compare to other surface roughnesses. The higher friction coefficients are most likely due to the greater real area of contact provided by the smooth surface. The Montana and Naples surfaces tend to have similar friction coefficients as well as roughnesses.

4.3 The Friction-Velocity Relationship

A typical stick-slip friction-time plot measured by the new test apparatus is shown in figure 4.22. Figure 4.23 shows the coefficient of friction versus velocity. The letters on both figure 4.22 and figure 4.23 identify the same phases of motion. The rise in friction at

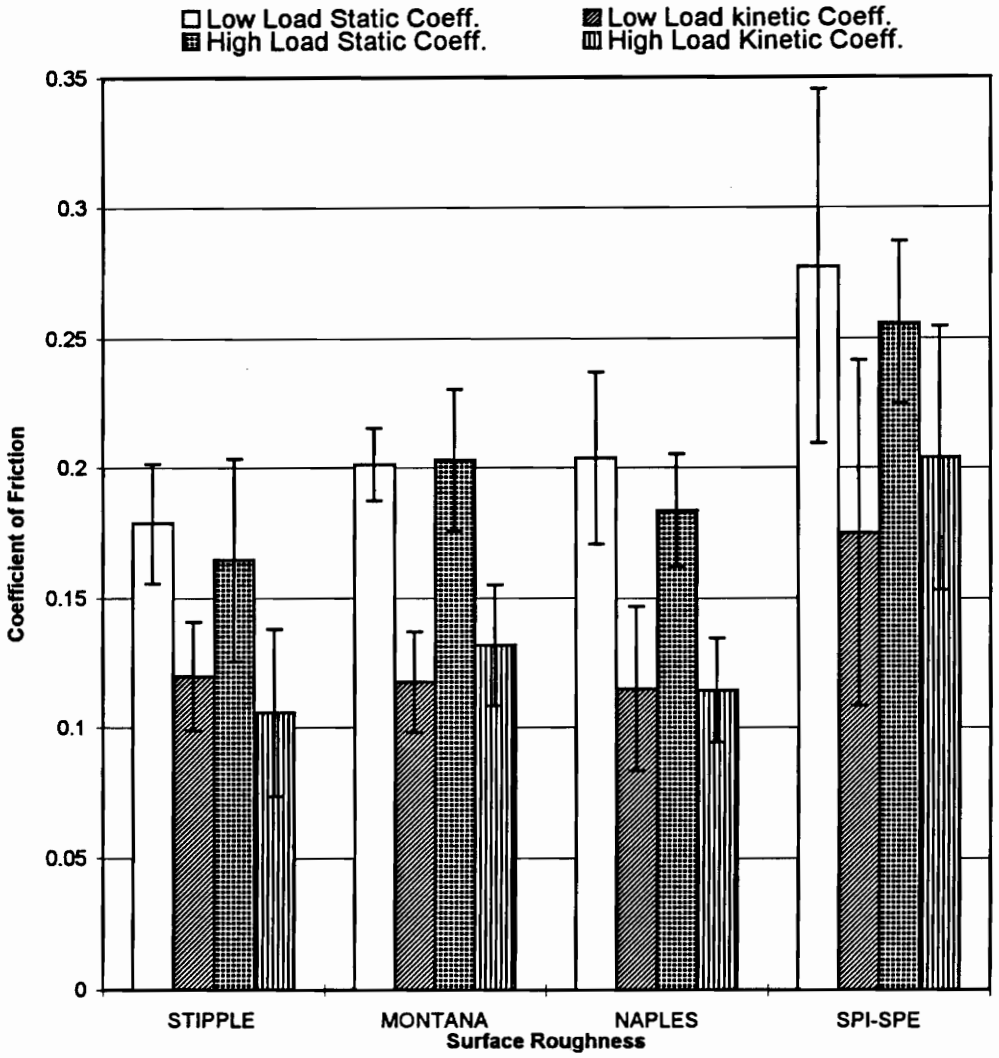

Figure 4.18 Static and kinetic coefficient of friction for ABS vs. surface roughness under 10.7 and 20.7 Newton loads.

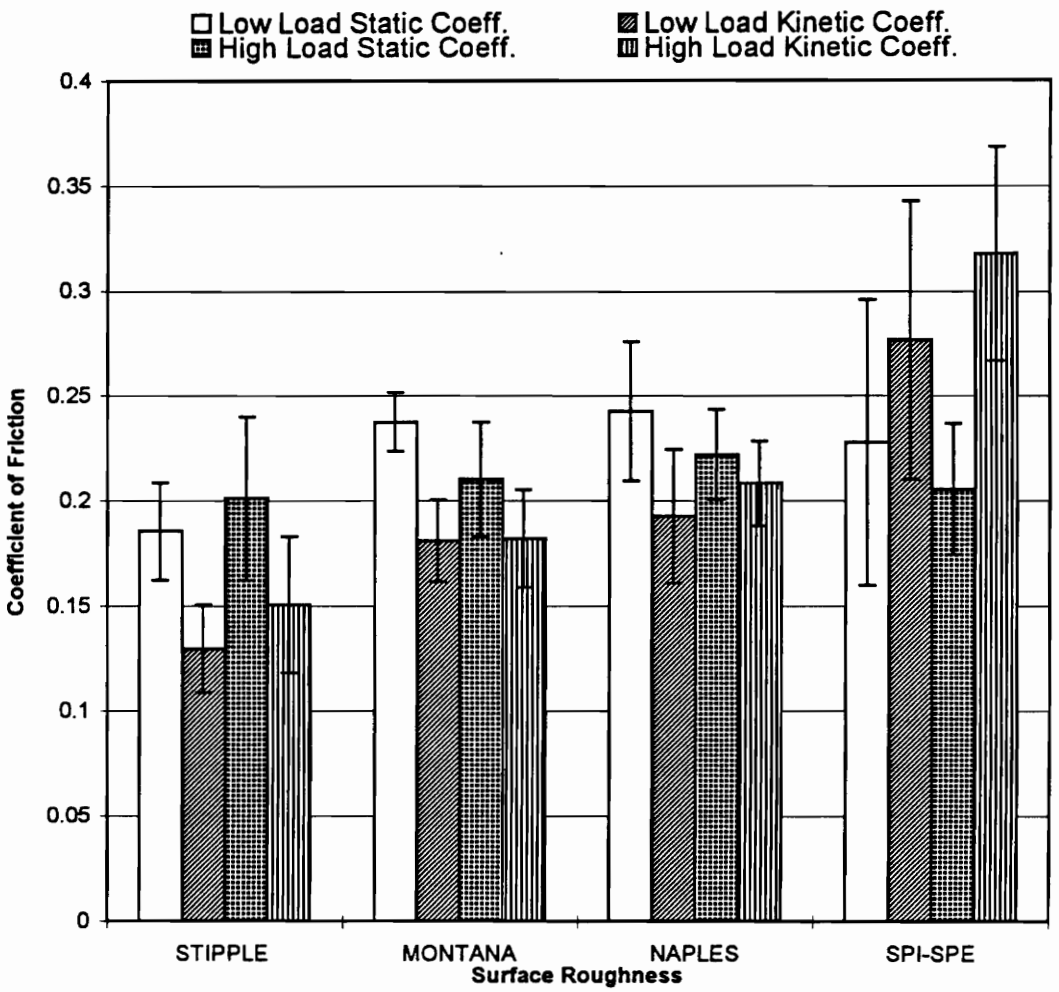

Figure 4.19 Static and kinetic coefficient of friction for polycarbonate vs. surface roughness under 10.7 and 20.7 Newton loads.

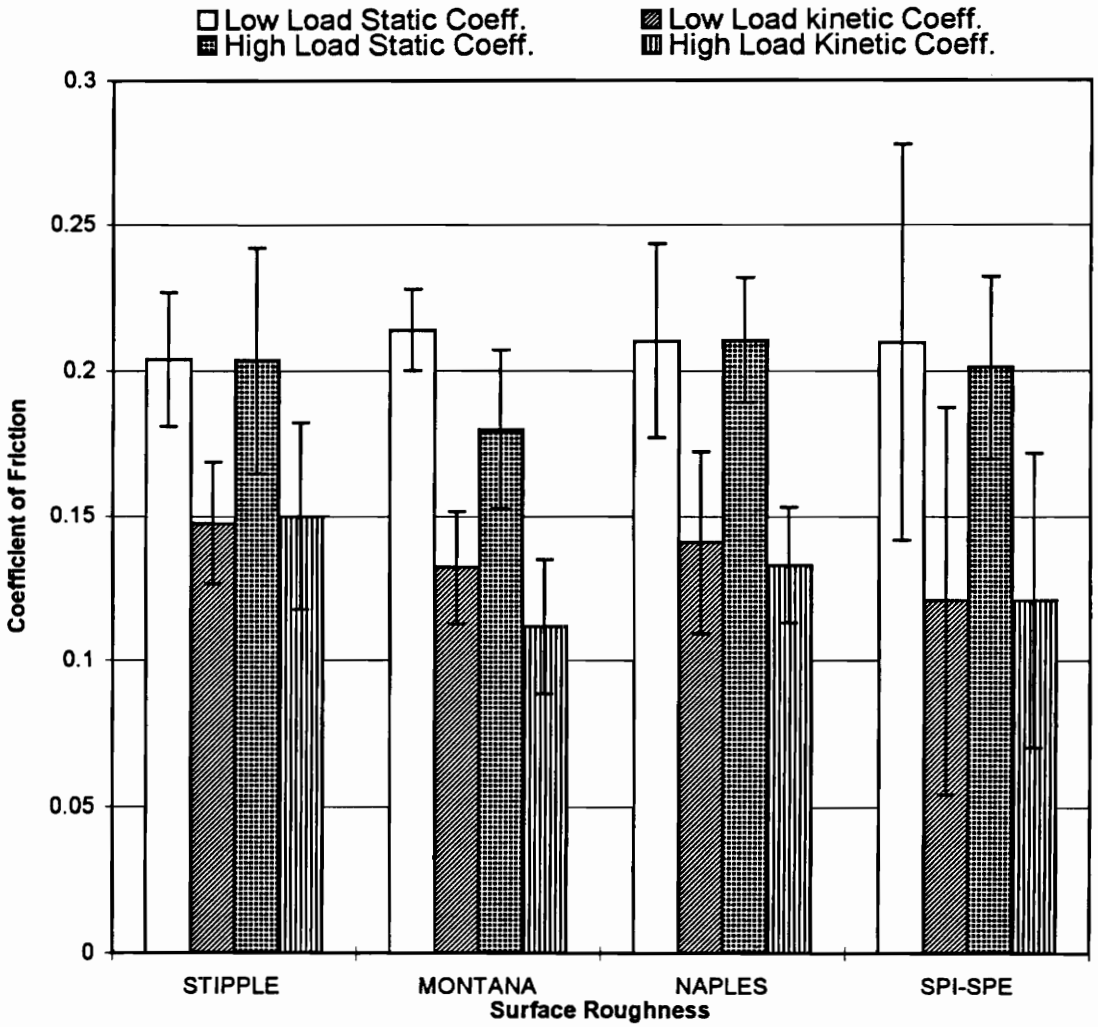

Figure 4.20 Static and kinetic coefficient of friction for fiberglass filled polypropylene vs. surface roughness under 10.7 and 20.7 Newton loads.

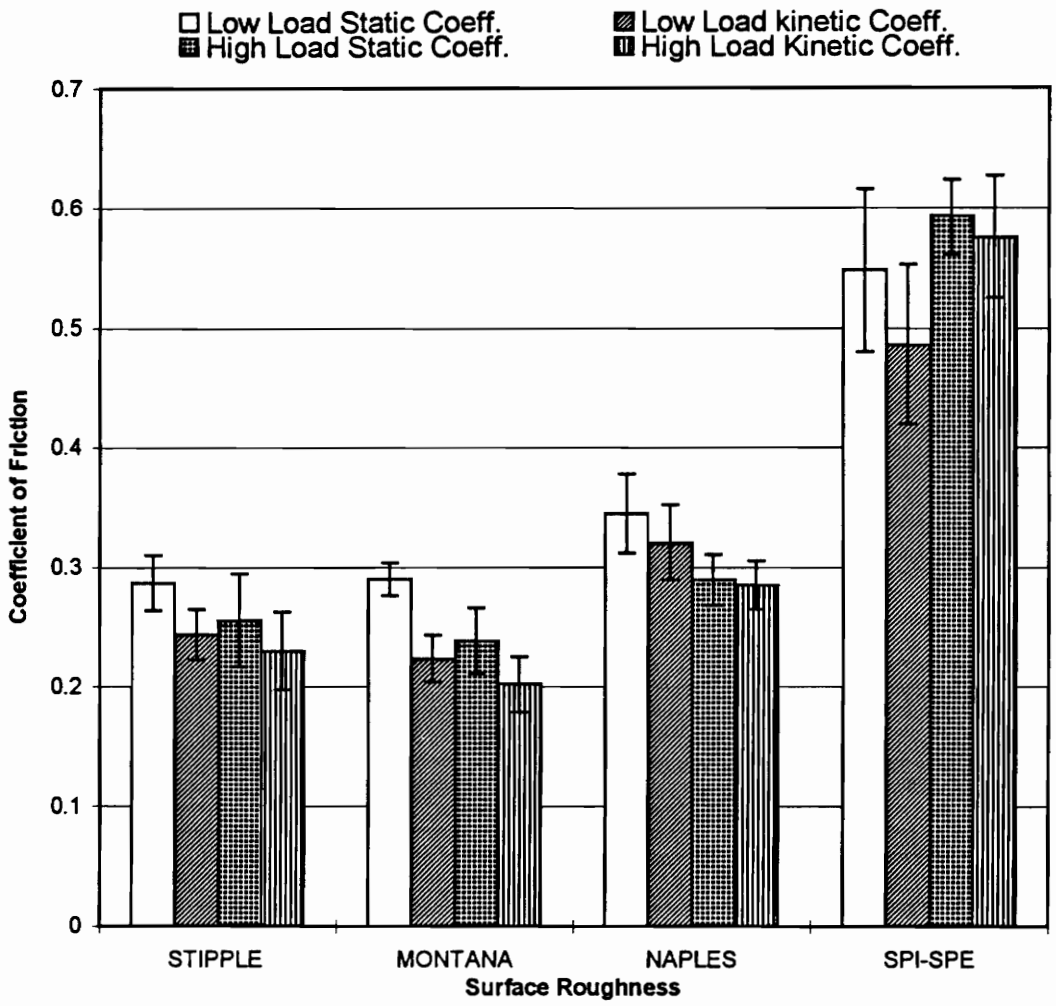

Figure 4.21 Static and kinetic coefficient of friction for unfilled polypropylene vs. surface roughness under 10.7 and 20.7 Newton loads.

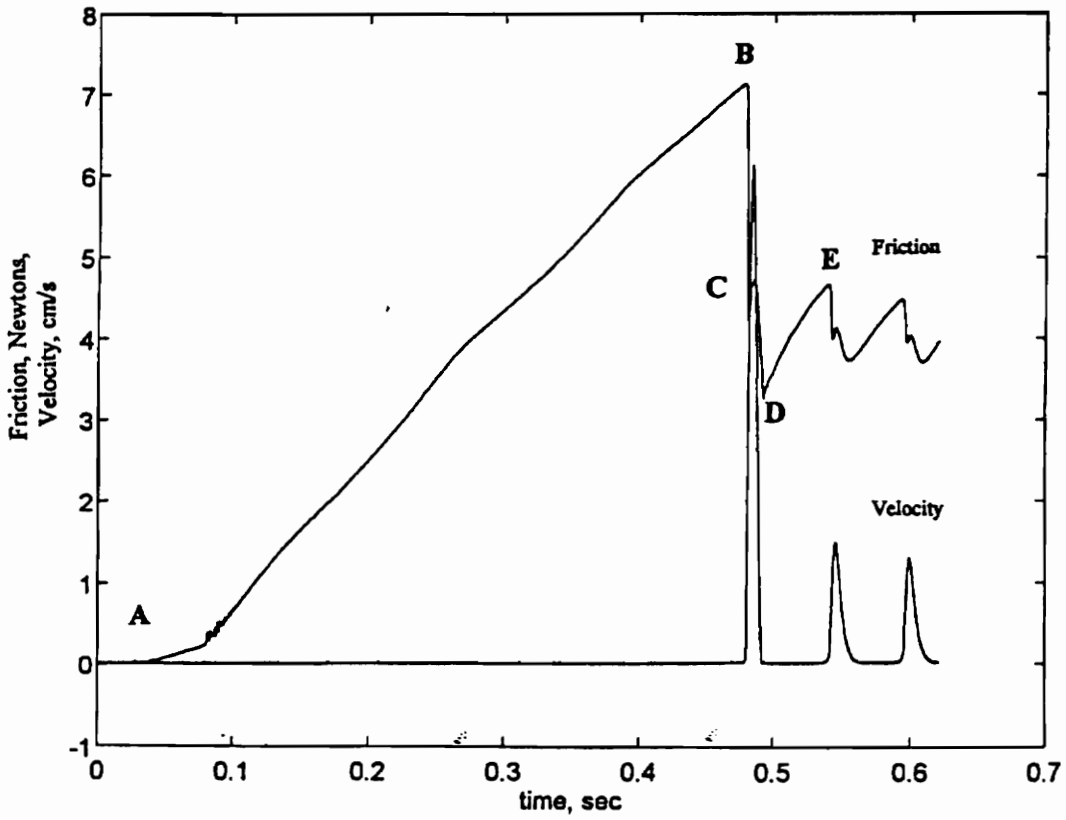

Figure 4.22 Friction-time trace of multiple stick slip for ABS SPI-SPE #1 surface under a 20.7 Newton load.

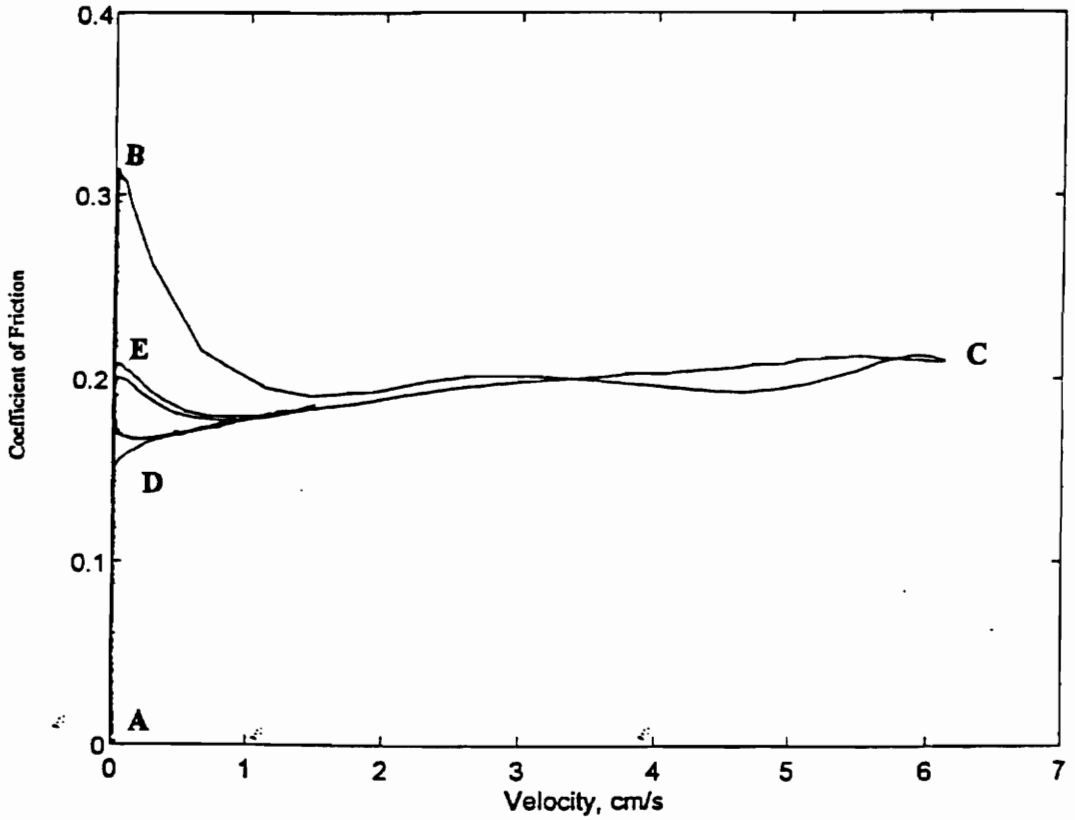

Figure 4.23 Friction-velocity trace of multiple stick slip for ABS SPI-SPE #1 surface under a 20.7 Newton load.

zero velocity from A to B is the increase in the interfacial contact force which culminates in the static friction at B. The initial stick phase from A to B indicates the motion of the actuator was accommodated by the elastomeric coupling and the force transducer measured the force build-up in the interface between the two flat polymer surfaces. The velocity signal indicates that during the initial stick no motion was detected.

When the two surfaces slipped relative to one another, the applied force exceeded the static friction at point B on the friction time curve. A sharp drop in friction along with a increase in velocity occurs from B to C. From C to D both friction and velocity decrease. Thus, the first slip occurs between B and D. At point D the two samples "stick" as revealed by the zero relative velocity. The interfacial contact force builds up during the second stick phase until at E the second "slip" occurs. The second stick phase was again identified by the average constant slope on the friction-time curve and the zero velocity. Note that the static friction is higher in the first stick than in subsequent sticks. This is caused by creep which occurs during a 5 minute period between the time the normal load was applied and the starting of the actuator motion. This stick-slip cycle continued until the test was completed.

The friction-velocity relationship is similar for cases of single stick and single stick-slip. During single stick-slip one stick-slip cycle occurs after the initial slip. After the second slip at point E, sliding initiates and continues to the end of the test with no further stick-slip cycles. In cases of single stick, after the initial slip the friction-velocity curve terminates to a point of constant sliding velocity at a constant kinetic friction instead of another stick-slip cycle.

Both friction-time and friction-velocity plots are distinctly different for cases such as polypropylene when a constant static-to-kinetic friction transition occurs (See figure 4.24-4.25.) The rise in friction from zero velocity from A to B occurs similar to the

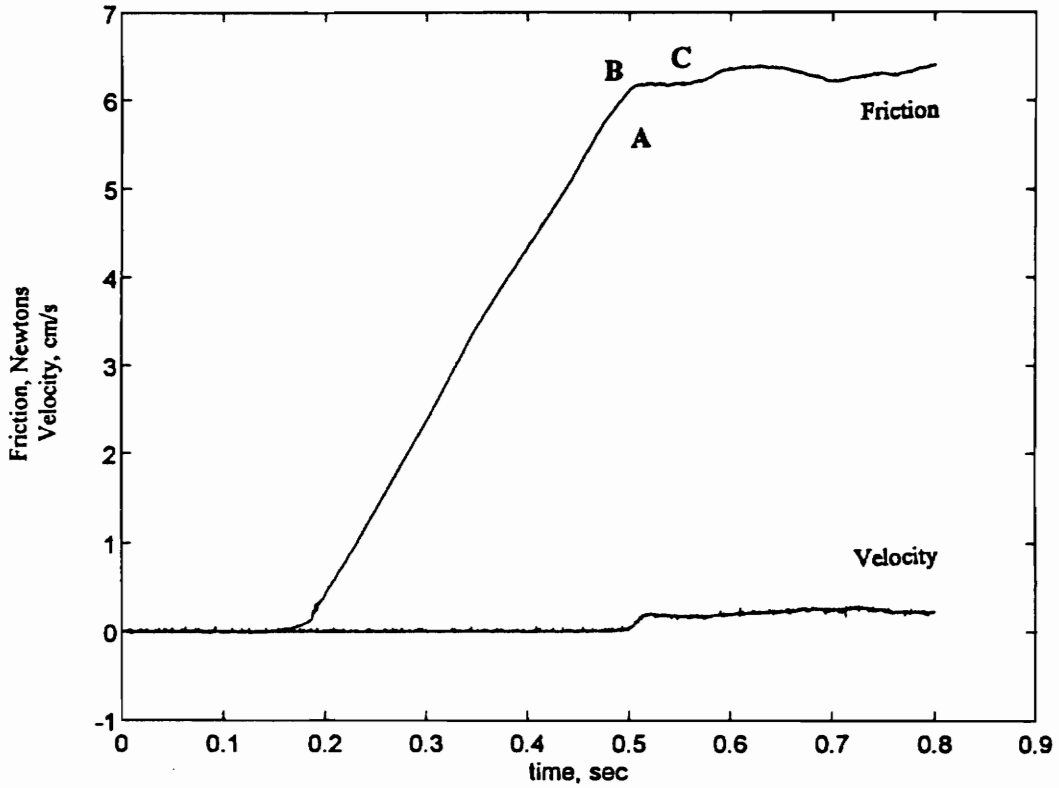

Figure 4.24 Friction-time trace of a smooth transition from static to kinetic friction for unfilled polypropylene Naples surface under a 20.7 Newton load.

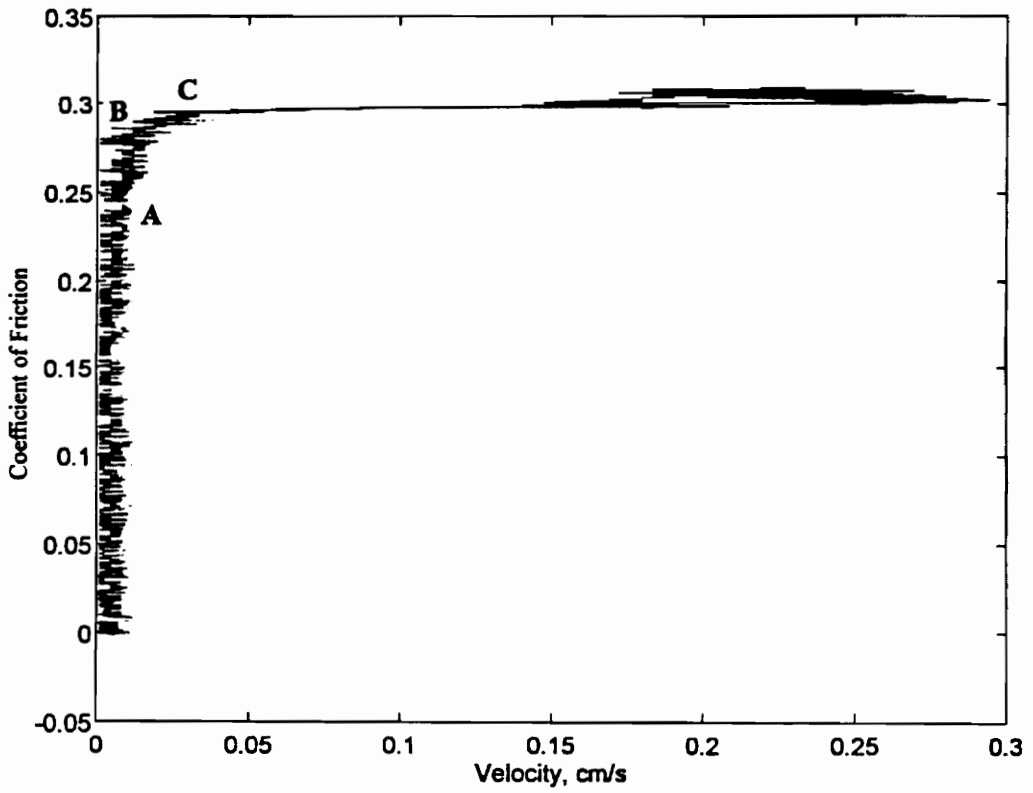

Figure 4.25 Friction-velocity trace of a smooth transition from static to kinetic friction for unfilled polypropylene Naples surface under a 20.7 Newton load.

previous curves. The similarity ends here, as the interfacial contact force increases, a series of micro-slips occur which slowly releases energy as indicated by the decrease in slope between A and B. Instead of a sharp drop and an sudden increase in velocity at B, a smooth transition occurs at B into a constant friction over a constant sliding velocity to point C.

4.4 Effects of Experimental Setup on Frictional Behavior

The friction-time and friction-velocity plots in figures 4.26-4.27 suggest that the horizontal system stiffness of the test apparatus has an effect on frictional behavior. The different combinations of elastic members produce different friction-velocity relationships. All friction-velocity plots for single stick and stick-slip were double valued. In some cases, the friction-velocity plot showed the friction retracing the curve and then separating into a double valued curve.

4.5 Stress-Strain Measurement

Figure 4.28-4.31 shows the stress-strain measurement results of ABS, polycarbonate and filled and unfilled polypropylene. The stress strain curves for ABS and polycarbonate show strain hardening (figure 4.28.4.29.) Necking occurred for both polycarbonate and ABS after yield. Unfilled polypropylene shows strain softening after yield (figure 4.31.) Figure 4.30 shows brittle fracture for fiberglass filled polypropylene shortly after yield. This is due to the brittle and stiff glass fibers which prevent the material from elongating.

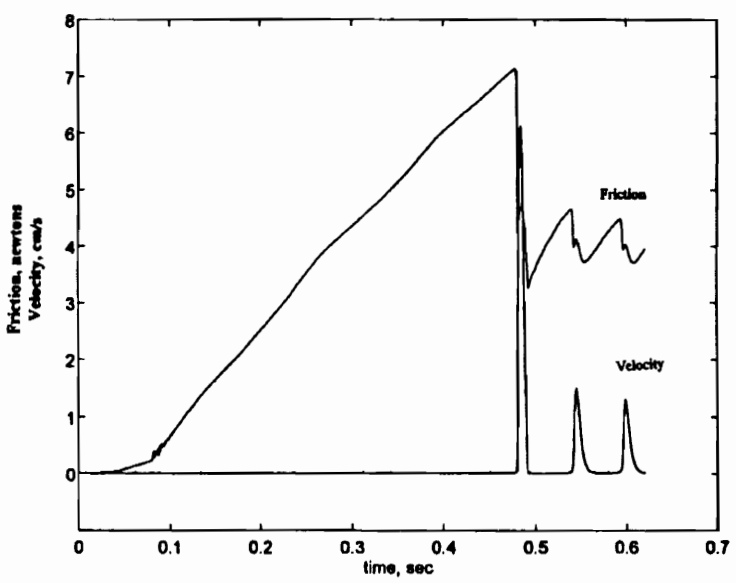

(a)

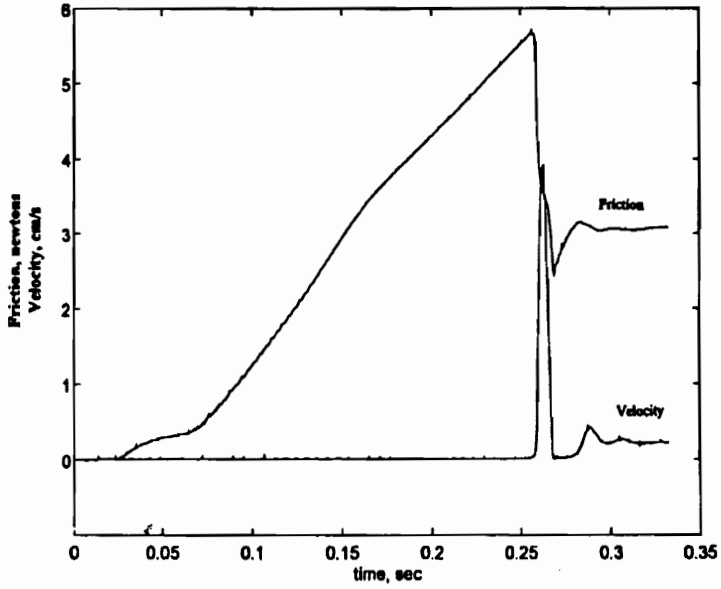

(b)

Figure 4.26 Friction-time trace for ABS SPI-SPE #1 surface under 20.7 newton load for different experimental configurations. The natural frequencies for each plot are: a) 54 Hz, b) 67 Hz, c) 58 Hz, and d) 100 Hz.

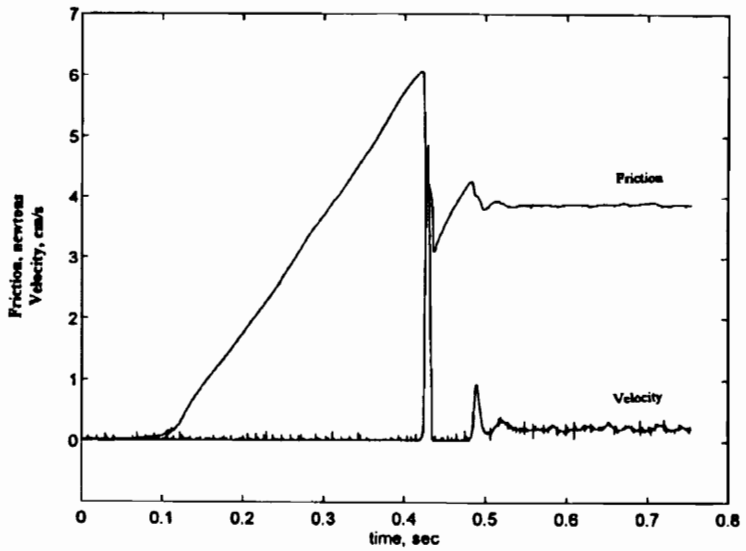

(c)

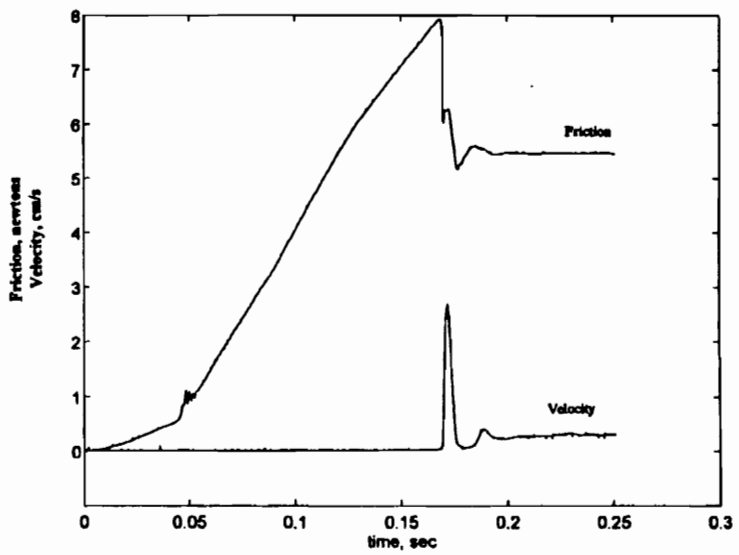

(d)

Figure 4.26 Friction-time trace for ABS SPI-SPE #1 surface under 20.7 newton load for different experimental configurations. The natural frequencies for each plot are: a) 54 Hz, b) 67 Hz, c) 58 Hz, and d) 100 Hz.

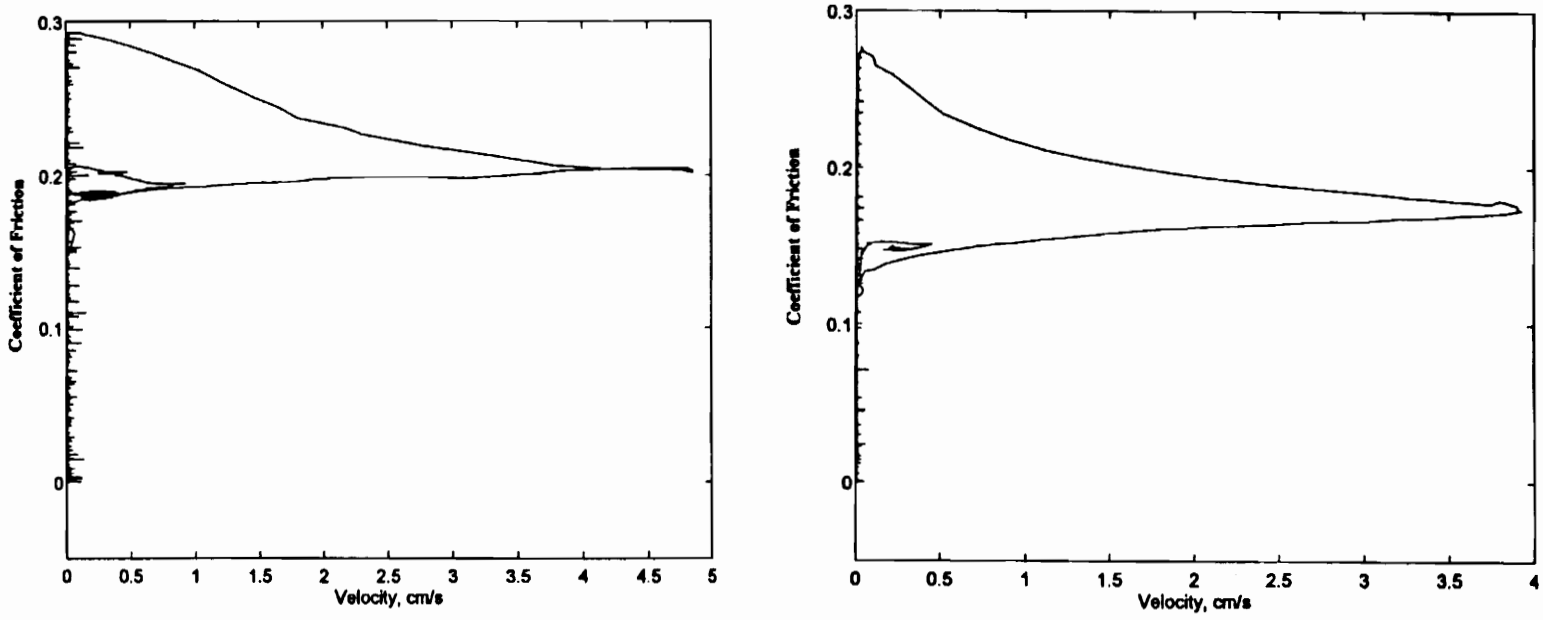

(a) (b)

Figure 4.27 Friction-time trace for ABS SPI-SPE #1 surface under 20.7 Newton load for different experimental configurations. The natural frequencies for each plot are: a) 54 Hz, b) 67 Hz, c) 58 Hz, and d) 100 Hz.

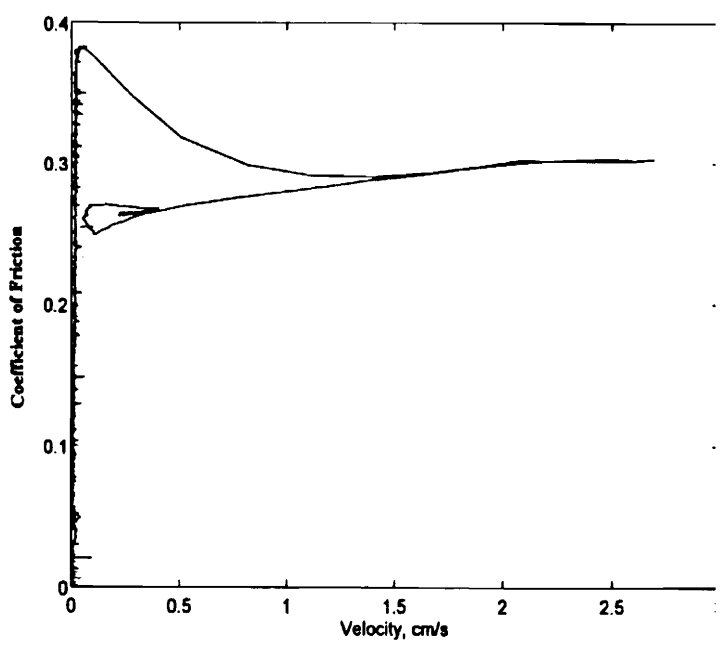

(c)

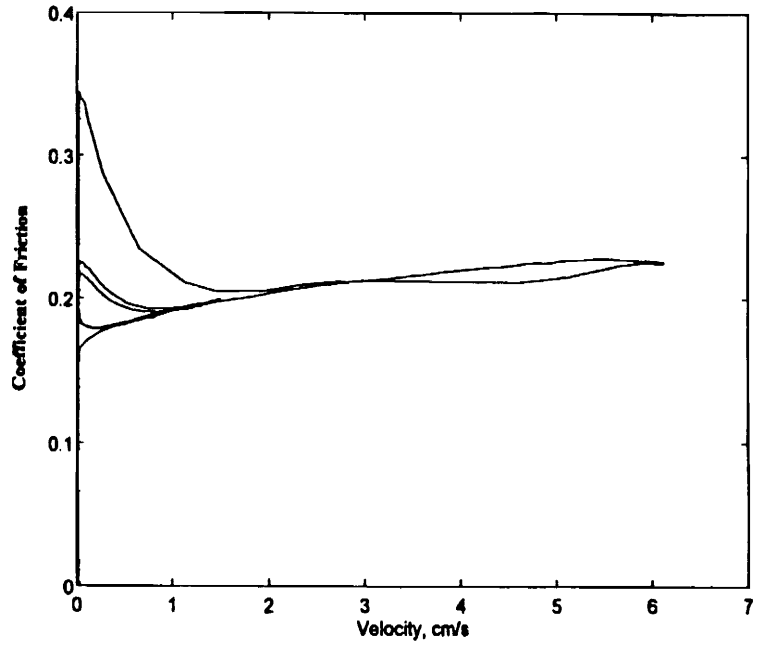

(d)

Figure 4.27 Friction-time trace for ABS SPI-SPE #1 surface under 20.7 Newton load for different experimental configurations. The natural frequencies for each plot are: a) 54 Hz, b) 67 Hz, c) 58 Hz, and d) 100 Hz.

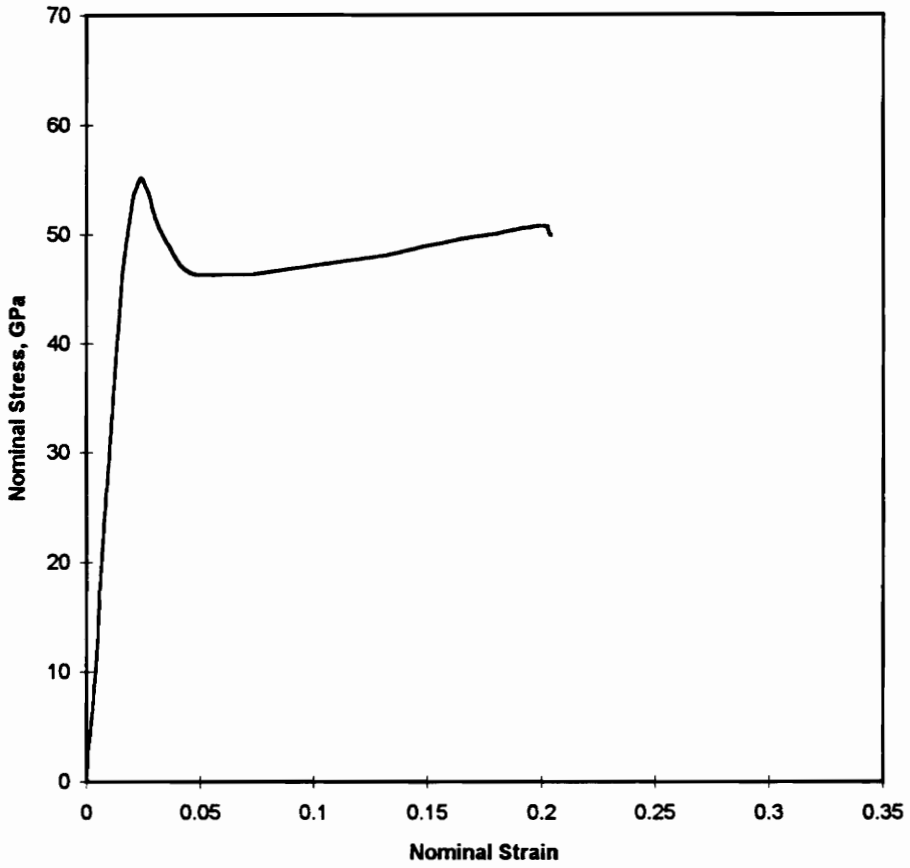

Figure 4.28 Stress strain curves for ABS, SPI-SPE #1 surface.

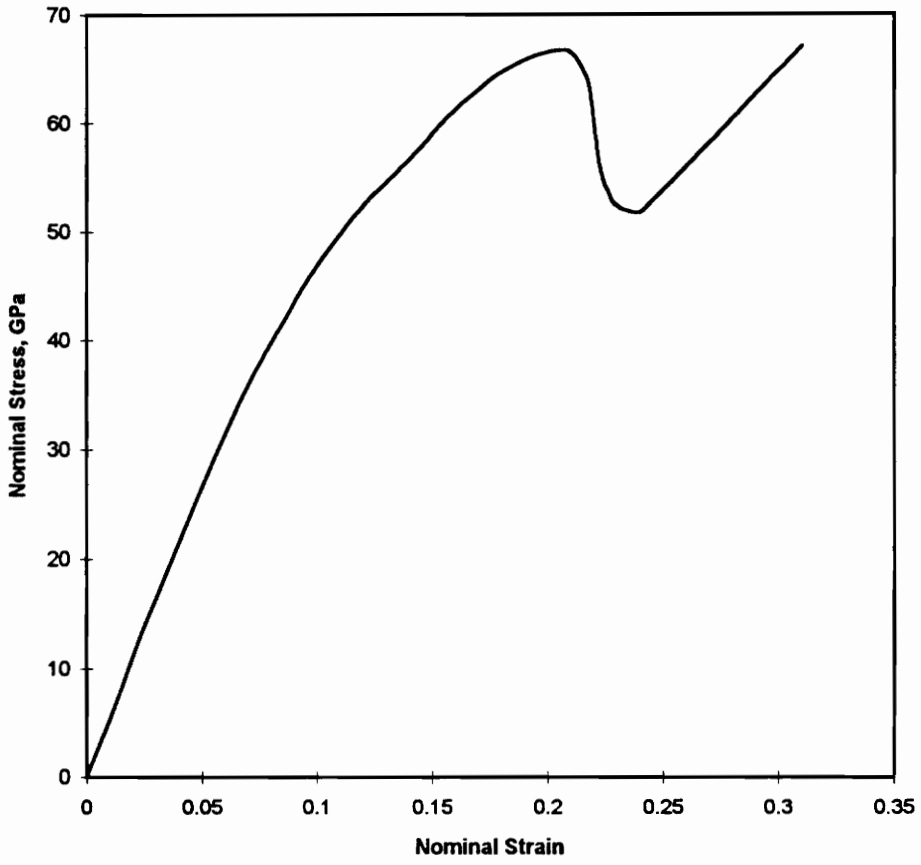

Figure 4.29 Stress strain curves for polycarbonate, SPI-SPE #1 surface.

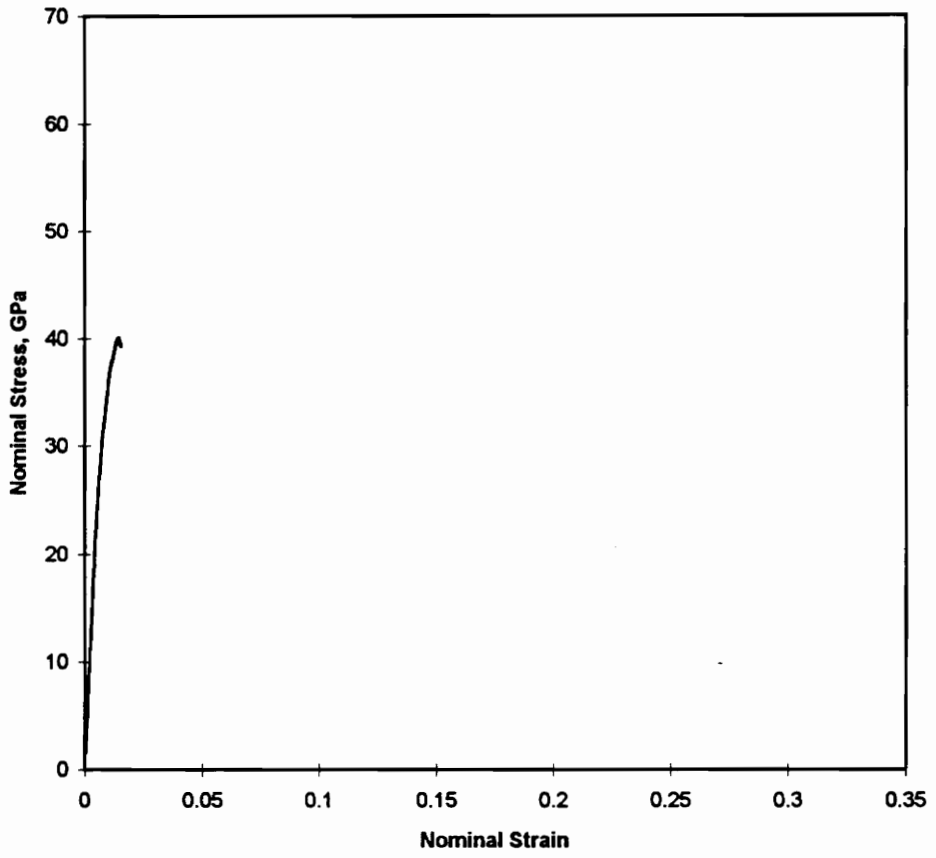

Figure 4.30 Stress strain curves for fiberglass filled polypropylene, SPI-SPE #1 surface.

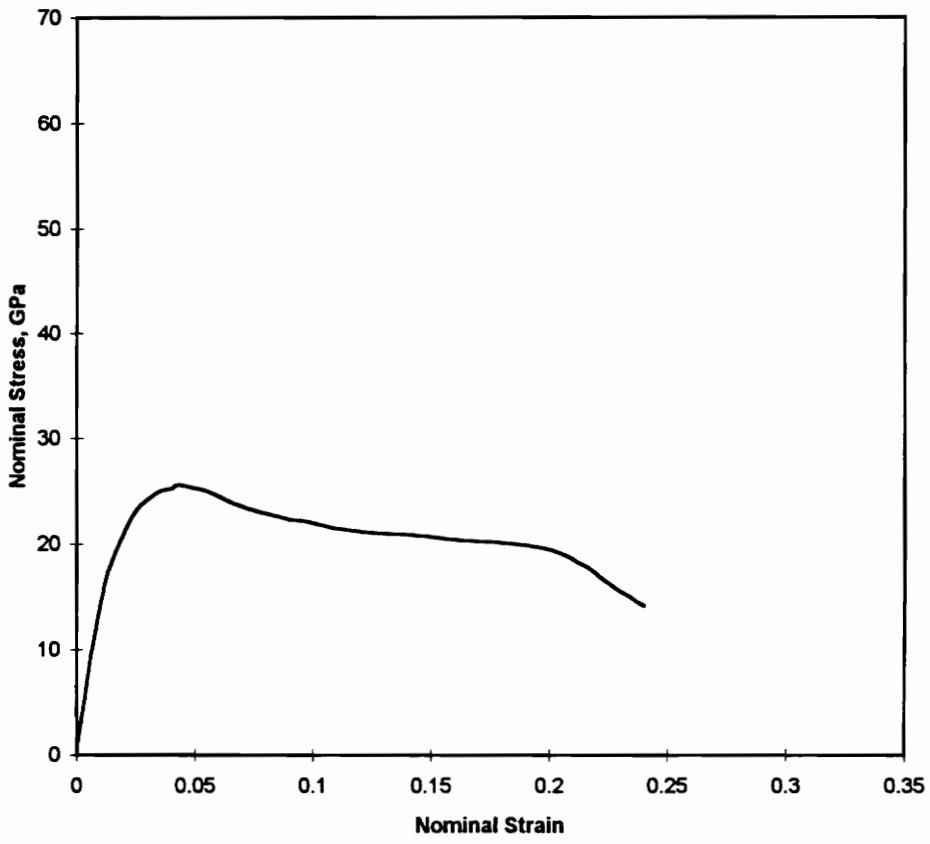

Figure 4.31 Stress strain curves for unfilled polypropylene, SPI-SPE #1 surface.

Table 4.3 lists the results of the stress strain testing. The effect of the fiberglass filler is obvious for polypropylene. Yield strength and modulus of fiberglass filled polypropylene is twice that of unfilled polypropylene and similar in magnitude to ABS.

Table 4.3 Mechanical Properties of ABS, PC, Fiberglass Filled and Unfilled PP

	ABS	PC	Unfilled PP	Filled PP
Modulus, E (kN/m^2)	2.96E5	5.32E4	2.96E5	4.67E5
Yield Strength, (kN/m^2)	5.54E4	6.71E5	2.14E4	4.04E4
Extension @ Break, mm	12.7	3.73	7.62	0.857
Peak Load, kN	0.733	1.23	0.382	0.729
Peak Extension, mm	1.21	2.19	1.93	0.840
Original Cross Sectional area, mm^2	13.02	18.33	17.81	18.26

5.0 Discussion

In this chapter, the experimental results are discussed to explain possible friction mechanisms or system affects on the transition from static and kinetic friction and the friction-velocity relationship. Section 5.1 discusses the static contact time tests performed to investigate creep effects on the static and kinetic friction. Section 5.2 discusses how computer modeling was used to understand how the system reacts to the friction-velocity relationship and how sampling rate affects the friction-velocity curve. Possible relationships between mechanical and frictional behaviors are described in section 5.3. Section 5.4 discusses the relationship between material composition and surface roughness on frictional behavior. Section 5.5 discusses the friction-velocity relationship and the limitations of the experimental setup.

5.1 Relationship Between Creep and Static Friction

In section 4.1 a positive correlation between creep and the static coefficient of friction was observed. Note that creep is measured as elongation under a constant tensile load. The cross-sectional area of the specimen will decrease which leads to higher real stresses. In this study, creep is defined as the increase in contact area due to a constant compressive load which leads to lower stresses. Creep is measured by the change in cross-sectional area under a constant load. If a material exhibits creep behavior, then the

real area of contact should increase as the contacting asperities are loaded over a period of time.

Polymers in general exhibit creep behavior due to a combination of mechanical and chemical properties. The static coefficient of friction increases with the static contact time and approaches zero as the contact time approaches zero for materials exhibiting creep. This increase is due to the increase in the real area of contact as more asperities come into contact and deform to support the load. Longer contact times encourage this behavior. The shearing of the larger area of contact results in a larger friction. Consequently, as the static contact time approaches zero, the static and kinetic coefficient of friction should approach the same values. Figure 4.9-4.10 show this phenomenon to be true.

Re-examining the magnitude of the friction coefficients in figure 4.1-4.10 show that surface roughness and load seem to have a minimal affect on the static friction coefficient as a function of contact time. Values of static and kinetic coefficients of friction for each contact time are not statistically different.

5.2 Computer Modeling

Computer simulation models of the friction tester were developed to predict how the friction tester would react to a given friction-velocity relationship and to determine the effect of the size of the integration time step on the friction variation with time.

The single degree of freedom system was used to model the current friction tester to understand how the friction-velocity characteristic affects the system response.

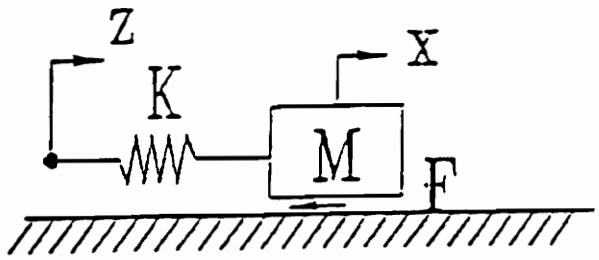

$$\ddot{x} = \frac{1}{M}(Kz - Kx - F)$$

Figure 5.1 Single degree of freedom system used to model friction test apparatus.

Friction-velocity relationships measured on the tester were incorporated in the model shown in figure 5.1 where M is the mass of the slider, K is the elastic member stiffness, F is the friction, and Z is the displacement applied by the actuator. The intention of this model is to focus on the transition from static to kinetic friction and the resulting velocity of the slider. The model showed that a negative slope of the friction-velocity curve causes the system to become unstable while a positive slope results in stable behavior.

Next the model was utilized to give insight on the data sampling rates required to obtain accurate friction and velocity data. The friction-velocity curve used in the simulation is shown in figure 5.2. Figure 5.3 shows the interface force during stick and the friction during slip for an integration time step of 0.1 ms. Figure 5.4 shows the corresponding velocity-time plot. Figures 5.5-5.6 show friction and velocity for a time step of 1 μs. Comparison of the friction plots shows that smaller integration step sizes (faster sampling rates) in figure 5.5 captures the detail of the friction-velocity relationship shown in figure 5.2 while the larger integration step size (slower sampling rate) in figure 5.3 does not. Following this simulation study, data sampling rates were increased from 3000 Hz to 6000 Hz to acquire friction and velocity data during the friction tests.

5.3 Relationships Between Mechanical and Frictional Behavior

Results in section 4.2 shows that ABS, fiberglass filled polypropylene and polycarbonate tend to exhibit single stick, single and multiple stick slip behavior. Unfilled polypropylene tends to exhibit a constant transition from static to kinetic friction. This section discusses the relationship between the mechanical and the system properties on

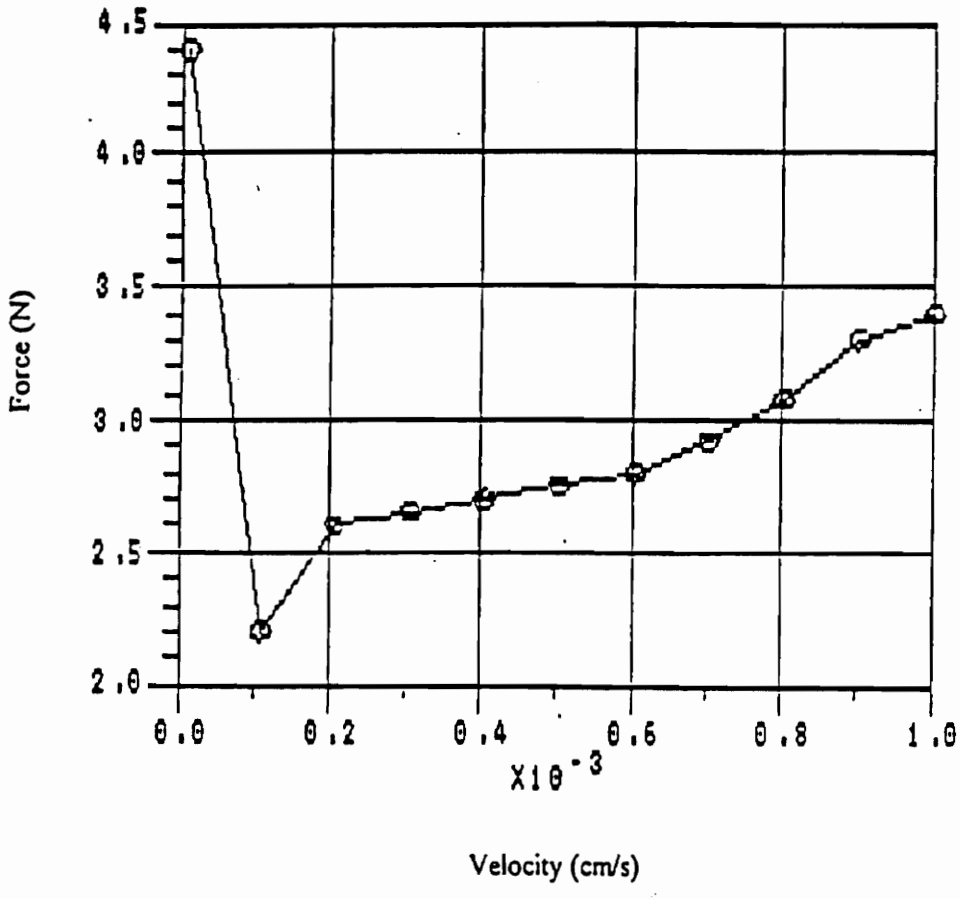

Figure 5.2 Friction-velocity relationship used in the simulation.

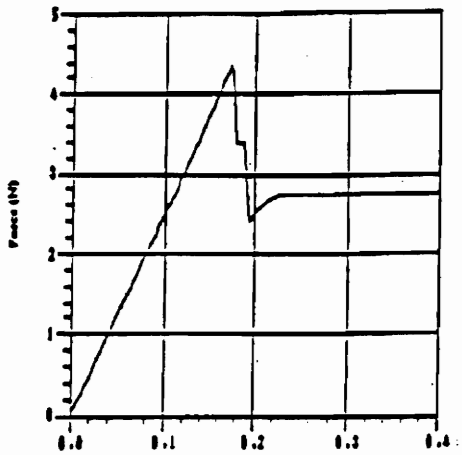

Figure 5.3 Simulated interface and friction forces for 0.1 ms time step.

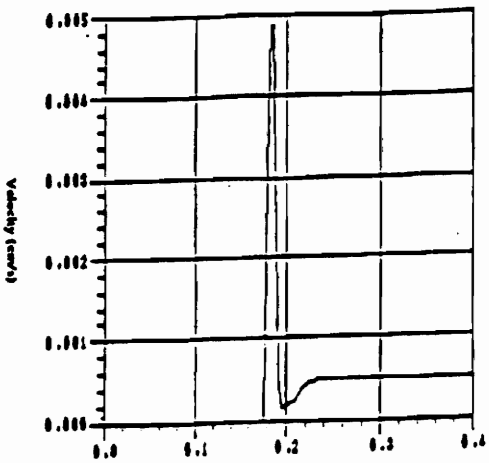

Figure 5.4 Simulated velocity for 0.1 ms time step.

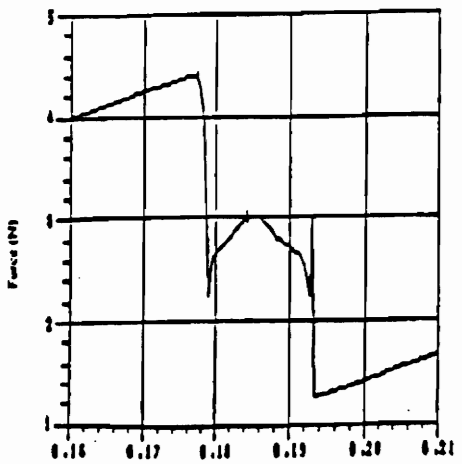

Figure 5.5 Simulated interface and friction forces for 0.1 μs time step.

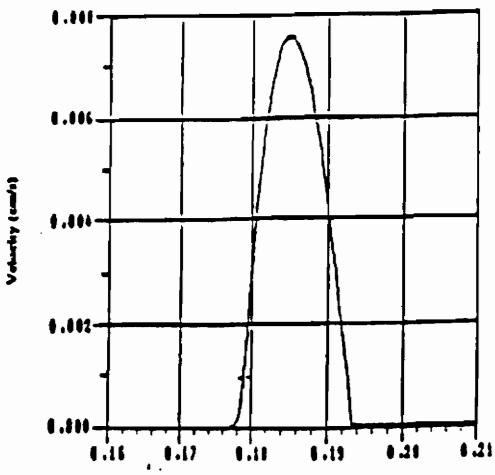

Figure 5.6 Simulated velocity for 0.1 μs time step.

frictional behaviors. The static-to-kinetic transition is affected by how energy is released prior to rupture of the adhesive bonds.

Relative motion between two contacting surfaces occurs when the applied force exceeds the interfacial force between two contacting surfaces. The work of friction is stored as potential energy in the elastic members of the system. A sudden release of energy is more likely to cause a drop in friction while a gradual release is likely to cause a smooth transition from static to kinetic.

Prior to yield, energy is fully recoverable because deformation is elastic. After yield, with the onset of plastic deformation, some of the energy is dissipated and thus is not fully recoverable. This behavior is true for materials which exhibit strain hardening, strain softening, or brittle fracture. In the case of brittle fracture, little plastic deformation occurs before the material ruptures.

The release of energy prior to slip may be governed by microslips due to plastic deformation after yield. Microslips occur as the tangential load is increased prior to gross sliding. The theory states that microslips occur when asperities in contact deform plastically due to the applied tangential force[18]. The microslip stops as new asperities come into contact and resist deformation. This process continues until the resistance of the asperities cannot prevent gross sliding from occurring.

Microslips are more likely to occur for strain softening materials than strain hardening materials because a lower level of force is required to plastically deform the material after yield for the former materials. These microslips release some of the potential energy accumulated in the elastic members during stick. The potential energy is gradually released into the system as microslips until the applied force exceeds the interfacial force. The release of energy to initiate sliding is not abrupt and the static-to-kinetic friction transition occurs without a significant drop in interfacial force.

Energy is not released through microslips for materials which exhibit strain hardening and brittle fracture. A large amount of potential energy is stored in the elastic members prior to sliding. When the applied force exceeds the friction at the interface, the adhesive bonds are ruptured leading to a large force imbalance. The energy stored in the elastic members is released all at once. A sharp drop from static to kinetic friction occurs which accelerates the moving surface to the sliding velocity.

Figure 4.21 reveals a higher static coefficient of friction for unfilled polypropylene than ABS, polycarbonate, or fiberglass filled polypropylene. The higher static coefficient is due to the larger area of contact. This means a larger number of asperities for the softer unfilled polypropylene deform to support the load. Note that unfilled polypropylene does not exhibit creep and thus the real area does not increase with time. Thus, it appears that the microslip mechanism is unaffected by the magnitude of the static friction coefficient.

5.4 Material Composition and Surface roughness effects on Friction

The surface roughnesses of the molded polymers are more a function of the material composition rather than the surfaces of the mold. The plates were made with prescribed surface roughness which theoretically should mold all polymers to the same roughness. Table 3.2 shows that there is considerable variation between surface roughness and material composition.

The results of this study has not found conclusive evidence that a smoother surface is more likely to exhibit stick slip behavior than a rougher surface. Table 4.1 shows that stick-slip occurs for all surfaces depending on which material composition was tested. This suggests that unsteady frictional behavior is more a function of material composition than surface roughness.

5.4.1 ABS

All cases of the ABS material exhibited either a sudden or a gradual drop in friction(see table 4.1 and 4.2.) Multiple and single stick slip occurred when the friction had a sudden drop for the Montana BG, Naples FY, and SPI-SPE #1 surfaces under both 10.7 and 20.7 Newton loads. This is interesting because the Montana and Naples surface have a 10 point height roughness of 53.6 and 36.4 microns respectively while SPI-SPE #1 has a roughness of 1.2 microns. The Stipple surface which has a roughness of 37.3 microns does not exhibit stick slip frictional behavior.

5.4.2 Polycarbonate

Polycarbonate has a unique range of friction characteristics with instances of multiple and single stick slip, single stick, and kinetic friction coefficients higher than the static friction coefficient. Like ABS, the Stipple surface under the 10.7 Newton load tends to have gradual transitions from static to kinetic(this is also observed by the lower maximum slip velocities and gradually negative slope during the initial drop.) But when the Stipple surface is under a 20.7 Newton load a sharp drop in friction occurs with large fluctuations in the kinetic friction.

The Montana and Naples surfaces under both loads exhibit sharp transitions from static-to-kinetic friction. Instances of multiple and stick slip are superimposed onto these large fluctuations. In cases where stick slip occurs, the magnitude of the slip cycle velocity fluctuates as well.

The smoothest surface tested was SPI-SPE #1 which provides a larger real area of contact. This particular surface had a peculiar transition from static-to-kinetic friction. Figure 4.18 shows a rise in friction, then an initial slip, followed by an increase in friction

to a steady kinetic friction value. The velocity remains constant during the increase in friction while the normal load increases in a similar manner.

5.4.3 Polypropylene

5.4.3.1 Fiberglass Filled Polypropylene

The fiberglass filler has affected frictional properties of polypropylene in a negative manner even though mechanical properties have been improved. From previous studies, polypropylene is known to have favorable frictional behavior which results in a constant static-to-kinetic friction transition. The fiberglass filled polypropylene exhibited single stick slip and single stick behavior. A gradual drop from static to kinetic was observed for the Naples surface under a low load and the Stipple surface under both loads. All other surfaces have a sharp drop in friction which resulted in single stick-slip behavior.

In figure 4.19 note that the surface roughness does not seem to greatly affect the static and kinetic coefficients for fiberglass filled polypropylene. The fiberglass filler appears to reduce the surface roughness effect on frictional behavior. This may be because the polymer matrix of a fiberglass filled polymer transfers the load to the glass fibers. Thus, the glass fibers support the load instead of the resin matrix and the friction becomes a function of the fibers. The surface roughness contributes to the friction but to a lesser extent. This may also explain why fiberglass filled polypropylene has a lower static and kinetic coefficient than unfilled polypropylene. The stiffer asperities allow less deformation on contact making the real area of contact smaller.

5.4.3.2 Unfilled Polypropylene

Three distinct frictional behaviors were evident for unfilled polypropylene. Most

cases exhibited a smooth transition from static to kinetic without a sharp drop in friction and a few cases showed a gradual drop from static to kinetic friction. Single stick was observed for the Montana and Stipple surfaces. For the SPI-SPE #1 surface, the kinetic coefficient of friction is higher than the static coefficient which was also observed for polycarbonate with the same surface. Figure 4.20 compares the static and kinetic coefficients under 95% confidence intervals which show the a transition from static to kinetic friction is constant.

5.5 The Friction-Velocity Relationship

In section 2.2.4 it was noted that a negative slope of the friction-velocity curve can cause friction instabilities. Computer simulation models have confirmed this relationship.

A more useful tool to analyze the friction-velocity relationship is the coherence function. The coherence function between friction and velocity during stick slip under 40 Hertz is high, ranging from 0.9-0.98 with a negative correlation. The negative correlation simply means the friction decreases as the velocity increases. A negative coherence function also means a negative slope to the friction-velocity curve exists while a positive coherence indicates a positive slope. The coherence function is also useful in examining harmonic oscillations in the kinetic friction.

The friction-velocity curves for the materials in this study have mostly been double valued with the exception of unfilled polypropylene. Figures 4.26-4.27 show the range of behaviors which can be obtained from different system stiffnesses through different

combinations of elastomeric combinations. In some curves, the region leading to and returning from the maximum slip velocity shows the friction tracing back upon itself instead of being doubled valued. No explanation can be given for this behavior at this time.

6.0 Conclusions

1. Strain softening polymers such as polypropylene are more likely to have equal static and kinetic friction values. One possible explanation is because potential energy is released prior to relative motion in the form of microslips. These microslips occur due to deformation of the asperities. Polymers which strain harden such as ABS and polycarbonate or exhibit brittle fracture like fiberglass filled polypropylene are more likely to have a abrupt drop friction. The possible explanation is due to the rupture of the adhesive bonds which releases all the potential energy during slip.

2. The friction-velocity curve is doubled valued when a drop in friction occurs from static to kinetic friction. The velocity increases as the friction decreases until the slip velocity reaches a maximum value. The velocity then decelerates to the sliding speed as the friction continually drops to the kinetic friction value.

3. Creep behavior which is independent of the surface roughness affects the static coefficient of friction. The static coefficient of friction increases with increasing contact time because of growth of the real area of contact. The maximum value is reached in 5 minutes.

4. The occurrence of stick slip is more a function of material composition rather than surface roughness. This contradicts McCann's conclusions[24]. Multiple and single stick-slip occurred for the rougher Montana and Naples surface and the smoother SPI-SPE #1 surface.

5. The occurrence of frictional oscillations are also affected by additives and fillers. Fiberglass filled polypropylene exhibited single stick slip behavior while unfilled polypropylene exhibited a smooth static to kinetic transition.

6. The stiffness of the horizontal slider on the test apparatus seems to affect the shape of the friction-velocity curve. The specific mechanism is unknown.

7. Strain hardening materials such as polycarbonate and ABS exhibit creep behavior, while strain softening materials, such as unfilled polypropylene, do not.

8. The measurements of the new test apparatus provides an excellent foundation for studying and understanding the static to kinetic friction transition. Friction, normal load, and relative velocity can be simultaneously measured and analyzed.

7.0 Recommendations

1. Select other strain softening polymers to determine if they also have equal static and kinetic frictions and if they do not make noises in typical automobile interior applications.
2. Determine how certain additives enhance or degrade frictional behavior. The results may guide the formulation of special blends to obtain favorable frictional properties. Tests with materials exhibiting desirable frictional characteristics may be refined by testing the same materials but with different additives. Analyze the chemical composition and microstructure to determine which parameters specifically affect friction.
3. Conduct tests on aged or UV exposed polymers to determine their effects on the transition from static to kinetic friction.
4. Develop models to identify material properties and system parameters which influence friction. Determine how and why these variables caused a doubled valued friction-velocity relationship. Identify any variables which predict unstable or stable frictional behavior.
5. Determine how processing (sample preparation and injection molding) affects the surface and structure of the material and how friction is affected.
6. Measure the roughness of the molds and compare to the roughness of the molded polymer. This is to determine the exact relationship between the surface roughness

of the molds to roughness of the injection molded polymer. At the time of this study the surface profilometer was out of service which prevented roughness measurements of the polymer specimens.

7. Design a new mold which produces specimens which can be directly used by the test apparatus to reduce cutting costs and vastly improve the consistency of the specimen size.

References

[1] Wood, Richard., *Automotive Engineering Plastics*. Pentech Press: London, 1-85, (1991).

[2] Briscoe, B. J., "The friction of Polymers: A Short Review," Friction and Traction, ed. by D. Dowson, M. Godet, C. M. Taylor, and D. Berthe, Westbury House, IPC Press, Guilford, 81-93 (1981).

[3] Eguchi, M. and Yamamoto, T., "Effect of Surface Geometry on Relationship Between Static Friction and Stationary Contact Time in Stick-Slip Oscillations," Proc. of the JSLE International Conference, July 8-10, 1053-1058 (1985).

[4] Seymour, R. B. and Carraher, C. E., "Structure-Property Relationships in Polymers," Plenum Press, New York, (1984).

[5] Chou, N. J., Kowalczyk, S. P., Saraf, R., and Tong, H., "Characterization of Polymers," Butterworth-Heinemann, Boston, (1994).

[6] Bowden, F. P. and Tabor, D. "Friction An Introduction to Tribology," Doubleday & Company, Inc., London, 79-81 (1973).

[7] Voorhes, W. G., "Investigation of Stick Slip In Simulated Slideways," Journal of the American Society of Lubrication Engineers, April 30-May 2, 457-469 (1963).

[8] Erhard, G., "Sliding Friction Behavior of Polymer-Polymer Material Combinations," Wear, 84, 167-181 (1983).

[9] Watanabe, M. and Yamaguchi, H,. "The Friction and Wear Properties of Nylon," Proceedings of the JSLE International Tribology Conference, July 8-10, 1985, Tokyo, Japan.

[10] Capone, G., D'Agostino, V., Della Valle, S. and Guida, D., "Influence of the Variation Between Static and Kinetic Friction on Stick-Slip Instability," Wear, 161, 121-126 (1993).

[11] Gao, C., Kuhlmann-Wilsdorf, D. and Makel, D. D. , "Fundamentals of Stick-Slip," Wear, 162-164, 1139-1149 (1993).

[12] Rabinowicz, E., *Friction and Wear of Materials,* John Wiley and Sons, Inc., New York, 152-153, (1965).

[13] Brockley, C. A., Cameron, R., and Potter, A. F., "Friction-Induced Vibration," ASME Journal of Lubrication Technology, Vol. 89, 101-108, April 1967.

[14] Ko, P. L., and Brockley, C. A., "The Measurement of Friction and Friction-Induced Vibration," ASME Journal of Lubrication Technology, Vol. 92, 550-556, October 1970.

[15] Ko, P. L., and Brockley, C. A., "The Measurement of Friction and Friction-Inducted Vibration," ASME Journal of Lubrication Technology, Vol. 92, 543-549, October 1970.

[16] Gao, C., Kuhlmann-Wilsdorf, D. and Makel, D. D. , "The Dynamic Analysis of Stick-Slip Motion," Wear, 173, 1-12 (1994).

[17] Johansen, A., Dimon, P. and Ellegaard, C., "Dynamics of Sliding in a Spring-Block Experiment," Wear, 172, 93-97 (1994).

[18] Simkins, T. E., "The Mutuality of Static and Kinetic Friction," Lubrication Engineering, 26-31, vol 25, (1967).

[19] Bahadur, S., "Dependence of Polymer Sliding Friction on Normal Load and Contact Pressure," Wear, 29, 323-336, (1974).

[20] Nakai, M, and Yokoi, M., "Generation Mechanism of Friction Noises in Dry Friction, " Japanese Journal of Tribology, Vol. 35, No. 5, 513-522, (1990).

[21] Bhushan, B., "Stick-slip Induced Noise Generation in Water-Lubricated Compliant Rubber Bearings, " Journal of Lubrication Technology, Vol. 102, 201-212, April 1967.

[22] Taniguchi, M., and Takagi, T., "Noise and Tribology in Electrical Sliding Contact Characteristics and Problems," Japanese Journal of Tribology, Vol. 34(No. 10), 1135-1145 (1989).

[23] Briscoe, B. J. and Tabor, D., "Shear Properties of Thin Polymeric Films," Journal of Adhesion, Vol. 9, 145-155 (1978).

[24] McCann, Brian P., "Frictional Vibrations in Structural Polymers." Master of Science Thesis, Virginia Polytechnic Institute and State University, May 1992.

[25] Arnell, R. D., Davies, P. B., Halling, J., and Whomes, T. L. *Tribology Principles and Design Applications.* Springer-Verlag, Hong Kong, (1993)

[26] Briscoe, B. J., and Tweedale, P. J., "A View of Polymer Composite Technology," Proc. of Amer. Soc. Mat. Conf., Tribology of Composite Materials, ed. by P. K. Rohatgi, P. J. Blau, and C. S. Yust, 15-23 (1990).

[27] Aronov, V., D'Souza, A. F., Kalpakjian, S., and Shareef, I., "Interactions Among Friction, Wear, and System Stiffness-Part 2: Vibrations Induced by Dry Friction," ASME Journal of Lubrication Technology, Vol. 106, January 1984, 56-64.

[28] Molique, Robert S., "Frictional Behavior of Polymers: the Transition from Static to Kinetic Conditions." Master of Science Thesis, Virginia Polytechnic Institute and State University, February 1994.

[29] Aronov, V., D'Souza, A. F., Kalpakjian, S., and Shareef, I., "Experimental Investigation of the Effect of System Rigidity on Wear and Friction-Induced Vibrations," ASME Journal of Lubrication Technology, Vol. 105, April 1983, 206-211.

[30] Aronov, V., D'Souza, A. F., Kalpakjian, S., and Shareef, I., "Interactions Among Friction, Wear, and System Stiffness-Part 1: Effect of Normal Load and System Stiffness," ASME Journal of Lubrication Technology, Vol. 106, January 1984, 54-58.

[31] Antoniou, S. S., Cameron, A. and Gentle, C. R. "The Friction-Speed Relation from Stick-Slip Data," Wear, 36, 235-254 (1976).

[32] Saeki, M., and Takano, E., "Oscillations Caused by Solid Friction in Mechanical Driving System, " Japanese Journal of Tribology, vol. 37, No. 10, 1308-1316, (1992).

[33] Margolis, J. M., "Engineering Thermoplastics properties and Applications," Marcel Dekker Inc., New York, (1985).

[34] Ward, I. M., "Mechanical Properties of Solid Polymers Second Edition," John Wiley & Sons, Chichester, (1983).

[35] Dorinson, A. and Ludema, K. C., "Mechanics and Chemistry in Lubrication," Elsevier Scientific Publishing Company, New York, 1985.

[36] Sakamoto, T., Abo, M., and Kakunai, S., "Friction Reduction in a Stick-Slip Process under Vibratory Load," Japanese Journal of Tribology, Vol. 36(no. 1), 71-82 (1991).

[37] Shimura, H. and Kitahara, T., "Effects of Vibration Characteristics of Measuring System on Friction and Wear," Japanese Journal of Tribology, Vol. 35(No. 5), 577-858 (1990).

APPENDIX A

Table A.1 Component List of Test Apparatus

Component Description	*Manufacturer*	*Part No.*
Linear Velocity Transducer (L.V.T.) w/ 4" threaded rod	Lucas Schaevitz	612-VTZ
Micro-slider	Schneeberger	ND2-80.50
Vertical Slider	Schneeberger	NVRD-3300
Piezoelectric Force Transducer Power Supply	PCB Piezotronics	208-AO2 484B11
Strain Gage Force Transducer	Sensotec	Model No. 41 w/ In-line amp Model UBP
DC servo actuator Cylinder Controller Limit switches Motor Cables	Industrial Devices Corporation	NH995A-4-MS6-MT1-ZH H3951 RPC QF1-12
#4-40 Elastic Members	Minor Rubber	VBM-1020
#6-32 Elastic Members	Minor Rubber	VBM-1028

APPENDIX B - Experimental Setup and Test Procedures

This section outlines the experimental setup and test procedures used to collect data for this thesis. All the arrows in the diagram below represent coaxial input/output connections between components. Note that all equipment must be connected to common ground to reduce unwanted noise problems caused by an open ground loop.

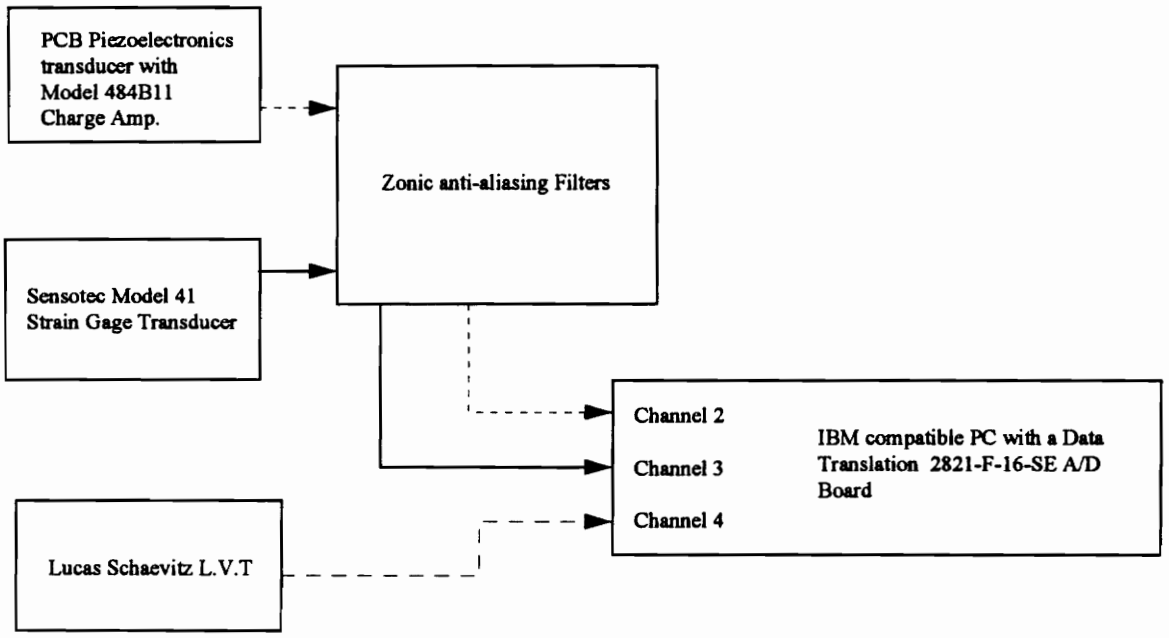

Figure B.1 Experimental Setup diagram for input/output connections of the components

Note: The filter setup is optional, the piezoelectric force transducer and strain gage can be directly connected to the A/D board.

Experimental Testing Procedures for the New Test Apparatus

Four 0.2 inch sliding distance tests over a fresh surface of the lower specimen can be conducted before being replaced. The actuator is moved 0.25 inches between tests to make sure a fresh surface is always encountered.

1. Turn on all the equipment:
   - PCB Model 484B11 Piezoelectronics charge amplifier
   - IDC DC servo actuator
   - Zonic anti-aliasing filters set to a frequency cutoff of 1500 Hz(if connected)
   - HP Model 6226B DC Power supply - This powers the Sensotec normal load strain gage transducer and must be set to 24 Volts
   - Personal Computer with the Data Translation 2821, 16 bit A/D board

2. Allow the components to warm up for 20-30 minutes. During this time the Global Lab data acquisition software can be setup.
   - Go into the directory to which the data is to be saved, e.g. cd\data\
   - Type *GL* <enter>
   - A menu screen appears, select the ***System*** menu, and then select the ***A/D module!***.
   - A new menu screen appears under the ***A/D module!***. Select the ***File*** menu and load an *.asu setup file which was created previously through the ***Load*** sub menu. If a new setup file is to be created or adjustment of the A/D board settings is required then go to the ***Edit*** submenu. For the 2821 16 bit A/D board channels 2, 3, and 4 are available. Activate these channels by pressing the space bar each time for the ***acq*** and ***D*** column.

The input voltages can be selected for each channel under the Range column by pressing the spacebar until the desired range is selected. Input voltage requirements for each component are:

L.V.T.	±1.25 V
Strain Gage	±2.5V, ±5V maximum
Piezoelectric	±2.5, ±5V, ±10V maximum

The settings will depend on experimental factors, such as the magnitude of the normal load, rate of change of speed, and/or the magnitude of the constant velocity.

The rest of the parameters are set accordingly(as their appear on the screen):

Sampling frequency

per channel: **6000 Hz** (recommended)

or total:

Sampling Duration

Samples/chan:

or duration: **2 seconds** (For one static to kinetic transition test)

Leave the next four parameters to default

Filename: enter filename of the data to be collected

3. To see if all the transducers are working properly use the digital oscilloscope in the Global lab software. This is done by pressing **F10**, going into ***Acquisition*** menu,

selecting ***Test***, and pressing any key. There now should be three plots showing the output of all three transducers. Lightly load or wiggle the transducers to see their output on the screen. If there is no output for any of the transducer recheck all connections between the components and the A/D board and make sure that all components are turned on.

4. Place a rectangular specimen on horizontal slider and secure each end with screws.

5. Then place a square specimen, cavity side up onto the square specimen. Align the square specimen with tweezers so that it is perpendicular to the direction of travel and underneath the specimen holder. The 1/8" OD steel ball should line directly above the square specimen.

6. Load program - 6 into the actuator by typing F6, 6, 6, <enter>. The program is then initiated by pressing button 1 of the external switch box to the controller. To set the actuator into the position for the next test, press button 2 after the test is completed. Four tests can be performed with this program over the length of the sample before the actuator must be returned to its start position. More on editing and programming can be found in the IDC instruction manual.

7. Place the stainless steel weights onto the top bracket of the vertical assembly. The weight of the vertical assembly without dead weights is 5.69 Newtons. See table B.1 for specific weights of the stainless steel weights.

Table B.1 Specific Weights of Stainless Steel Weights

Stainless Steel Weight Number	Measured Weight	
1	510.36 g	5.01 N
2	511.03 g	5.01 N
3	256.36 g	2.51 N
4	256.11 g	2.51 N

Lower the vertical assembly (which includes the piezoelectric transducer and weights) on to the square specimen on the horizontal slider. The stainless steel ball should line up with the cavity of the square.

8. Once lowered, use a stopwatch to wait 5 minutes before conducting a test (for a polymer sample.)

9. During this time, the data acquisition software should still be in the digital oscilloscope mode. Adjust the span on the PCB charge amplifier for the piezoelectric transducer so that the screen shows zero volts output. Otherwise data will be collected at an offset by this transducer.

10. At approximately 15 seconds before 5 minutes you should be getting ready to acquire data with Global Lab. This is done by pressing escape, and then selecting go. A message then appears on the bottom of the screen:

"Acquisition prepared press any key to start"

This means that the data acquisition software is awaiting you to trigger it to begin collecting data.

11. At five minutes, press any key to trigger the digital acquisition software, and then press the button one on the external switchboard to the controller of the actuator. This process must be done quickly in this sequence.

12. Once the data is collected, move the vertical assembly up and remove the square specimen. Then press button 2 on the external switchboard to the actuator to setup for the next experiment. Replace the old square specimen with a fresh

sample as described in step 5. Return to step 2 to change the filename and repeat steps 7 through 11.

13. Upon completing the fourth test, remove the upper square sample and simultaneously press buttons 1 and 2 to return the actuator to its start position. Now remove the lower rectangular sample. To continue more tests, make a new file(see step 2) and redo steps 4 through 12.

APPENDIX C - Equipment Specifications and Calibration Data

This section describes in further detail the components of the new linear test apparatus. The test apparatus has two separate force transducers, one to measure friction forces and the other to measure changes in normal load. The reasons for separate transducers include the reduction of cross-talk, the high frequency response of the piezoelectric friction force transducer, and the ability of the strain gage normal load transducer to measure static forces during creep testes. Relative velocity is measured by a linear velocity transducer(L.V.T.) A DC servo actuator was chosen to minimize velocity variation while providing constant velocity. A discussion on the data sampling and processing techniques concludes this section.

Piezoelectric Force Transducer

The new test apparatus incorporates a PCB Piezotronics 208AO2 series piezoelectric force transducer to measure the friction force. The crystals in the transducer produce an electrical charge only when a change in load is experienced. Therefore, it is not necessary to measure deflection which allows the piezoelectric to be extremely rigid and provide fast frequency response times (high natural frequencies and fast rise times.)

Performance was the deciding factor in choosing the piezoelectric transducer over conventional strain gage transducers to measure friction force. Transducers such as strain gages measure deformation to determine the force. Force in any transducer cannot be measured without disturbing the event being measured. Thus the measuring element must deform sufficiently in order to obtain any useful sensitivity which limits the frequency

response of the measuring systems. Measurement errors, such as linearity and hysteresis, arise because the deformations introduce geometric changes to the measuring element. Piezoelectric transducers do not have this problem because the sensing element of the piezoelectric is the same as the transduction element producing the electrical output force signal. This makes piezoelectrics suitable to measure a step change in the transition from static to kinetic friction force.

The piezoelectric transducer measures friction force at an offset distance from the center of the transducer of approximately 0.6 inches. Two calibration tests were conducted to ensure that the transducer accurately measured the friction force. The transducer was loaded in-line and then offset 0.6 inches to the applied force. These results produced two linear calibration curves with similar slopes. Calibration of the transducer was the directly performed on the new test apparatus. The calibration curve and specifications are in figure C.1 and table C.1 respectively.

The major disadvantage of piezoelectrics is that true static force can not be measured. This is because the electrical change generated by the force cannot be stored for an infinite amount of time. Piezoelectric transducers are ideally suited for measuring dynamic and quasi-static events. Short term friction measurements such as those conducted in this study are quasi-static events which occur approximately 2 seconds. Quasi static events up to 100 seconds can be measured with the current transducer and the Model 484B11 power supply in the DC coupled mode because this combination of transducer and power supply has a time constant of 1000 seconds. A static event measured at 1/10 of the time constant will have an error of 10 percent.

Table C.1 PCB Model 208AO2 Piezoelectronics Specifications Voltage Output Force Transducer.

Max. Compression	1000 lbs	Resonant frequency	70 kHz
Tension Range	100 lbs	Rise Time	10 μsec
Resolution	0.002 lbs.	Linearity	1 % F.S.
F.S. output voltage	± 5 V	Temperature Range	-100 to +250
Sensitivity	50 mV/lbs.	Stiffness	10 lbs./μin
Weight	25gm (0.9oz)		
Power Supply Model No.	484B11	Time constant in DC coupled mode	1000 seconds*

*The output signal response to a step input dropped less than 1% in a 10 second period

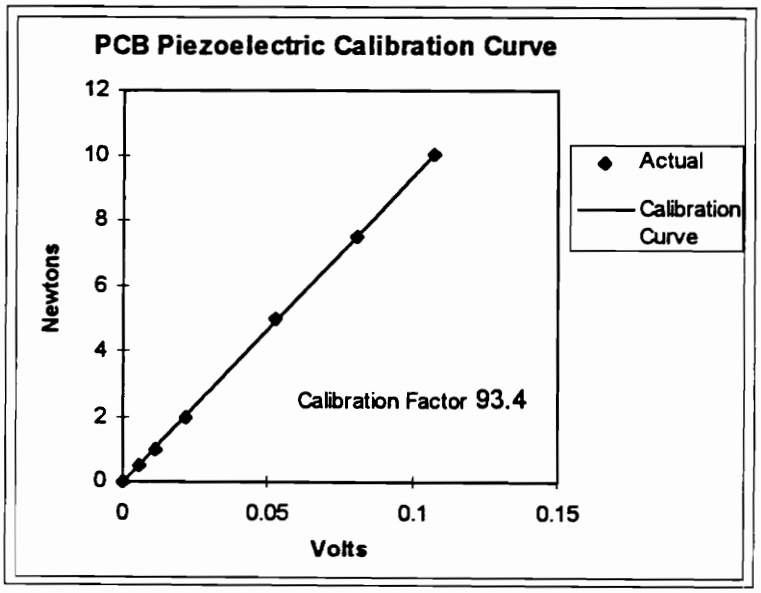

Figure C.1 PCB 208AO2 Piezoelectric friction transducer calibration curve.

Linear Velocity Transducer

Relative velocity is measured by a Lucas Schaevitz VT-Z Series linear velocity transducer which produces an DC voltage output directly proportional to velocity. This transducer does not require a power supply. The L.V.T possesses an extremely wide range of measurement, of at least 1,000 inches per second with the minimum velocity limited by the noise threshold of the signal conditioning equipment. Resolution is essentially infinite. The transducer data is given in table C.2.

The magnetic core of the L.V.T. should be positioned at the mid stroke position to ensure linear operation within the displacement range of the device. Zero velocity can change depending on what the impedance is on the output. During operation the threaded end of the magnet core is attached to the edge of the micro-slider table while the outside core remains fixed.

Table C.2 VT-Z Series Linear Velocity Transducer

Type: 6L2VT-2 Serial No. 6569 Range± 2.0 inches	**Calibration Factor** **0.434 Volt/inch/s** **1.102 Volts/cm/s**
Core	Alnico V
Sensitivity	434 mC/inch/second
Total DC Resistance	14.415 ohms
Total Inductance	3500 millihenrys
Insulation Resistance	Tested from all windings to case. At 500V DC insulation resistance is greater than 50 megaohms.

Normal Load Transducer

Normal load is measured by a Sensotec Model 41 full bridge strain gage load cell which measures loads up to 10 lbs. The signal of this transducer is amplified by an Model UBP in-line amplifier with an output range of ±5 volts. This transducer will also be used to measure any changes in load at the interface during stick slip. The transducer has ample sensitivity and resolution to measures these changes which occur during low frequency stick slip cycles. The specifications are listed in table C.3 and the calibration curve is shown in figure C.2.

Table C.3 Sensotec Load Cell and In-Line Amplifier Specifications

Model 41 Load Cell		Model UBP In-line Amplifier	
Load Range	10 lbs	Operating Voltage	24 -32 VDC
Non-Linearity	±0.2% F. S.	Operating Temp.	-20 to 180°F
Hysteresis	±0.1% F. S.	Excitation Voltage	3,5,10 VDC@70ma
Non-Repeatability	±0.1% F. S.	Output Voltage Range	±5 VDC @ 2ma.
Output	2 mv/v	Zero Adjustment Range	±50% coarse ±15% fine
Operating Range	-65°F to 250°F	Span Adjustment Range	0.5 mv/v to 10 mv/v
Strain Gage	Bonded Foil	Shunt Calibration	Solid state relay
Excitation	10 VDC	Frequency Response	DC - 5000 Hz
Deflection-F. S.	0.003	Linearity	±0..1% F. S.
Stiffness - F. S.	3333 lbs./in (5.86E5 N/m)	Natural Frequency	85 Hz

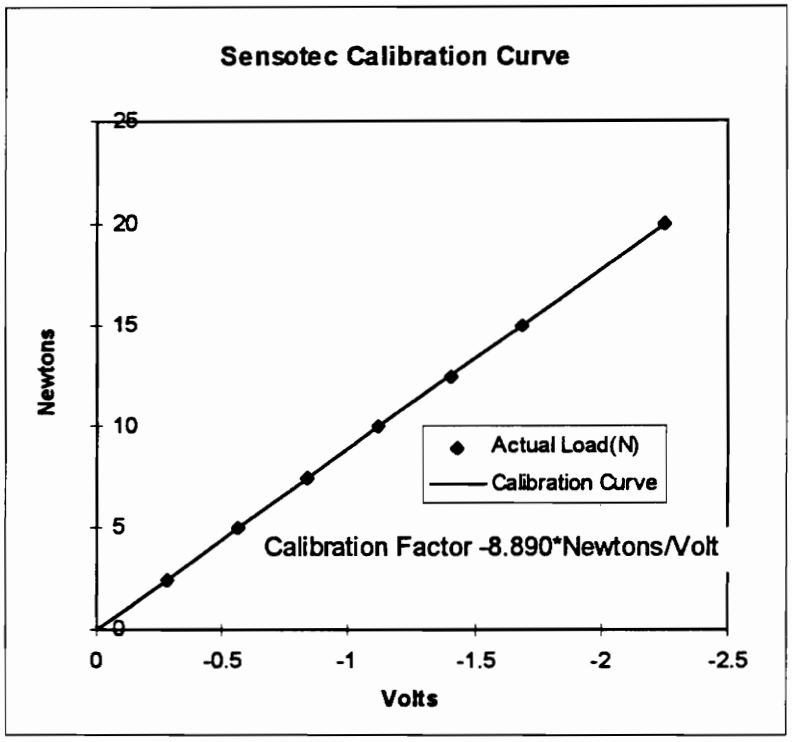

Figure C.2 Sensotec normal load transducer calibration curve.

Linear Sliding Motion

Linear sliding motion is provided by an Industrial Devices Corporation direct drive DC servo actuator. The actuator is driven by a self programmable feed back controller. The PID gains in the controller allow fine tuning of the feedback control providing better control of velocity variations. These settings can be adjusted to allow the controller to adopt to specific load and move conditions. Velocity profiles can be programmed to a maximum velocity at 12 in/s when not attached to the test apparatus. Acceleration will depend on the length of travel and the constant velocity. The acceleration ranges form 0.05 - 15 seconds to ramp to constant velocity.

Maximum constant velocity for the actuator is a function of acceleration and the distance traveled. A triangular velocity profile results if the velocity of the actuator cannot ramp up to the desired constant velocity given the sliding distance. This means constant velocity cannot be obtained. The maximum constant velocity of the actuator is approximately 6 in/s to traverse the entire 1.8 inches of the horizontal slider. The maximum obtainable constant velocity decreases as the sliding distance shortens. Therefore, a constant velocity profile must be experimentally confirmed if the sliding distance and sliding velocity setup is changed. This can be done by measuring the relative velocity of the horizontal slider(which is connected to the actuator) with the L.V.T and viewing the velocity profile on Global Lab.

Appendix D - Data Acquisition and Signal Processing

Data acquisition was performed by a personal computer based analog-to-digital (A/D) board with the Global Lab data acquisition software. The Data Translation DT2821 A/D board has a maximum A/D throughput of 150 kHz (50 kHz maximum each for three channels) and a sample and hold delay of 100 nano-seconds. The impedence of the A/D board is better than 100 kohms.

The sampled friction force, normal load, and velocity signals were then exported from Global Lab to an ASCII format. This data was then processed by a MatLab program which does the following:

1. Calibrates all three signals, if required
2. Corrects for any DC offset in the friction signal and velocity signal
3. Plots the coefficient of friction vs. velocity and friction, velocity, and normal load vs. time relationships shown in the results section.

```
%Edward Lee - Virginia Tech Mechanical Engineering Dept - Version 4.1
%MatLab computer routine to import ascii data files acquired by friction
%test apparatus, and to correct for the DC offset.  The data can be
% converted from volts to Newtons(friction & normal), and cm/s(velocity).


clear
%sr=input('Enter sampling rate(Hz);')
sr = 6000;

%Imports ASCII files for friction force, normal load, and velocity
%     in units of volts
load c:\ <enter your path and filename with extension here>
data = <filename>
;

%Define global variables v,x,z to respective filenames for
% friction, normal, and velocity
fric = data(:,1);
norm = data(:,2);
vel = data(:,3);
num=length(fric)
%Procedure finds maximum friction force and determines
%Scaling of the data to focus on transition zone.  Omit %
%signs to run this subroutine
%fricmax=max(fric);
%limit=0.001*fricmax;
%peak=find(fric>(fricmax-limit));
%lower=peak(1)-750;
%upper=peak(1)+700;



%Procedure to correct for DC offset when PCB model 484B11
%power source is used
query=input('Press <Enter> to compensate for offset ','s')
   if isempty(query)
        for j=1:10
           const(j)=fric(j);
           velcon(j)=vel(j);
        end
        offset=sum(const)/10
```

```
        vlofst=sum(velcon)/10
    else
        offset=0
        vlofst=0
    end



%Procedure to calibrate friction and velocity data
%Multiply velcal, friccal, and normcal, by the calibration
%factor.  In global lab, the units can be loaded into the
%data acquisition setup


for j=1:num
   time(j)=j/sr;
   velcal(j)=abs(vel(j)-vlofst);
   friccal(j)=(fric(j)-offset);
   normcal(j)=abs(norm(j));
   mu(j) = friccal(j)/20.7;
end


%Plots various friction velocity relationships
%Axis scaling can be adjusted if desired, axis([x1 x2 y1 y2])
%Title and labels can be changed, title, xlabel, ylabel
%grids can be added or removed(put a '%' symbol before it)

figure(1)
plot(velcal,mu)
%title('Friction Velocity Curves')
xlabel('Velocity, cm/s')
ylabel('Friction, N')
%grid


figure(2)
plot(time,friccal,time,velcal)
%title('Friction Force and velocity vs. Time')
xlabel('time, sec')
ylabel('friction force, Velocity')
%grid

%figure(3)
```

```
%plot(time,mu,time,velcal)
%title('Coeff of Friction vs. Time')
%xlabel('time, sec')
%ylabel('Coeff of Friction')
%grid

%figure(4)
%plot(time,friccal,time,velcal,time, normcal)
%title('Friction Force, Normal Load and velocity vs. Time')
%xlabel('time, sec')
%ylabel('Friction force, Normal Load, and Velocity')
%grid
```

APPENDIX E - Cutting and Surface Preparation Techniques for Test Specimens

A new procedure was developed to replace the original method of cutting the samples with a bandsaw. The samples were milled with a jig to ensure that the sample sizes were consistent between tests. The first step of this new process is to tape samples to jig and then make parallel cuts in one direction then cut perpendicular to the original direction. Both the quarter inch squares and the rectangles are cut the same way. The last step is to drill holes on both ends of the rectangles and mill the hemispherical cavities in the quarter inch squares. Refer to figure 3.1 for specific dimensions.

Prior to testing all samples were deburred, washed in mild detergent, and rinsed in tap water(deionized water is recommended) to remove surface debris. The samples were then allowed to air dry before storage. The samples were carefully wrapped in Chem-wipes and stored in plastic bags for future testing.

A standardized cleaning and storage procedure should be developed for future studies. The importance of a standardized cleaning procedures was not realized until after the tests had been completed. Consequently, future studies should include surface characterization such as FTIR to determine what surface films are present.

APPENDIX F

Table F.1 Listing of available injection molded polymers

Polymer Type	Manufacturer/ Industry Designation	Composition	
ABS	*Dow/Pulse 930 Engr Resin Natural	ABS resin and bisphenol A/phosgene resin terminated w/ p-tertiary butyl phenol Styrene Monomer	100% 0.25%
	Dow/Magnum 357 HP ABS Resin Natural	Blend of N-phenyl maleimide modified ABS and ABS resin Bis stearamide wax	100% 2%
	Dow/Magnum 541 ABS Natural	ABS Mineral Oil Wax Styrene Monomer	90-99% 0-2% 0-2% <3000 ppm
Polycarbonate	*Miles/APEC HT DP9-9351 1510 Black	Modified Polycarbonate Bisphenol A Polycarbonate Methylene Chloride	min 70% max 30% <3ppm
Polypropylene	*Ferro/HPP30GP-GZ	Fiberglass/mineral filled	n/a
	*Ferro/NPP00GC-GE	Unfilled	n/a
Nylon 6/6	Allied Signal/CAPRON 8233 HS Nylon	Glass fiber reinforcement	33%

ppm - parts per million

APPENDIX G

Table G.1 Injection Molding Conditions

	Dow Pulse 930 ABS	Allied Signal Glass Filled Nylon	APEC Polycarbonate	Ferro NPP Series Unfilled Polypropylene	Ferro HPP Series Glass filled Polypropylene
Drying Conditions					
Temp.	110C max.	180°F	265°F	125°F	200°F
Time	4 hours	n/a	4 hours	2-3 hours	2-3 hours
Barrel Temp.					
Rear	245-265°C	480-520°F	610°F	390-400°F	400-415°F
Middle	225-275°C	500-540°F	615°F	400-400°F	410-420°F
Front	265-280°C	520-560°F	625°F	400-400°F	420-425°F
Nozzle	260-275°C	520-560°F	635°F	400-410°F	425-440°F
Mold Temp. Range	70-90°C	180-200°F	175-250°F	100-110°F	110-125°F
Back Press.	0.35-1.7 MPa	500-1800 psi	50-100psi	50-100 psi	50-100 psi
Injection Speed	38-64 mm/s	fast	slow to moderate	Medium	slow-medium
Screw Speed	2-3sec full recovery	1 inch of ram travel/sec	50-100 rpm	Medium(fast if necessary)	Medium

APPENDIX H - Surface Roughness Measurements of Plastic Master Panels

The following table provides the surface texture characteristics (roughness measurements Ra, Rq, and Rt) measured by the Ford Motor Company. Two master panels made of plastic from Eastman and Ferro were evaluated.

	Ra(microns)	Rq(microns)	Rt(microns)
Ferro, Plastic Master 4-19-93			
Montang BG			
Upper	0.09	0.12	0.80
Lower	0.12	0.14	0.70
Stipple#1			
Upper	0.13	0.17	0.80
Lower	0.14	0.17	0.80
Naples FY			
Upper	0.11	0.14	0.60
Lower	0.12	0.14	0.90
Eastman, Plastic Master 9-27-89			
Montana BG			
Upper	0.18	0.22	0.80
Lower	0.15	0.18	0.90
Stipple #1			
Upper	0.13	0.16	0.70
Lower	0.15	0.19	0.90
Naples FY			
Upper	0.16	0.20	1.5
Lower	0.11	0.13	1.30
SPE-SPI 1			
Upper	0.00	0.00	0.00
Lower	0.00	0.00	0.10
SPE-SPI 3			
Upper	0.00	0.00	0.00
Lower	0.00	0.00	0.10
SPE-SPI 5			
Upper	0.01	0.01	0.10
Lower	0.01	0.01	0.10

Ra = Arithematic Average Roughness
Rq = Root mean square (RMS) roughness
Rt = Maximum peak-to-valley height

APPENDIX I

Table I.1 List of Available Polymer Resins

#	Company	Polymer Resin
1	Allied Signal	Capron 8233GH3 Nylon
2		PETRA 230BK-112 PET
3	AMOCO	ACCTUF 61-3950 Enhanced polypropylene
4		ACCPRO 10-9433 Enhanced polypropylene
5		HOMOPOLYMER RESIN 10-1016
6		AMODEL A-1133 HS BK324 Polyphthalamide(PPA)
7	ARCO	Dylark Glass reinforced "P" Grade 480P16-0N5 SMA Copolymer
8		Dylark Glass reinforced "P" Grade 378P20-0N5 SMA Copolymer
9		Dylark Glass reinforced "A" Grade 378P20A0N5 SMA Copolymer
10	BASF	ABS resin, TERLUX 2802 TR Transparent 0161
11		548010-ULTRADUR B4300G4 Uncolored
12		Product Code 530749 Description N 2325 U
13	DOW Chemicals	Magnum 358 HP ABS 27 Natural 7
14		Pulse 930 Engr Resin FP770031 ABS
15		Magnum 357 HP ABS 27 Natural

#	Company	Polymer Resin
16		Magnum 541 ABS 27 Natural 7
17	Whiting Brownston Dist. for DOW Chemicals	Calibre 101-15 ID2801QCE1 Type 100 Polycarbonate Sample
18		Pulse 0830 Natural II0601Q04 Type 100 ABS Sample
19		Pulse 0959 IE2001QCEI Type 100 ABS Sample
20	Ferro	FF 21795-1922 9408223 Black
21	Ferro	Mineral Filled Polypropylene: WPP10SD-02NA
22	Ferro	Unfilled Polypropylene: NPP00GW01BK
23		Fiberglass/mineral filled Polypropylene: HPP30GR05BK
24	Himont	SB891 Polypropylene
25		SB823 Polypropylene
26		SG702 Polypropylene
27		SD242 Polypropylene
28		SB821 Polypropylene
29	Hoechst Celanese	112 CELCON - Acetal Copolymer GB25 DB93101A5 LB
30		112 VECTRA - Liquid Crystal Polymer A435 VB00551A1 LB
31		112 FORTRON - Polphenylene Sulfide 1140L4 SB11061D1 LB
32		CELCON ACETAL COPOLYMER TX90 BC40818151 2C4L
33		CELCON ACETAL COPOLYMER M90 BC40816062 2D4R

#	Company	Polymer Resin
34		CELANEX
35		CELANESE 1003 Nylon Natural
36		CELCON - BLACK Acetal Copolymer
37	Miles*	APEC HT DP9-9351 1510 Black Polycarbonate
38	Miles	Bayblend T-85 MN 1510 BK Polycarbonate
39		Makrolon T-7435 1510 Black
40	Monsanto	Vydyne Resin 21SP
41	Monsanto	Plastic Resin Elite HH 1827-1000
42		Resin Centrex 821-90867 Black
43		ABS Resin LGA Elite-1000 Natural
44		Lustran ABS 1146 Q774 Natural
45	Monsanto	CADON - Glass 2320 90807 Black
46	Monsanto	Lustran 1450 black/gray
47		TRIAX 2753 Q294 001000

Appendix J

Table J.1 Time Dependent Friction Data for Nylon

Montana Surface							
Min.	**Test**	**#**	**μ_s**	**μ_k**	**$\Delta\mu$**		
.5 min. contact time	**NYLMTAR**	1	0.188	0.112	0.0764	**AVG μ_s**	0.199
		2	0.192	0.145	0.0464	**AVG μ_k**	0.127
		3	0.226	0.149	0.0770	**AVG $\Delta\mu$**	0.0719
		4	0.191	0.103	0.0878		
1 min. contact time	**NYLMTBR**	1	0.226	0.110	0.117	**AVG μ_s**	0.224
		2	0.201	0.129	0.0718	**AVG μ_k**	0.126
		3	0.253	0.139	0.115	**AVG $\Delta\mu$**	0.0890
		4	0.216	0.127	0.0891		
2 min. contact time	**NYLMTCR**	1	0.235	0.113	0.122	**AVG μ_s**	0.238
		2	0.256	0.137	0.119	**AVG μ_k**	0.118
		3	0.207	0.110	0.0965	**AVG $\Delta\mu$**	0.120
		4	0.255	0.114	0.141		
3 min. contact time	**NYLMTDR**	1	0.280	0.139	0.141	**AVG μ_s**	0.267
		2	0.288	0.141	0.147	**AVG μ_k**	0.127
		3	0.245	0.130	0.145	**AVG $\Delta\mu$**	0.140
		4	0.257	0.0999	0.157		
5 min. contact time	**NYLMTER**	1	0.275	0.129	0.146	**AVG μ_s**	0.277
		2	0.264	0.156	0.108	**AVG μ_k**	0.142
		3	0.303	0.149	0.154	**AVG $\Delta\mu$**	0.136
		4	0.267	0.132	0.135		
Naples Surface							
Time	**Test**	**#**	**μ_s**	**μ_k**	**$\Delta\mu$**		
.5 min. contact time	**NYLNTAR**	1	0.176	0.0820	0.0937	**AVG μ_s**	0.184
		2	0.187	0.134	0.0522	**AVG μ_k**	0.113
		3	0.179	0.112	0.0678	**AVG $\Delta\mu$**	0.0706
		4	0.194	0.125	0.0689		
1 min. contact time	**NYLNTBR**	1	0.234	0.123	0.111	**AVG μ_s**	0.239
		2	0.256	0.137	0.119	**AVG μ_k**	0.121
		3	0.212	0.115	0.0975	**AVG $\Delta\mu$**	0.118
		4	0.254	0.108	0.146		
2 min. contact time	**NYLNTCR**	1	0.259	0.131	0.128	**AVG μ_s**	0.231
		2	0.235	0.139	0.0955	**AVG μ_k**	0.119
		3	0.208	0.0997	0.108	**AVG $\Delta\mu$**	0.112
		4	0.222	0.106	0.116		
3 min. contact time	**NYLNTDR**	1	0.264	0.120	0.144	**AVG μ_s**	0.253
		2	0.270	0.126	0.144	**AVG μ_k**	0.120
		3	0.241	0.102	0.139	**AVG $\Delta\mu$**	0.133
		4	0.238	0.133	0.105		
5 min. contact time	**NYLNTER**	1	0.302	0.0971	0.205	**AVG μ_s**	0.284
		2	0.293	0.141	0.152	**AVG μ_k**	0.110
		3	0.268	0.0982	0.169	**AVG $\Delta\mu$**	0.174
		4	0.274	0.103	0.171		

SPI-SPE #1 Surface							
Time	Test	#	μ_s	μ_k	$\Delta\mu$		
.5 min. contact time	NYLSTAR	1	0.175	0.113	0.0622	AVG μ_s	0.189
		2	0.197	0.130	0.0662	AVG μ_k	0.115
		3	0.183	0.111	0.0724	AVG $\Delta\mu$	0.0745
		4	0.203	0.106	0.0970		
1 min. contact time	NYLSTBR	1	0.216	0.118	0.0975	AVG μ_s	0.197
		2	0.183	0.103	0.0799	AVG μ_k	0.112
		3	0.1184	0.103	0.0809	AVG $\Delta\mu$	0.0845
		4	0.204	0.125	0.0796		
2 min. contact time	NYLSTCR	1	0.237	0.139	0.0975	AVG μ_s	0.222
		2	0.214	0.116	0.0981	AVG μ_k	0.121
		3	0.228	0.117	0.111	AVG $\Delta\mu$	0.101
		4	0.209	0.112	0.0967		
3 min. contact time	NYLSTDR	1	0.300	0.141	0.159	AVG μ_s	0.276
		2	0.269	0.123	0.146	AVG μ_k	0.125
		3	0.266	0.112	0.153	AVG $\Delta\mu$	0.150
		4	0.269	0.126	0.142		
5 min. contact time	NYLSTER	1	0.256	0.129	0.127	AVG μ_s	0.258
		2	0.222	0.0969	0.125	AVG μ_k	0.137
		3	0.281	0.167	0.112	AVG $\Delta\mu$	0.121
		4	0.272	0.151	0.121		
Stipple Surface							
Time	Test	#	μ_s	μ_k	$\Delta\mu$		
.5 min. contact time	NYLITAR	1	0.227	0.181	0.0466	AVG μ_s	0.203
		2	0.189	0.146	0.0432	AVG μ_k	0.151
		3	0.192	0.125	0.0670	AVG $\Delta\mu$	0.0523
		4	0	0	0		
1 min. contact time	NYLITBR	1	0.245	0.192	0.0535	AVG μ_s	0.236
		2	0.215	0.172	0.0434	AVG μ_k	0.173
		3	0.264	0.179	0.0854	AVG $\Delta\mu$	0.0634
		4	0.220	0.149	0.0713		
2 min. contact time	NYLITCR	1	0.236	0.178	0.0573	AVG μ_s	0.225
		2	0.244	0.153	0.0904	AVG μ_k	0.152
		3	0.230	0.160	0.0700	AVG $\Delta\mu$	0.0735
		4	0.192	0.116	0.0762		
3 min. contact time	NYLITDR	1	0.273	0.178	0.0958	AVG μ_s	0.263
		2	0.258	0.159	0.108	AVG μ_k	0.158
		3	0.260	0.166	0.0934	AVG $\Delta\mu$	0.104
		4	0.260	0.140	0.120		
5 min. contact time	NYLITER	1	0.293	0.201	0.0914	AVG μ_s	0.268
		2	0.252	0.175	0.0763	AVG μ_k	0.171
		3	0.286	0.154	0.133	AVG $\Delta\mu$	0.0965
		4	0.241	0.156	0.0856		

Denotation for Appendix

μs - Static Coefficient of Friction
μk - Kinetic Coefficient of Friction
Δμ - μs-μk

The first two letters denote the material:	NY	Nylon
The third letter denotes the applied normal load:	L	10.7 Newtons or
	H	20.7 Newtons
The fourth letter denotes the surface roughness	M	Montana BG or
	N	Naples FY or
	S	SPI-SPE #1 or
	I	Stipple #1
The 5th and 6th letter denotes the contact time	TA	0.5 minute contact time or
	TB	0.5 minute contact time or
	TC	0.5 minute contact time or
	TD	0.5 minute contact time or
	TE	0.5 minute contact time
The 7th and 8th characters denote the replicate #.	R1	Replicate 1
	R2	Replicate 2
	R3	Replicate 3
	R4	Replicate 4

Note: Data for NYLITAR test sessions was not available for analysis.
A nylon data was filtered through Zonic anti-aliasing lowpass filters set at a frequency cutoff of 1500 Hz.

Appendix K

Table K.1 Friction Data for ABS, Polycarbonate, Polypropylene(Unfiltered Data)

	ABS Montana Surface							
	Load: 10.7 Newtons Test Series: ABLMTER				Load: 20.7 Newtons Test Series: ABHMTER			
#	μ_s	μ_{min}	μ_k	$\mu_s-\mu_{min}$	μ_s	μ_{min}	μ_k	$\mu_s-\mu_{min}$
1	0.191	0.0373	0.107	0.154	0.200	0.0676	0.131	0.133
2	0.201	0.0792	0.120	0.122	0.191	0.785	0.142	0.113
3	0.218	0.0566	0.103	0.161	0.236	0.0461	0.150	0.190
4	0.195	0.0775	0.140	0.118	0.184	0.0674	0.105	0.117
	ABS Naples Surface							
	Load: 10.7 Newtons Test Series: ABLNTER				Load: 20.7 Newtons Test Series: ABHNTER			
#	μ_s	μ_{min}	μ_k	$\mu_s-\mu_{min}$	μ_s	μ_{min}	μ_k	$\mu_s-\mu_{min}$
1	0.221	0.0890	0.135	0.131	0.158	0.0499	0.0923	0.108
2	0.224	0.0852	0.131	0.139	0.201	0.0998	0.134	0.101
3	0.207	0.0312	0.119	0.176	0.188	0.0620	0.117	0.0126
4	0.163	0.0505	0.0763	0.112	0.188	0.0948	0.115	0.0929
	ABS SPI-SPE #1 Surface							
	Load: 10.7 Newtons Test Series: ABLSTER				Load: 20.7 Newtons Test Series: ABHSTER			
#	μ_s	μ_{min}	μ_k	$\mu_s-\mu_{min}$	μ_s	μ_{min}	μ_k	$\mu_s-\mu_{min}$
1	0.338	0.174	0.225	0.164	0.237	0.117	0.180	0.120
2	0.316	0.1118	0.173	0.198	0.236	0.147	0.180	0.0894
3	0.222	0.119	0.136	0.102	0.257	0.181	0.268	0.0762
4	0.235	0.111	0.136	0.124	0.293	0.149	0.187	0.144
	ABS Stipple Surface							
	Load: 10.7 Newtons Test Series: ABLITER				Load: 20.7 Newtons Test Series: ABHITER			
#	μ_s	μ_{min}	μ_k	$\mu_s-\mu_{min}$	μ_s	μ_{min}	μ_k	$\mu_s-\mu_{min}$
1	0.196	0.0741	0.107	0.122	0.200	0.101	0.131	0.0991
2	0.168	0.0956	0.103	0.0690	0.184	0.124	0.124	0.0601
3	0.194	0.131	0.140	0.0627	0.145	0.0784	0.0984	0.0665
4	0.157	0.0855	0.129	0.0712	0.130	0.0546	0.0705	0.0751

Polycarbonate Montana Surface

	Load: 10.7 Newtons Test Series: PCLMTER				Load: 20.7 Newtons Test Series: PCHMTER			
#	μ_s	μ_{min}	μ_k	$\mu_s-\mu_{min}$	μ_s	μ_{min}	μ_k	$\mu_s-\mu_{min}$
1	0.251	0.0492	0.174	0.202	0.229	0.175	0.0741	0.155
2	0.250	0.130	0.181	0.120	0.219	0.192	0.165	0.0537
3	0.218	0.169	0.190	0.0490	0.225	0.197	0.147	0.0784
4	0.231	0.0927	0.180	0.138	0.168	0.164	0.129	0.0392

Polycarbonate Naples Surface

	Load: 10.7 Newtons Test Series: PCLNTER				Load: 20.7 Newtons Test Series: PCHNTER			
#	μ_s	μ_{min}	μ_k	$\mu_s-\mu_{min}$	μ_s	μ_{min}	μ_k	$\mu_s-\mu_{min}$
1	0.231	0.130	0.170	0.101	0.202	0.140	0.227	0.0617
2	0.249	0.172	0.218	0.0770	0.220	0.154	0.189	0.0656
3	0.261	0.177	0.187	0.0841	0.245	0.0790	0.198	0.166
4	0.230	0.155	0.196	0.0746	0.221	0.0743	0.219	0.147

Polycarbonate SPI-SPE #1 Surface

	Load: 10.7 Newtons Test Series: PCLSTER				Load: 20.7 Newtons Test Series: PCHSTER			
#	μ_s	μ_{min}	μ_k	$\mu_s-\mu_{min}$	μ_s	μ_{min}	μ_k	$\mu_s-\mu_{min}$
1	0.206	0.126	0.180	0.0801	0.227	0.192	0.405	-.0357
2	0.205	0.189	0.358	-.0159	0.202	0.173	0.343	-.0291
3	0.261	0.224	0.273	-.0374	0.198	0.131	0.296	-.0669
4	0.245	0.315	0.315	-.0708	0.195	0.149	0.227	-.0462

Polycarbonate Stipple Surface

	Load: 10.7 Newtons Test Series: PCLITER				Load: 20.7 Newtons Test Series: PCHITER			
#	μ_s	μ_{min}	μ_k	$\mu_s-\mu_{min}$	μ_s	μ_{min}	μ_k	$\mu_s-\mu_{min}$
1	0.199	0.133	0.143	0.0656	0.190	0.0822	0.136	0.108
2	0.183	0.117	0.138	0.0667	0.211	0.131	0.156	0.0795
3	0.193	0.111	0.116	0.0816	0.184	0.124	0.147	0.0599
4	0.166	0.122	0.122	0.0445	0.220	0.115	0.163	0.105

Fiberglass Filled Polypropylene Montana Surface

	Load: 10.7 Newtons Test Series: FPLMTER				Load: 20.7 Newtons Test Series: FPHMTER			
#	μ_s	μ_{min}	μ_k	$\mu_s-\mu_{min}$	μ_s	μ_{min}	μ_k	$\mu_s-\mu_{min}$
1	0.206	0.100	0.136	0.106	0.193	0.0868	0.119	0.107
2	0.222	0.109	0.141	0.113	0.184	0.0711	0.112	0.113
3	0.212	0.120	0.136	0.0921	0.159	0.0908	0.107	0.0685
4	0.215	0.114	0.115	0.100	0.182	0.0849	0.108	0.0975

Fiberglass Filled Polypropylene Naples Surface

	Load: 10.7 Newtons Test Series: FPLNTER				Load: 20.7 Newtons Test Series: FPHNTER			
#	μ_s	μ_{min}	μ_k	$\mu_s-\mu_{min}$	μ_s	μ_{min}	μ_k	$\mu_s-\mu_{min}$
1	0.230	0.152	0.152	0.0778	0.218	0.149	0.152	0.0778
2	0.206	0.143	0.143	0.0623	0.226	0.127	0.143	0.0623
3	0.202	0.139	0.139	0.0634	0.199	0.120	0.139	0.0634
4	0.203	0.129	0.129	0.0741	0.198	0.0958	0.129	0.0741

Fiberglass Filled Polypropylene SPI-SPE #1 Surface

	Load: 10.7 Newtons Test Series: FPLSTER				Load: 20.7 Newtons Test Series: FPHSTER			
#	μ_s	μ_{min}	μ_k	$\mu_s-\mu_{min}$	μ_s	μ_{min}	μ_k	$\mu_s-\mu_{min}$
1	0.236	0.124	0.155	0.112	0.229	0.105	0.148	0.124
2	0.207	0.104	.0.126	0.103	0.195	0.0795	0.113	0.115
3	0.210	0.0974	0.111	0.112	0.190	0.0788	0.112	0.111
4	0.186	0.0627	0.0918	0.123	0.190	0.100	0.111	0.0898

Fiberglass Filled Polypropylene Stipple Surface

	Load: 10.7 Newtons Test Series: FPLITER				Load: 20.7 Newtons Test Series: FPHITER			
#	μ_s	μ_{min}	μ_k	$\mu_s-\mu_{min}$	μ_s	μ_{min}	μ_k	$\mu_s-\mu_{min}$
1	0.205	0.146	0.146	0.0592	0.217	0.152	0.152	0.0650
2	0.213	0.172	0.172	0.0411	0.194	0.145	0.145	0.0484
3	0.197	0.137	0.137	0.0598	0.201	0.149	0.149	0.0521
4	0.199	0.135	0.135	0.0643	0.203	0.154	0.153	0.0488

Unfilled Polypropylene Montana Surface

	Load: 10.7 Newtons Test Series: UPLMTER				Load: 20.7 Newtons Test Series: UPHMTER			
#	μ_s	μ_{min}	μ_k	μ_s-μ_{min}	μ_s	μ_{min}	μ_k	μ_s-μ_{min}
1	0.261	0.264	0.264	-0.003	0.240	0.223	0.223	0.017
2	0.299	0.224	0.224	0.075	0.218	0.207	0.207	0.011
3	0.304	0.235	0.235	0.070	0.262	0.225	0.225	0.038
4	0.292	0.169	0.169	0.122	0.233	0.153	0.153	0.080

Unfilled Polypropylene Naples Surface

	Load: 10.7 Newtons Test Series: UPLNTER				Load: 20.7 Newtons Test Series: UPHNTER			
#	μ_s	μ_{min}	μ_k	μ_s-μ_{min}	μ_s	μ_{min}	μ_k	μ_s-μ_{min}
1	0.388	0.388	0.388	0	0.318	0.301	0.301	0.0170
2	0.297	0.269	0.269	0.027	0.305	0.305	0.305	0.000
3	0.351	0.321	0.321	0.03	0.280	0.280	0.280	0.000
4	0.342	0.303	0.303	0.039	0.254	0.254	0.254	0.000

Unfilled Polypropylene SPI-SPE #1 Surface

	Load: 10.7 Newtons Test Series: UPLSTER				Load: 20.7 Newtons Test Series: UPHSTER			
#	μ_s	μ_{min}	μ_k	μ_s-μ_{min}	μ_s	μ_{min}	μ_k	μ_s-μ_{min}
1	0.706	0.572	0.572	0.134	0.669	0.673	0.673	0.004
2	0.570	0.489	0.489	0.081	0.569	0.569	0.569	0.000
3	0.610	0.567	0.567	0.043	0.597	0.597	0.597	0.00
4	0.307	0.317	0.317	0.011	0.537	0.464	0.464	0.073

Unfilled Polypropylene Stipple Surface

	Load: 10.7 Newtons Test Series: UPLITER				Load: 20.7 Newtons Test Series: UPHITER			
#	μ_s	μ_{min}	μ_k	μ_s-μ_{min}	μ_s	μ_{min}	μ_k	μ_s-μ_{min}
1	0.323	0.279	0.279	0..044	0.243	0.225	0.225	0.017
2	0.293	0.272	0.272	0..022	0.266	0.237	0.237	0.029
3	0.278	0.221	0.221	0..057	0.264	0.245	0.245	0.020
4	0.251	0.202	0.202	0..049	0.248	0.212	0.212	0.035

3 vbm 1020s in series
ABS Montana Surface

	Load: 10.7 Newtons Test Series: ABLMTER				Load: 20.7 Newtons Test Series: ABHMTER			
#	μ_s	μ_{min}	μ_k	μ_s-μ_{min}	μ_s	μ_{min}	μ_k	μ_s-μ_{min}
1	0.199	0.124	0.154	0.0748	0.221	0.117	0.139	0.104
2	0.193	0.0807	0.133	0.112	0.209	0.104	0.104	0.105
3	0.227	0.111	0.130	0.115	0.226	0.0469	0.120	0.179
4	0.202	0.0913	0.161	0.111	0.213	0.106	0.116	0.107

ABS Naples Surface

	Load: 10.7 Newtons Test Series: ABLNTER				Load: 20.7 Newtons Test Series: ABHNTER			
#	μ_s	μ_{min}	μ_k	μ_s-μ_{min}	μ_s	μ_{min}	μ_k	μ_s-μ_{min}
1	0.249	0.0864	0.165	0.163	0.269	0.087	0.149	0.164
2	0.225	0.0904	0.118	0.135	0.258	0.090	0.146	0.192
3	0.249	0.159	0.131	0.091	0.191	0.159	0.109	0.083
4	0.203	0.162	0.162	0.041	0.192	0.162	0.079	0.095

ABS SPI-SPE #1 Surface

	Load: 10.7 Newtons Test Series: ABLSTER				Load: 20.7 Newtons Test Series: ABHSTER			
#	μ_s	μ_{min}	μ_k	μ_s-μ_{min}	μ_s	μ_{min}	μ_k	μ_s-μ_{min}
1	0.259	0.193	0.193	0.066	0.248	0.183	0.216	0.065
2	0.278	0.182	0.193	0.096	0.258	0.178	0.186	0.080
3	0.211	0.018	0.153	0.193	0.325	0.118	0.187	0.207
4	0.288	0.191	0.191	0.175	0.321	0.152	0.176	0.169

ABS Stipple Surface

	Load: 10.7 Newtons Test Series: ABLITER				Load: 20.7 Newtons Test Series: ABHITER			
#	μ_s	μ_{min}	μ_k	μ_s-μ_{min}	μ_s	μ_{min}	μ_k	μ_s-μ_{min}
1	0.171	0.106	0.111	0.066	0.159	0.101	0.113	0.058
2	0.204	0.110	0.104	0.094	0.192	0.152	0.147	0.040
3	0.201	0.058	0.103	0.143	0.171	0.135	0.133	0.036
4	0.177	0.138	0.148	0.039	0.151	0.112	0.116	0.039

Appendix L - Analysis of Variance(ANOVA) Results

An analysis of variance using SAS software was performed by the Statistical Consulting Center. The effect of material composition, surface roughness, and normal load were compared to the mean of the static, kinetic, and drop from static to kinetic coefficient of friction. Significant differences and interactions are shown in table L.1.

Table L.1. Statistics - ANOVA method

Does a significant difference exist?

Main Effects	μ_s	μ_k	$\Delta\mu$
Material(4)	yes	yes	yes
Surface(4)	yes	yes	yes
Load(2)	no	no	yes
1st Order Interactions			
Material*Surface	yes	yes	yes
Material*Load	no	no	no
Surface*Load	no	no	no
Material*Surface*Load	no	no	no

Table L.2 SAS Data Inputs

Number of observations: 128		
Class	**Levels**	**Values**
Material (M)	4	ABS, PC, filled PP, and unfilled PP
Surface (S)	4	Montana BG, Naples FY, SPI-SPE#1, Stipple #1
Load (L)	2	High load(20.7 N), low load(10.7 N)

	DOF	Sum of Squares	Mean Square	F-Value	P-Value
Dependent Variable: Static					
Model	31	1.0921	0.0352	23.4	0.0001
Error	96	0.1446	0.0015		
Corrected Total	127	1.2367			

R-Squared	Root Mean Square	Mean
0.8831	0.0388	0.2462

Source	DoF	Type I SS	Mean Square	F-value	P-value
M	3	0.5115	0.1705	113.24	0.0001
S	3	0.2147	0.0716	47.53	0.0001
L	1	0.0074	0.0074	4.90	0.0292
M*S	9	0.3400	0.0378	25.09	0.0001
M*L	3	0.0007	0.0002	0.16	0.9215
S*L	3	0.0038	0.0013	0.83	0.4795
M*S*L	9	0.0140	0.0016	1.03	0.4212

	DOF	Sum of Squares	Mean Square	F-Value	P-Value
Dependent Variable: Kinetic					
Model	31	1.4429	0.0465	29.12	0.0001
Error	96	0.1534	0.0016		
Corrected Total	127	1.5964			

R-Squared	Root Mean Square	Mean
0.9039	0.0400	0.1968

Source	DoF	Type I SS	Mean Square	F-value	P-value
M	3	0.7454	0.2485	155.45	0.0001
S	3	0.3510	0.1170	73.20	0.0001
L	1	0.0004	0.0004	0.26	0.6120
M*S	9	0.3129	0.0348	21.75	0.0001
M*L	3	0.0008	0.0003	0.17	0.9187
S*L	3	0.0161	0.0054	3.36	0.0220
M*S*L	9	0.0162	0.0018	11.13	0.3514

	DOF	Sum of Squares	Mean Square	F-Value	P-Value
Dependent Variable: ΔFriction					
Model	31	0.4006	0.0129	5.42	0.0001
Error	96	0.2290	0.0024		
Corrected Total	127	0.6296			

R-Squared	Root Mean Square	Mean
0.6363	0.0488	0.0705

Source	DoF	Type I SS	Mean Square	F-value	P-value
M	3	0.1167	0.0389	16.31	0.0001
S	3	0.0409	0.0136	5.71	0.0012
L	1	0.0171	0.0171	7.16	0.0088
M*S	9	0.1802	0.0200	8.39	0.0001
M*L	3	0.0043	0.0014	0.60	0.6159
S*L	3	0.0138	0.0046	1.93	0.1295
M*S*L	9	0.0277	0.0031	1.29	0.2523

VITA

The author was born in New York City, New York on April 26, 1971, the first of two sons, to Dr. Kun Chieh Lee and Mrs. Shiow Yeh Lee. He graduated from Nitro High School in Nitro, West Virginia, in the spring of 1989 and enrolled at Virginia Polytechnic Institute and State University. Four years later he graduated with a Bachelor of Science degree in Mechanical Engineering and continued his education by enrolling in the Master of Science degree in Mechanical Engineering. The author will be employed by the Cryovac division of W.R. Grace & Company as a mechanical engineer in Duncan, South Carolina.